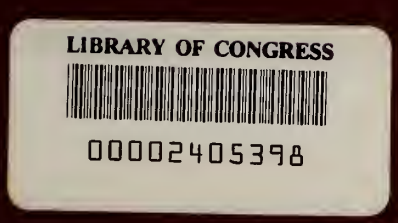

IC 9195

Bureau of Mines Information Circular/1988

New Steelmaking Technology From the Bureau of Mines

Proceedings of an Open Industry Briefing Held in Association With the Electric Furnace Conference, December 8, 1987, Chicago, IL

Compiled by Staff, Bureau of Mines

UNITED STATES DEPARTMENT OF THE INTERIOR

Information Circular/9195

New Steelmaking Technology From the Bureau of Mines

Proceedings of an Open Industry Briefing Held in Association With the Electric Furnace Conference, December 8, 1987, Chicago, IL

Compiled by Staff, Bureau of Mines

UNITED STATES DEPARTMENT OF THE INTERIOR
Donald Paul Hodel, Secretary

BUREAU OF MINES
T S Ary, Director

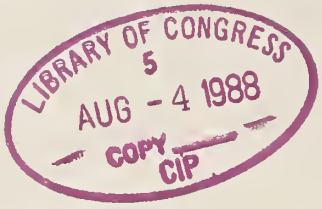

Library of Congress Cataloging-in-Publication Data

New steelmaking technology from the Bureau of Mines.

(Bureau of Mines information circular ; 9195)

Bibliographies.

Supt. of Docs. no.: I 28.27: 9195.

1. Steel—Metallurgy—Congresses. I. Electric Furnace Conference (1987 : Chicago, IL). II. United States, Bureau of Mines. III. Series: Information circular (United States. Bureau of Mines) ; 9195.

TN295.U4 [TN730] 622 s [669'.1424] 88-600072

PREFACE

On December 8, 1987, the Bureau of Mines held an open industry briefing in association with the Electric Furnace Conference sponsored by AIME's Iron and Steel Society. The papers presented at that briefing are contained in this Information Circular, which serves as a proceedings of the meeting. The papers highlight the Bureau's most recent research aimed at improving steelmaking technology. Areas addressed by this research include arc stability in electric steelmaking furnaces, stainless steel pickling processes, substitutes in steelmaking, steelmaking refractories, and recycling of steelmaking dusts and wastes.

The open industry briefing used as a forum for the transfer of this research is one of the many mechanisms used by the Bureau of Mines in its efforts to move research developments, technology, and information resulting from its programs into industrial practice and use. To learn more about the Bureau's technology transfer program and how it can be useful to you, please write or telephone:

Bureau of Mines
Office of Technology Transfer
2401 E Street, NW.
Washington, DC 20241
Telephone: 202-634-1224

CONTENTS

UNIT OF MEASURE ABBREVIATIONS USED IN THIS REPORT

A	ampere
A/dm^2	ampere per square decimeter
Å/min	angstrom per minute
atm	atmosphere, standard
at·pct	atomic percent
Btu/(lb·mol)	British thermal unit per pound per mole
Btu/st	British thermal unit per short ton
Btu/yr	Brithsh thermal unit per year
cm	centimeter
cm^2	square centimeter
°C	degree Celsius
°F	degree Fahrenheit
dB	decibel
dm^2	square decimeter
ft	foot
ft/s	foot per second
g	gram
gal	gallon
g/cm^3	gram per cubic centimeter
g/L	gram per liter
g/m^2	gram per square meter
g-mol/dm^2·h	gram mole per square decimeter per hour
gr/dscf	grain per dry standard cubic foot
h	hour
Hz	hertz
in	inch
K	kelvin
kcal/mol	kilocalorie per mole
keV	thousand electron volts
kHz	kilohertz
kW	kilowatt
kW·h	kilowatt hour
kW·h/lb	kilowatt hour per pound
kW·h/st	kilowatt hour per short ton
kW·h/yr	kilowatt hour per year
kV·A	kilovolt ampere
L	liter
lb	pound
lb/ft^3	pound per cubic foot
lb/min	pound per minute
lb/st	pound per short ton
Mgal	thousand gallons
mg/(min·cm^2)	milligrams per minute per square centimeter
min	minute
mL	milliliter
mm	millimeter
MMBtu	million British thermal units
MΩ-cm	megohm centimeter
mol/L	mole per liter
ms	millisecond
m/s	meter per second
mt	metric ton
mV	millivolt
μA/cm^2	microampere per square centimeter
μF/cm^2	microfarad per square centimeter
μm	micrometer
μs	microsecond
nm	nanometer
Ωcm^2	ohm centimeter squared
P	poise
pct	percent
ppm	part per million
ppt	part per thousand
psi	pound per square inch
s	second
scfm	standard cubic foot per minute
st	short ton
st/d	short ton per day
st/yr	short ton per year
V	volt
V/h	volt per hour
vol pct	volume percent
wt pct	weight percent
yr	year

NEW STEELMAKING TECHNOLOGY FROM THE BUREAU OF MINES

Proceedings of an Open Industry Briefing Held in Association With the Electric Furnace Conference, December 8, 1987, Chicago, IL

Compiled by Staff, Bureau of Mines

ABSTRACT

This report is a proceedings of a briefing recently sponsored by the Bureau of Mines at which Bureau personnel presented findings from their research efforts to improve steelmaking techology currently used in the United States. The papers contained in this report address many areas of concern to the iron and steelmaking industry. Among these are improving arc stability in electric arc furnaces, preheating ferrous scrap to reduce energy consumption, fluorspar substitutes in steelmaking, basic steelmaking refractories, corrosion of iron-based materials, improvements in stainless steel acid pickling processes, recycling of stainless steel dusts and other wastes, and use of wastes as a source of zinc for electro/galvanizing.

INTRODUCTION

For over 50 years the Bureau of Mines has worked to improve technology used by a major constituent of the U.S. minerals industry—the iron and steelmakers. The most recent promising results of this research are presented in this report. Some of the research described has been completed; other research studies highlighted are in progress. However, this report focuses on many significant findings with a probable high positive impact on the industry. For instance, the Bureau is studying the fundamental behavior of arcs in electric furnaces in order to improve the efficiency of this steel manufacturing technology. Past research has shown that electrical disturbances caused by the unpredictable arc are responsible for power surges and fluctuations and for noise levels in excess of 120 dB. Understanding fundamental arc behavior may enable researchers to control the arc and therefore optimize electric furnace operation and efficiency. Already these studies have yielded positive results in the identification of potential areas for change in furnace designs and operating procedures to greatly increase efficiency.

In addition to this research, the Bureau has also evaluated the feasibility of preheating ferrous scrap charges in electric furnace operations to decrease energy consumption by using furnace offgases. During a laboratory test, furnace offgases from a 1-st-capacity electric arc furnace were used to preheat continuously charged automotive scrap and metal stampings up to 1,110° F. Results showed that about 7 pct less electrical energy was used in charging preheated scrap than was used when cold scrap was charged.

Other research conducted by the Bureau may help reduce costs associated with basic oxygen and electric furnace operations by providing a less expensive substitute for fluorspar fluidizers. Substitutes evaluated as alternatives in basic oxygen furnace operations include colemanite, fused boric acid, synthetic fluorspar, and used aluminum smelter potlining. Alternatives for electric arc furnace operations were synthetic fluorspar, boric acid, hydroboracite, used aluminum potlining and anode tailing wastes, and Soreflux B (ilmenite). The substitute fluidizers did not adversely affect the steel produced in test operations.

Along with optimizing the efficiency of furnace operations, the Bureau is searching for ways to reduce the loss of strategic and critical metals during various phases of steelmaking and to reduce waste generation. This can be accomplished by recycling pickling solutions, wastes, and dusts. The Bureau has experimented with ion-selective membrane technology in developing a means to recycle acid solutions used during the pickling of stainless steels. Disposal of these acid solutions is costly to the steel manufacturing industry and results in the loss of valuable chromium and nickel. Preliminary research has revealed that an electrodialysis cell using ion-selective membranes does have the potential for separating dissolved metals from spent pickling acid solutions while regenerating the acids for return to the pickling process. Through other research studies, the Bureau has developed a process permitting in-plant recovery of about 90 pct of the chromium, molybdenum, nickel, and iron from stainless steelmaking dusts and wastes. By using yet another Bureau-developed process, zinc extracted from electric arc furnace dust can be used for electrogalvanizing.

Detailed accounts of the laboratory tests and results for each of these research studies are presented in this report. The report also provides a description of other studies conducted including an economic analysis of the technique to pelletize flue dusts and other waste resulting from steel manufacture in order to recover contained metals.

IMPROVED ARC STABILITY IN ELECTRIC ARC FURNACE STEELMAKING

By Thomas L. Ochs[1] and Alan D. Hartman[2]

ABSTRACT

In order to improve the performance of electric arc furnaces used to manufacture steel, the Bureau of Mines is studying the fundamental behavior of the electric arc in the electric arc furnace. Improvements in control and processes will allow more efficient and quieter operation of the electric furnaces. Presently, electrical disturbances caused by the unpredictable arc are responsible for flicker and surges on the power grid and sound levels in excess of 120 dB in the vicinity of the furnace. It is these disturbances that the Bureau is investigating.

In the Bureau experiments, electrical signals are sampled at 50,000 Hz and photographs of the arc are taken at up to 40,000 images per second using high-speed cinematography. These images are then correlated with the electrical signals to study the physical events in the arc plasma. Arcs studied to date indicate that the electrical waveforms have unique signatures preceding some voltage excursions. Initial Bureau investigations indicate that mathematical techniques of analysis in the field of nonlinear dynamics have characteristics that enable these methods to speed up processing of the electrical signals from the arc for use as control parameters.

The behavior of the arc in the experimental environment has led to the conclusion that there are new furnace design changes and operating procedures possible. The potential areas for change include the furnace shell geometry, continuous feeding methods, electromagnetic pumping of molten metal, electrical control, furnace atmosphere, waste heat recovery, and electrode design. These changes could greatly increase efficiency, which is typically in the 60-pct range, improve furnace operation, and reduce noise. Interactions of these changes are complicated and must be considered together.

INTRODUCTION

The share of steel produced by electric arc furnaces has increased over the past 20 yr because of the flexibility of the minimill concept and the consequent reduction in costs to produce steel in the environment of rapidly fluctuating demand. There have been many changes in the arc furnace over the past 30 yr of use, including ladle metallurgy, ultrahigh power operation, water jacket cooling, oxyfuel burners, and scrap preheating. Control of the furnaces, however, has remained a initiative process based on the prior experience of the furnace manufacturer and the operator. This is because the high-current arcs used in electric arc furnace steelmaking are violent high-temperature conducting plasmas and have proven very difficult to understand over the past 100 yr of study. Because of this limited knowledge, the arcs are difficult to control (*1*, pp. 15–16, *2*).[3] Currents of 100,000 A are common in commercial arc furnaces. These currents can produce temperatures in the core of the arc of 12,000 to 15,000 K, which is more than twice as hot as the surface of the Sun.

Although these arcs have been used in smelting and melting metals since the turn of the century, the fundamental processes taking place inside the arc and at the points where the arcs attach to the electrodes and the charge are poorly understood. Disruptions of these high-current arcs during operation can produce fluctuations on the power grid *(3)*, ablation of the furnace refractory, and poor heat transfer to the melt. At the present time, control of the furnace is based on the experience of the operators and the control manufacturers, not on any fundamental understanding of the processes taking place in the arc. Presently, control systems react to reverse a past event *(2)* as opposed to acting to prevent a future event.

Prevention of future events is possible only if the future situation is predictable, based upon the past events. However, arc behavior presently is unpredictable. New methods of examining the signals available from the voltage and current waveforms in the transformer secondary circuitry, and therefore in the arc itself, may be able to supply unique signatures useful over the span of a wavelength for indicating disruptive events. If the arc and its interactions with the furnace interior were better understood, then there could be improved control methods or modified equipment designs that would result in gains in efficiency and a reduction of disruptive electrical and acoustical noise.

[1] Mechanical engineer.
[2] Chemical engineer.
Albany Research Center, Bureau of Mines, Albany, OR.

[3] Italic numbers in parentheses refer to items in the list of references at the end of this paper.

The electric arcs studied in the Bureau investigations have shown deterministic behavior that is sensitive to the conditions of operation. Extreme sensitivity to operating conditions leads to a lack of predictability of the arc behavior since the furnace operating conditions cannot be measured exactly. This unpredictable arc behavior has been characterized as stochastic, or random, in prior studies, but instead is indicative of chaotic behavior resulting from nonlinear interactions. Viewing the arc as a chaotic, deterministic system of discrete events, it is possible to look at electrical waveforms and expect short-term precursors (half-cycle) to the seemingly random events. Short-term precursors indicate the possibility of anticipation and control of arc disruption. It is disruption of the arc while it is carrying a high current that causes both electrical and acoustical noise.

From these investigations, it is becoming clear that traditional transform methods of analysis and statistical analysis of the electrical waveforms are of limited use. These methods are normally used on smooth waveforms or waveforms with a small number of periodic discrete events. The waveforms that were obtained in this research are composed of many nonperiodic discrete events on distorted square and sine waves. These discrete events must be treated using discrete digital methods.

STOCHASTIC VERSUS CHAOTIC BEHAVIOR

The electric arc has been described as a random, or stochastic, system, with events taking place at unpredictable intervals. The present investigation shows that the arc is not a stochastic system, but rather a nonlinear system that is very sensitive to initial conditions. This sensitivity gives the appearance of random behavior since the internal conditions cannot be measured closely enough to predict the next operational state of the arc *(4–5)*. Behavior of these nonlinear chaotic systems is not possible to predict for any length of time from a mathematical solution based on measured system conditions. Instead, the system can be treated using the methods of nonlinear dynamics. Using these techniques, there is the possibility of short-term (one ac cycle) prediction of future events based upon the inferred conditions as deduced from the signature analysis of the real-time waveforms.

The basic premise of this method of predictive control is that the system is mathematically well behaved (continuous and single valued), and over a short term (one cycle) the arc behavior can be predicted. Over the long term (longer than a cycle), the minor variations in operating conditions that cannot be measured will produce unpredictable behavior even though the system is deterministic. This means that the control system must take real-time data of the arc waveforms, compare it against a library of waveform signatures, and make decisions in a short time frame, typically about a quarter-cycle (4 ms). Recent increases in computational capabilities and decreases in cost have made data analysis and system control of the type described feasible.

EQUIPMENT

An experimental 200-lb-capacity single-phase electric arc furnace was used for conducting the experiments. The furnace used two 3-in-diam graphite electrodes. The power was supplied by two single-phase ac welders connected in parallel. Each welder was rated at 1,500-A current and had a rated full-load voltage of 40 V. The primary rating was 440 V and 170 A single-phase.

The furnace was modified in order to simplify the data analysis. Three types of arc targets were used in the furnace. The arc target block materials were graphite, steel, and copper. These blocks were used to study different system configurations and obtain calorimetric data. The calorimetric data are for assessment of heat transfer rates and efficiency. Initially, electrical signals in the single-phase furnace were taken across both arcs, one from each of the electrodes. In this configuration, the two arcs consisted of one with the electrode acting as the cathode and one with the electrode acting as the anode. This averaged the events attributable to each arc and made data analysis difficult. Therefore, a simplifying modification was made to the experimental system. This consisted of threading one of the electrodes into the conductive target block (fig. 1). Threading the electrode into the block eliminated one of the arcs and its associated signals, while it maintained the current path that normally would be taken by the current flowing through the arc. This made the magnetic field in the furnace similar to that present in the two-arc system.

The second modification to the experimental furnace involved replacing the furnace shell with an airtight enclosure. By using this enclosure, the atmosphere within the furnace could be controlled (fig. 2). This allowed experimentation to be conducted with gases other than air, as well as gas injection through the electrode.

A third modification was the addition of two viewports at 90° to each other (fig. 3). Thus two perpendicular images of the arc could be captured simultaneously by a high-speed motion picture camera. The two images of the arc were directed into the lens of a high-speed camera by the use of mirrors. The camera used 450-ft rolls of 16-mm film and operated at up to 11,000 frames per second. The actual image capture can take place at up to 44,000 image pairs per second, which was accomplished by using the camera's internal prism to divide a frame into quarters (fig. 4). After 200 ft of film had been exposed, allowing the camera to reach maximum speed, a waveform analyzer was triggered that recorded the simultaneous voltage and current electrical signals corresponding with the film images. Synchronization between the waveforms and the film is achieved by the use of timing pulses on the film. The waveforms were digitized at 50 kHz per channel.

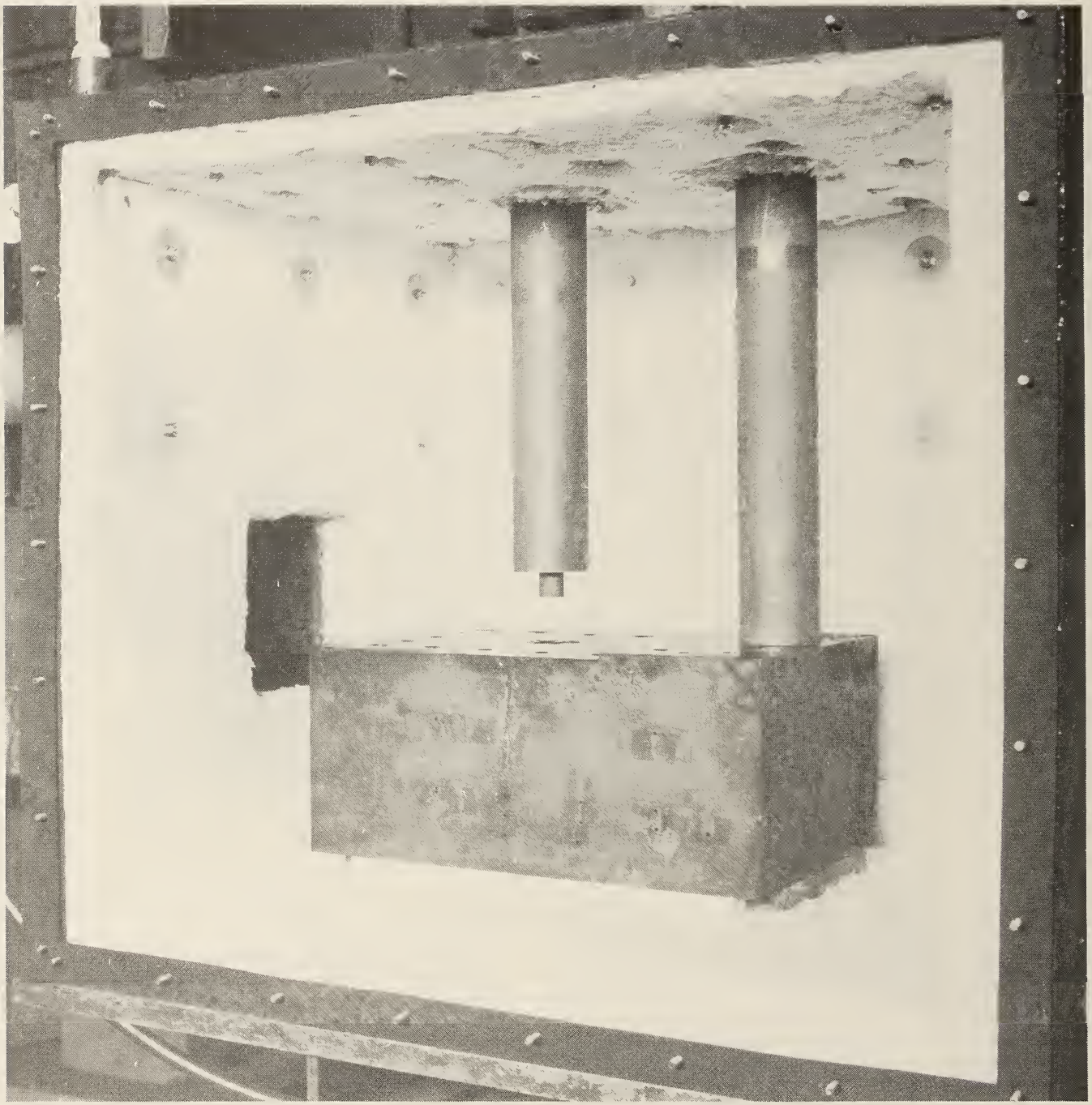

Figure 1.—Electrode threaded into target block to simplify target path.

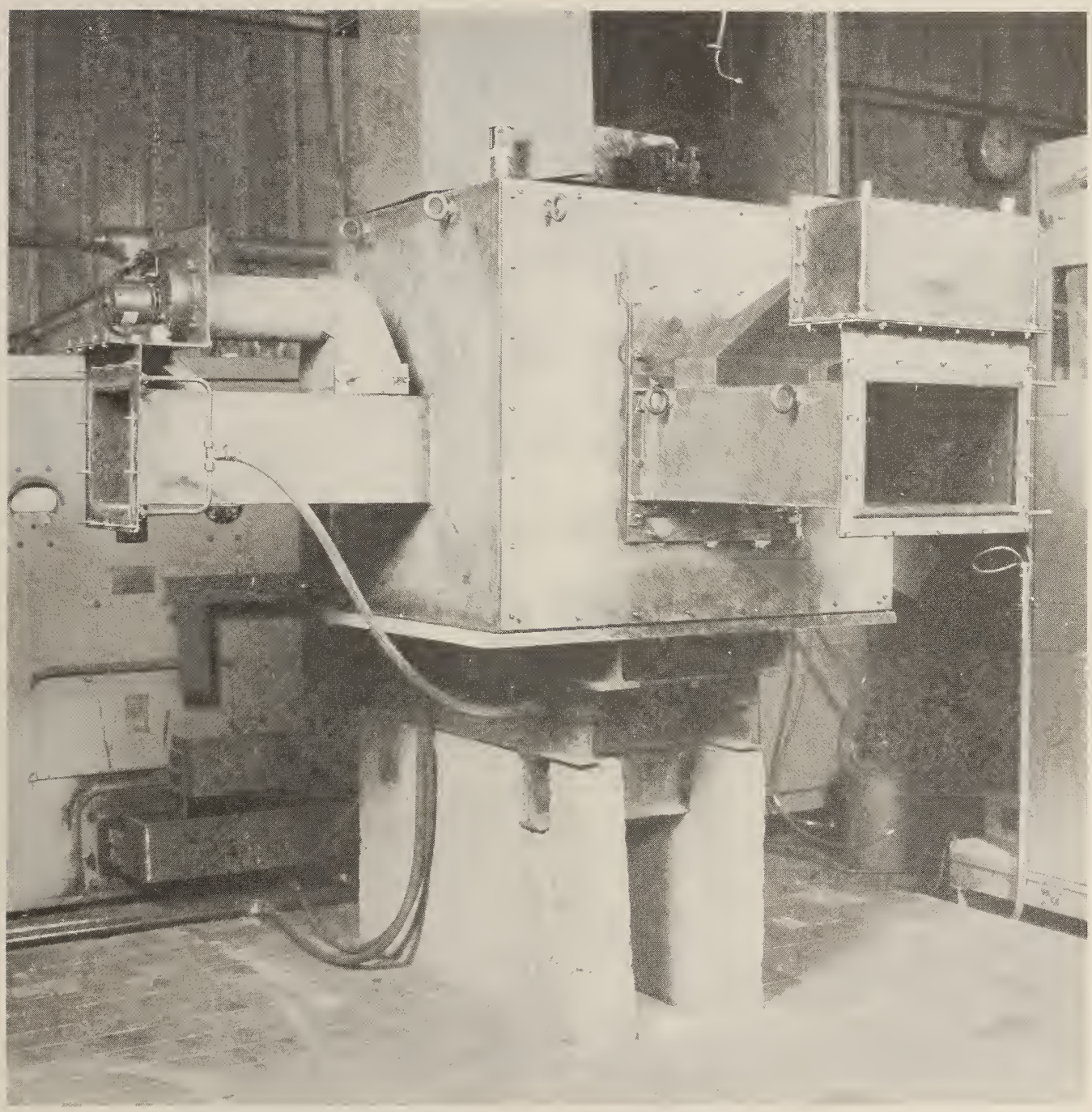

Figure 2.—Experimental furnace shell showing gas inlets.

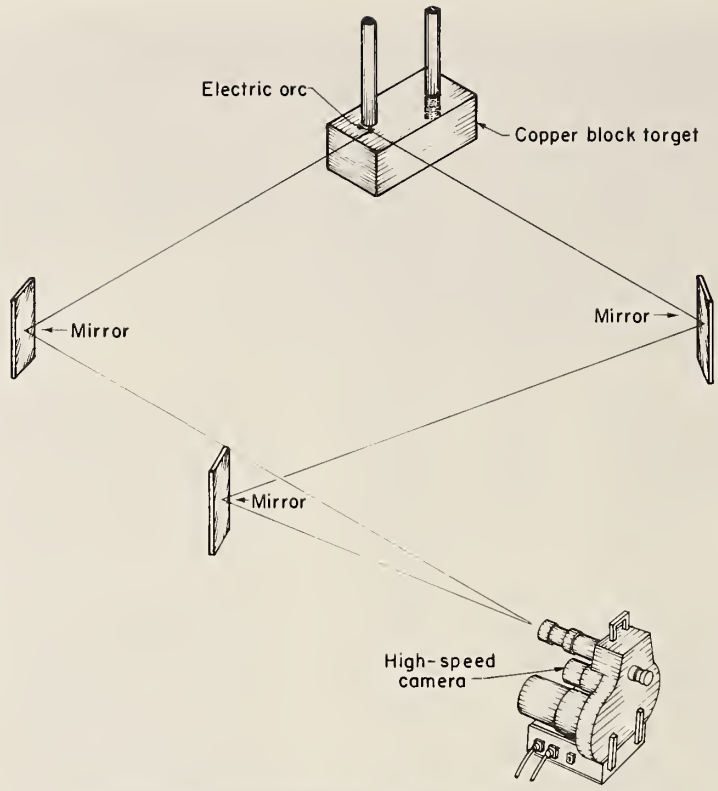

Figure 3.—Orthogonal views by use of mirror system.

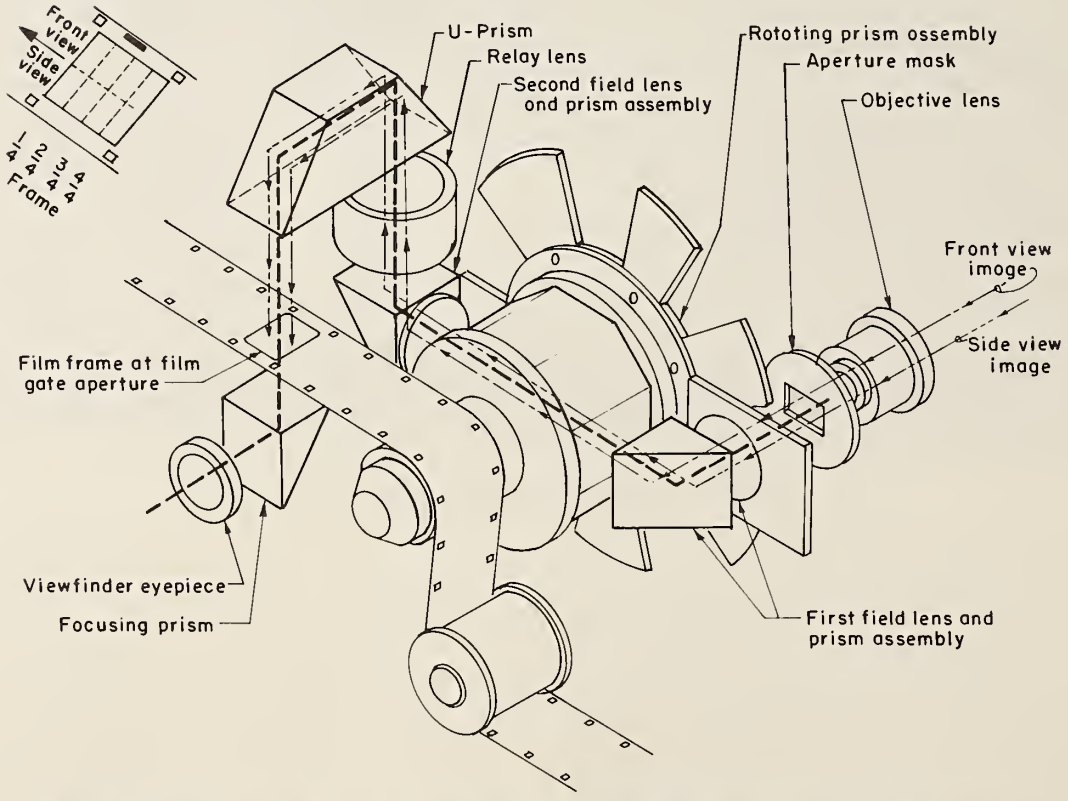

Figure 4.—View of single frame showing eight images and their relationship to original image.

EXPERIMENTAL PROCEDURE AND RESULTS

Areas investigated by the Bureau include (1) electrode tip design, (2) inert gas injection, and (3) arc analysis. Electrode tip design was investigated since the structure of the electrode providing the arc has been related to the unsteadiness of arcs *(6)*.

ELECTRODE TIP DESIGN

Electrodes providing a concave tip were found to reduce arc flare and maintain the arc under the electrode tip *(7)*. In reference 7, the author described attempts to reproduce this effect by testing hollow versus solid electrodes. Although the hollow electrodes increased the heating efficiency of the test furnace by approximately 10 pct over solid electrodes, the hollow electrode consumption was 2 to 10 pct above that of the solid electrodes. In order to improve energy efficiency while reducing electrode consumption, the Bureau designed alternative electrode tips. A basic electrode tip design used in the Bureau's research was a 1-in-diam tip machined onto the end of the 3-in-diam electrode (fig. 5). The theory behind this tip design is that the arcing between the workpiece in the furnace and the electrode will remain concentrated onto the 1-in-diam tip. The tip will become heated while the remaining 3-in-diam section of the electrode will remain relatively cool. This phenomenon was demonstrated in the high-speed films of the arc since the tip glowed white hot while the remaining, larger diameter electrode section surface remained black.

By making the smaller diameter electrode tip section an expendable section, the larger outer section of the electrode could become a semipermanent structure, thus reducing the amount of graphite needed for arcing (fig. 6).

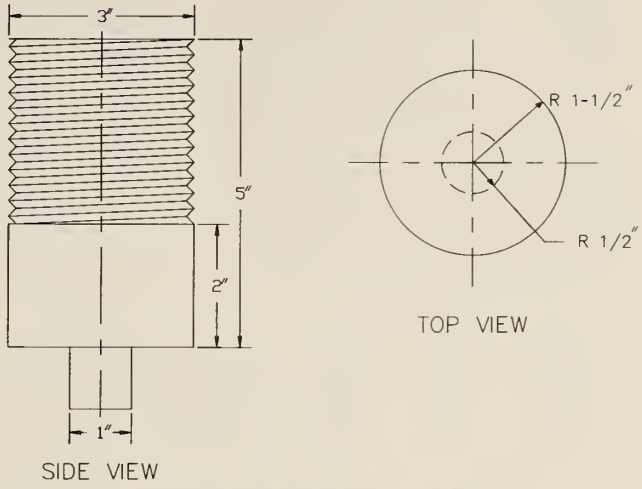

Figure 5.—Button electrode tip.

INERT GAS INJECTION

Inert gas injection was investigated to decrease electrode consumption by replacing the oxidizing atmosphere with an inert atmosphere. The inert gas was introduced into the furnace at three locations, through each viewport and also through the arcing electrode. Holes 1/32 in. in diameter on a 1-in-diam circle encompassing the electrode tip were used to introduce the gas (fig. 7). The gas from the 15 exit holes shrouded the arc and maintained it in a vertical direction, thus allowing more of the heat to be directed to the melt. The gas also helped to confine the arc to the tip section while it cooled the outer portion of the electrode, again decreasing electrode consumption.

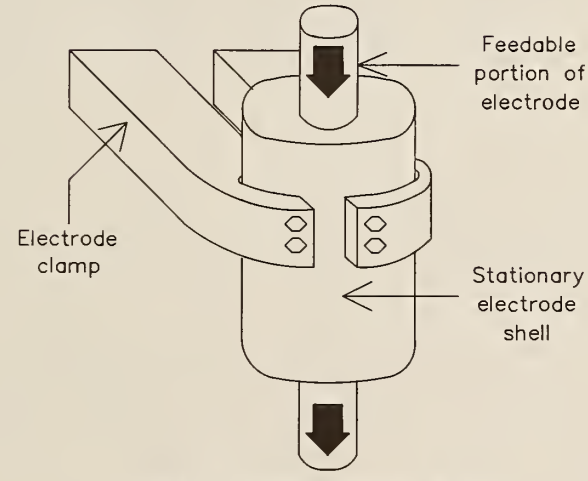

Figure 6.—Center feed electrode tip.

ARC ANALYSIS

Electrical waveforms of voltage and current were monitored across the arc with a waveform analyzer. The waveforms differed markedly depending upon the target composition. The differences between arc waveforms when using graphite, steel, and copper targets, are easily visible (fig. 8). These differences are expected since the thermal and electronic properties, such as the melting point and the amount of energy needed to free an electron from the surface of a material, vary dramatically from material to material. Figure 8 shows the voltage as a solid line and the current as a dashed line. The spikes on the voltage waveforms corresponded to the movement of the arc as seen in the high-speed films. In figure 8 (top), the positive and negative half-cycles have roughly the same absolute amplitude because the arc occurred between a graphite electrode and a graphite target. However, in the center and bottom

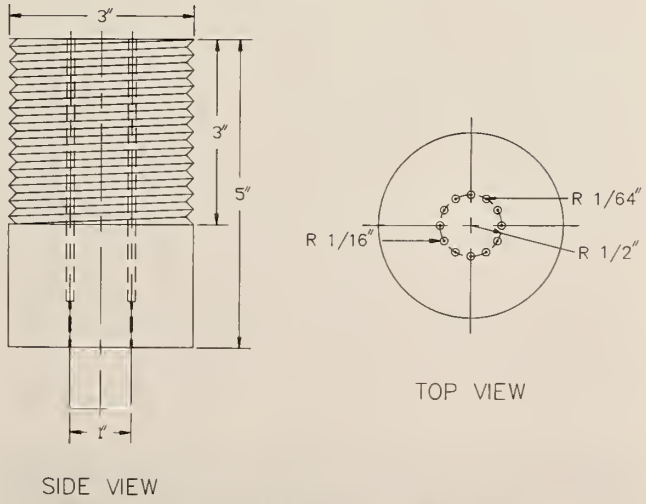

Figure 7.—Button electrode tip with gas injection.

panels of figure 8, the positive and negative half-cycle amplitudes show asymmetry owing to arcing between a graphite electrode and steel or copper, respectively. This asymmetry is due to the ability of graphite to emit electrons thermionically, whereas metals melt before thermionic emission occurs. In each of the waveforms, the electrode is acting as the anode in the positive half-cycles.

Waveforms and the corresponding high-speed films were analyzed together to identify the arc characteristics that were associated with the millisecond events on the waveforms. An example is shown in figure 9. In this case, the furnace atmosphere was 100 pct Ar and the arc was between a graphite electrode and a copper block. In the figure, voltage is the solid waveform and current is the dashed waveform. Positive half-cycles 1 and 3 are at a relatively low voltage as compared to positive half-cycles 2 and 4. Half-cycles 1 and 3 could be matched to short arcs between the graphite tip and copper block as the arc target, whereas half-cycles 2 and 4 correspond to long arcs on the film that were between the 3-in-diam section of the electrode and the copper block arc target.

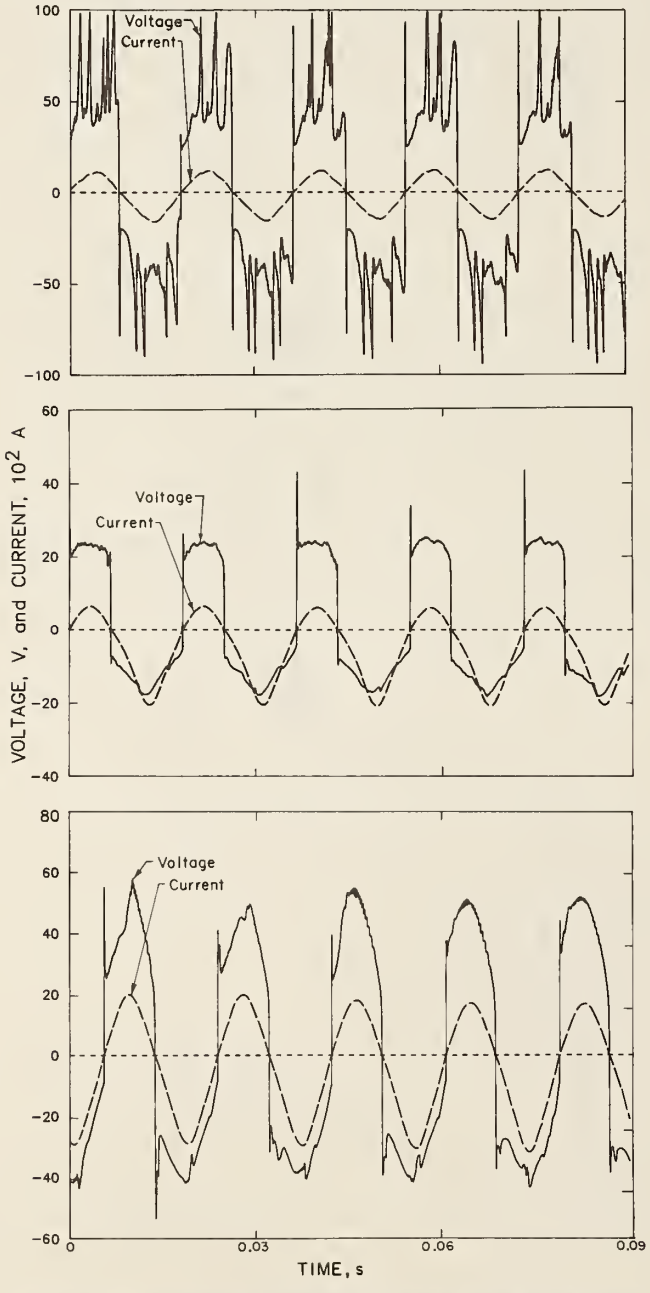

Figure 8.—Waveform of voltage and current for arc from graphite electrode to graphite (top), steel (center), and copper (bottom) target in 90-pct-He, 10-pct-Ar atmosphere.

Many shorter term discrete events of much less than a half-cycle duration have been identified in both voltage and current waveforms. In figure 10, four major events on a single-cycle voltage waveform have been correlated with the arc movement in the high-speed films. These events took place in a 90-pct-He, 10-pct-Ar atmosphere. Event A, which is a positive voltage spike, corresponded to the arc changing positions from arcing a short distance from the electrode tip, to arcing a longer distance, between the 3-in-diam section of the graphite electrode and the copper block as the arc target. The maximum voltage for event A was 53 V and occurred as the arc developed into the long arc column as depicted in sequence A of figure 10. Event B, on the positive side, showed that the rapid fluctuation of the voltage related to a long arc decreasing to a short arc on the tip section of the electrode and then back again to a long arc for each fluctuation. Event C, termed a shark's tooth, on the negative half-cycle could be related to the arc's movement across the tip section in a right-to-left motion, and finally event D was the opposite motion of the arc moving from the left to the right side on the electrode tip section.

A similar experiment with an atmosphere of 90 pct He-10 pct Ar produced the arc motions as shown in figure 11. Five areas are related to the arc's movement in the high-speed films. Area 1 related to a short arc rotating directly beneath the electrode's tip. Area 2 showed the gradual movement of a long arc, between the 3-in-diam graphite electrode and copper block, from the tip to the outer edge of the electrode. Area 3 is a short, very stationary arc on the negative half-cycle of the voltage waveform. Area 4 was correlated with the quick movement of the short arc from the left side to the right side on the tip. Area 5 was a rotating short arc directly beneath the electrode tip.

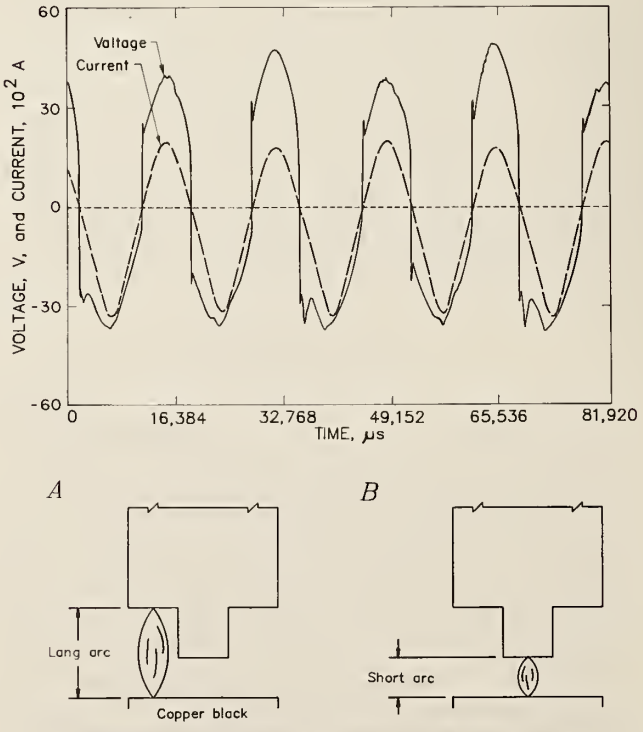

Figure 9.—Waveform. *A*, Long arc; *B*, short arc.

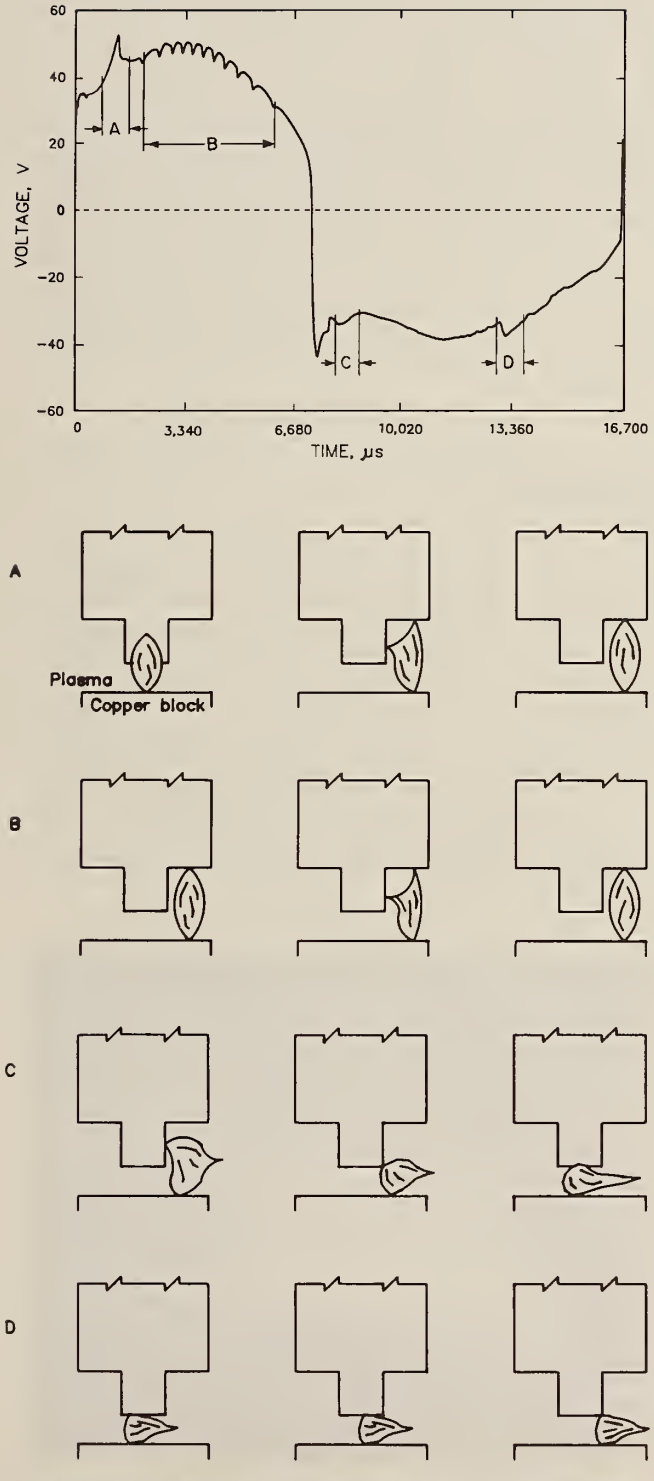

Figure 10.—One cycle with discrete events (A–D) delineated and diagramed.

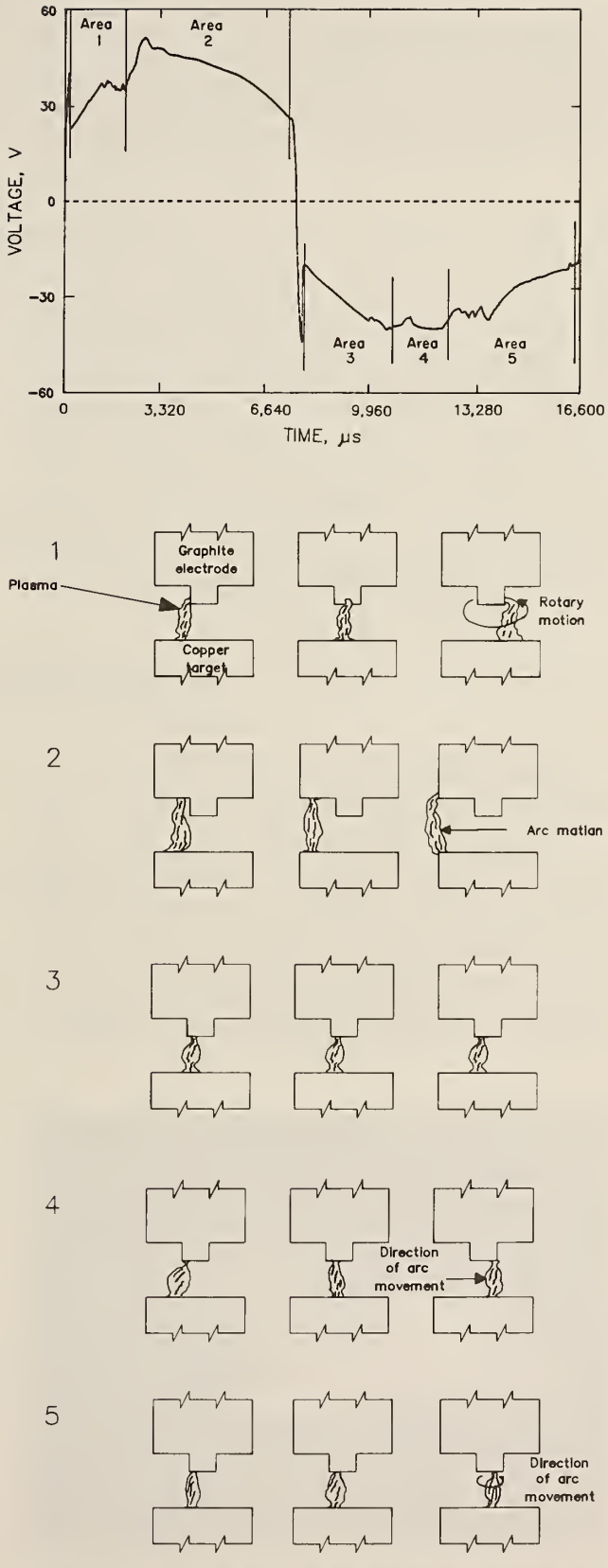

Figure 11.—One cycle with five discrete areas delineated and diagramed. 1, rotating, short arc; 2, arc moving right to left, arcing between 3-in-diam section and copper block; 3, very stationary arc; 4, arc movement; 5, rotating arc under tip.

Image analysis is being used to help define the arc's core within the plasma shown on the high-speed film frames. The arc structure is difficult to resolve because of the high luminosity that tends to saturate photographic emulsions, producing a seemingly white arc. Image analysis is helping to resolve the inner structure by digitally filtering the images to reconstruct the actual radiant intensity gradients. From these intensity gradients, the electron paths can be used to relate arc parameters to the resistance of the arc. For instance, image analysis is used to map areas of highest light intensity so that an arc path of conduction can be defined. By using this technique it has been possible to measure an arc length (fig. 12).

SYSTEM INTERACTION

The occurrence of a break in the arc at high current or the shorting of scrap to the electrode is responsible for electrode breakage, increased melt times, and voltage spikes that can damage electrical equipment, cause flicker on the electric power grid, and cause excessive noise. The identified events that cause these disruptions of the furnace arc are related to motion of the arc, scrap, electrodes, and/or magnetic fields, as seen in the Bureau experiments. When methods of stabilizing the arc in the furnace environment are considered, it is necessary to consider all of the interactions between the furnace variables, such as slag composition, atmosphere composition, type of scrap, temperature of the melt, composition of the electrodes, electrode geometry, and control methods. Early in this investigation, it became clear that there is a synergistic relationship between the variables in the furnace interior that is a direct result of the nonlinear relationships of the coupled magnetohydrodynamic equations governing the electric arc behavior. Because of this interactive behavior, it is not possible to change one variable without affecting the other furnace variables. Presently, most of the important parameters in the electric furnace are allowed to float at whatever value they may take. For example, there is no mechanism to control furnace atmosphere composition, instantaneous voltage, or geometry of the electrodes. These variables have been shown in experimentation to be very important for arc operation.

ATMOSPHERE CONTROL

One of the most influential variables in the arc experiments is the furnace atmosphere. Diatomic molecules such as oxygen and nitrogen must be disassociated before they can be ionized, and therefore, they are more difficult to ionize than inert gases. If inert gases are used, then the electrode consumption is dramatically decreased since there is no oxygen or nitrogen to react with the graphite. These reactive diatomic gases also will react with the steel if they are present, and if they are absent, then the steel composition can be more closely controlled. The gases found to be most promising in this study are mixtures of helium and argon. These mixtures have good heat transfer properties and are easy to ionize.

It has also been indicated in the studies of the arc fluid dynamics that shrouding the arc in a flowing gas will help to stabilize the arc as in a plasma torch. This comes about by a combination of a thermal pinch (contraction of the arc due to cooling of the outer arc surface and a subsequent reduction in electrical conductivity, forcing the electron flow into the center of the arc), causing wall stabilization and actual fluid dynamic forces preventing the arc from migrating through the gas shroud (fig. 13). This indicates that properly engineered gas injection through the electrode would help to stabilize the arc. This plasma jet effect also will increase convective heat transfer to the melt, thereby increasing thermal efficiency. The nonreactive inert gases also will permit the use of a wide range of slags that cannot be used in the traditional air atmosphere, and the gas injection through the electrodes possibly could be used to introduce reductants as needed.

Figure 12.—Processed image (actual size) showing arc path between 3-in-diam section of graphite electrode (upper right-hand attachment point) and graphite block as the arc target (near bottom of 1-in button on electrode).

Figure 13.—Gas shroud around transferred arc showing forces tending to stabilize arc (actual size).

CONTROL SYSTEM

A computerized control system could be operated by using a data base of historical waveform information and pattern matching information to determine the real-time furnace operating conditions. Using the data such as voltage and current waveforms, atmosphere composition, feed material, and slag type, the control system could adjust the furnace operating conditions for optimal performance. The adjustments would include variables such as atmosphere composition, feed rate, feed composition, voltage, gas injection rate, magnetic stirring, and electrode position. These adjustments could be made at rates that depend on the parameter being adjusted. For instance, if the parameter is voltage, then the adjustments must be made in the course of a half-cycle (8 ms). On the other hand, if the parameter is feed material, then the adjustment will be allowed to take place over a period of minutes. For indicators of a catastrophic disruption such as breaking of the arc during high-current conditions, the most simple control strategy would be to turn the current off at a zero current crossing, then position the electrodes to restart seconds later. More complex control would involve electronic tap changing and electrode control to maintain the arc under adverse conditions. This would prevent disruption at high current.

The type of system best suited to this process of decisionmaking based on data and experience is an expert system. The system could maintain a knowledge base of waveforms and past experience. Over a period of time, the system can be customized to the individual furnace it operates on by logging any uncataloged events and the corresponding results so that future decisions could be made based on this experience. These expert systems are beginning to be seen throughout industry. Adaptive expert systems are now being developed and within the next few years will be commercially available.

SUMMARY

A new perspective is available for investigation of electric arc behavior through the use of high-speed motion pictures and synchronized electrical waveforms. Analysis of the seemingly random occurrences in the arc on an event-by-event basis shows that the arc is deterministic and hence theoretically controllable. High-speed computers now make it possible to economically control factors such as transformer tap settings, furnace atmosphere, and electrode positions. These control factors coupled with new electrode geometry can improve efficiency and yield while stabilizing the electric arc.

New ways have been developed for investigating electric arc behavior through the use of high-speed motion pictures synchronized with electrical waveform data.

REFERENCES

1. Ochs, T. L., A. D. Hartman, and S. L. Witkowski. Waveform Analysis of Electric Furnace Arcs as a Diagnostic Tool. BuMines RI 9029, 1986, 19 pp.

2. Paschkis, M. E., and J. Persson. Open-Arc Furnaces. Ch. in Industrial Electric Furnaces and Appliances. Interscience, 2d ed., 1960, pp. 179–228.

3. Schwabe, W. E. Arc Furnace Power Delivery Scoping Study. Electric Power Res. Inst., Palo Alto, CA, EPRI RP-1201-24, 1982, 146 pp.

4. Abraham, R. H., and C. D. Shaw. Chaotic Behavior. Part 2 of Dynamics, The Geometry of Behavior. Aerial Press Inc., Santa Cruz, CA, 1983, pp. 99–105.

5. Crutchfield, J. P., J. D. Farmer, N. H. Packard, and R. S. Shaw. Chaos. Sci. Am., v. 255, No. 6, 1986, pp. 46–57.

6. Schwabe, W. E. Lighting Flicker Caused by Electric Arc Furnaces. Iron and Steel Eng., Aug. 1958, pp. 93–100.

7. _____. Experimental Results With Hollow Electrodes in Electric Steel Furnaces. Iron and Steel Eng., June 1957, pp. 84–92.

PREHEATING OF FERROUS SCRAP

By R. H. Nafziger[1] and G. W. Elger[2]

ABSTRACT

Energy conservation is an important consideration in all steelmaking operations. Energy consumption impacts on the productivity and costs of producing steel. Accordingly, the Bureau of Mines has evaluated the feasibility of preheating ferrous scrap charges in basic oxygen furnace (BOF) and electric furnace steelmaking operations to decrease energy consumption. Offgases generated during oxygen blowing of a molten charge in a ¼-st-capacity BOF were passed through a static bed of shredded auto scrap. Final bed temperatures ranged from 1,150° to 1,650° F. The thermal energy recovered can contribute up to 44 pct of the energy necessary to melt the scrap. Furnace offgases from a 1-st-capacity electric arc furnace were used to preheat continuously charged automotive scrap and metal stampings up to 1,110° F. Approximately 7 pct less electrical energy was used compared with that consumed in continuously charging cold scrap. Conventional backcharging techniques also were used for comparison purposes.

INTRODUCTION

In 1985, electric arc furnaces produced 34 pct or nearly 30 million st of raw steel in the United States *(1)*.[3] Most of the remainder (59 pct) was produced in BOF's. Electric furnace steelmaking operations use cold ferrous scrap nearly exclusively as charge materials, and a considerable amount of cold scrap is used by the BOF. Energy consumption is one of the primary concerns and a major cost in domestic steelmaking operations. For example, approximately 535 kW·h/st of steel produced is required in electric arc furnace steelmaking *(2)*. This represents approximately 1.8×10^6 Btu/st of steel. The fuel and electrical energy consumption in a BOF is approximately 0.9×10^6 Btu/st *(3)*. This represents 1.14×10^{14} Btu/yr consumed in domestic steelmaking. A 1-pct decrease would save 1.14×10^{12} Btu/yr or 334×10^6 kW·h/yr.

In both types of steelmaking operations, the Bureau is striving to increase the recycling of scrap. The BOF experiments were conducted to assess the feasibility of increasing the proportion of scrap used in the charge mixture. In addition, the use of hot offgases for preheating offers the potential of decreasing energy consumption and costs. The additional amount of scrap used could offset the limited availability of hot metal owing to blast furnace shutdowns, for example. The evaluation of preheated scrap in electric arc furnace steelmaking was aimed at promoting scrap use by making electric arc furnace steelmaking more competitive through decreased electrical energy consumption and costs. Early Bureau research involved the use of waste heat in electric arc furnace offgases to preheat prereduced iron ore pellets during continuous charging of the furnace *(4–5)*.

Others have discussed the preheating of scrap in BOF operations. Several methods have been described, including (1) in-vessel preheating, (2) separate vessel preheating with the thermal energy provided by oxygen-natural gas or oxygen-fuel oil burners *(6–7)*, and (3) waste gas preheating with the heat derived from offgases generated during oxygen blowing of the BOF charge *(8)*. In one application, natural gas-oxygen burners preheated scrap charges prior to the molten iron addition. Increased productivity and lower ingot costs were realized, but excessive scrap oxidation was noted *(9)*. In another study, increased scrap could be charged to a BOF when it was preheated to 1,700° F. This decreased lime and flux consumption, decreased slag volume, and decreased metal blowing time. However, refractory consumption was increased *(10)*.

Developments in preheating scrap charges for electric furnace steelmaking occurred as early as 30 yr ago. In nearly all cases, some means of external heating was used. Three techniques for preheating have been used. The first utilizes a special vessel for preheating. Typically, external fuel burners supplement the heat from the offgases used. After preheating, the scrap is transferred to a charging bucket prior to introduction into the furnace *(11)*. Considerable scrap handling, large space requirements, and high costs for the vessel pit are cited as disadvantages.

A second method involves placing the charge bucket into a preheating vessel. In this case, the scrap cannot be preheated to a high temperature, and there is more dust *(12)*. Variations in this technique involve the direction of hot furnace offgases to preheating stands or to a preheating chamber to heat the scrap in a charging bucket *(13–14)*.

In the third technique, a bucket lined with castable refractories serves as a preheating vessel and a charging bucket. Potential bucket distortion, dust losses, and a weight that requires a high crane capacity can cause problems with this method.

---

[1] Research supervisor.

[2] Research chemist.

Albany Research Center, Bureau of Mines, Albany, OR.

[3] Italic numbers in parentheses refer to items in the list of references at the end of this paper.

Oil burners either mounted in the charging bucket or in the furnace, natural gas lances, the use of charging buckets with louvers placed over hot billets or ingots, or the use of preheat chambers are additional preheating techniques that have been used *(15–22)*.

All of these techniques involve backcharging methods for feeding the furnace. Relatively high capital costs have precluded the adoption of fuel-fired preheaters. Other disadvantages include (1) distortion or warpage of the charging bucket doors, (2) uneven heat distribution within the charge, and (3) scrap oxidation.

Objectives of the Bureau research reported herein include (1) an evaluation of preheating BOF scrap charges using recovered hot offgases that are passed through a scrap bed in a separate chamber to eliminate oxygen-fuel preheating, and (2) a determination of the feasibility of continuously charging fragmented scrap into an electric arc furnace whereby the scrap is heated by countercurrent hot furnace offgases to realize decreased electrical energy requirements compared with those necessary in conventional backcharging tests.

BOF EXPERIMENTS

EXPERIMENTAL EQUIPMENT, MATERIALS, AND PROCEDURES

All of the tests were performed in a ¼-st capacity BOF, shown in figure 1. Offgases generated during oxygen blowing of the furnace charge were drawn through an adjacent preheat vessel by a blower located downstream from the preheater in the dust collecting system. The preheat vessel contained the scrap charge. A schematic diagram of the system is depicted in figure 2. Further details have been published previously *(23–24)*.

The furnace charge consisted of shredded automobile scrap having pieces no larger than 3 by 3 in, with a bulk density of 92 lb/ft^3.

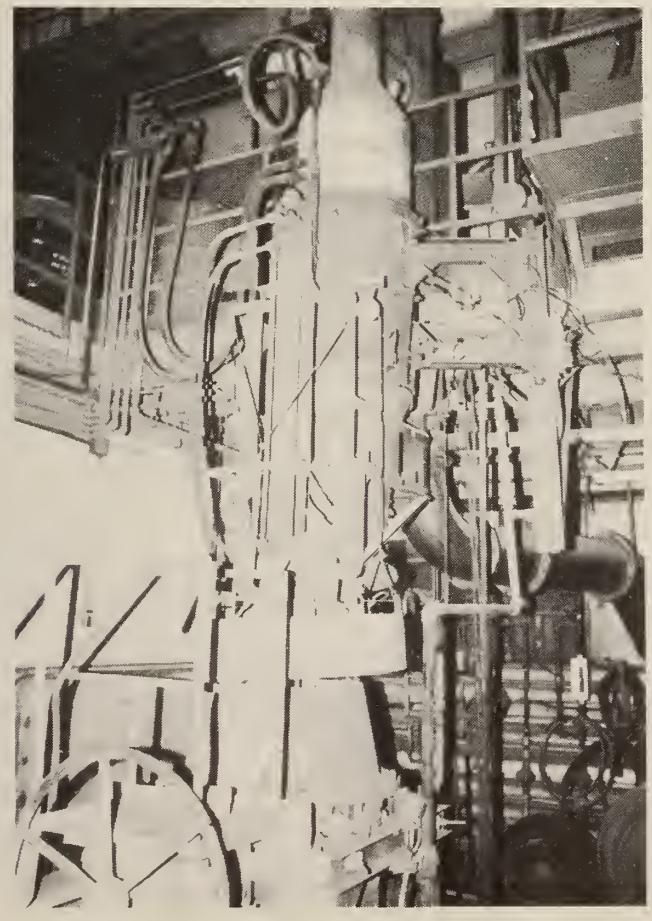

Figure 1.—Basic oxygen furnace and preheater system.

This material was fed into the preheat vessel prior to blowing the BOF metallic charge. After the blow, the heated scrap was used in the next test as a replacement for the normal cold scrap charge. Offgas flow was controlled by a manual slide damper located downstream from the preheater. The BOF charges contained 100 to 180 lb of preheated automobile scrap and 270 to 350 lb of molten pig

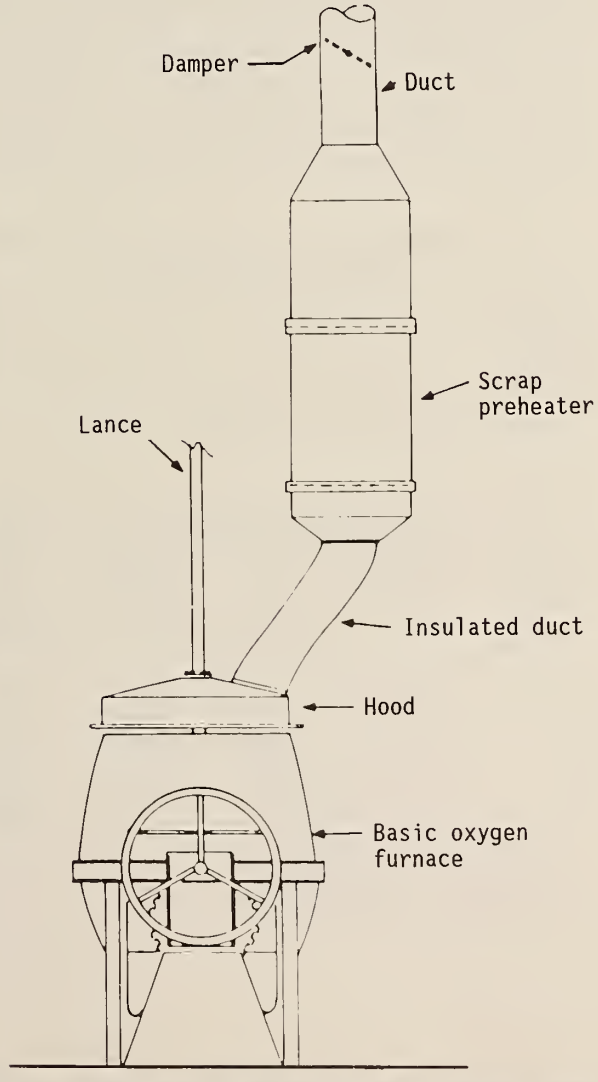

Figure 2.—Schematic diagram of the BOF-preheater system.

iron. Typical charge compositions are summarized in table 1 *(23–24)*.

After the preheated scrap-hot metal mixtures were charged, the oxygen lance was positioned, and blowing began after 25 lb of lime and 1 lb of fluorspar were added to the furnace. Oxygen blowing, at a fixed rate of 27 scfm, was terminated when visual observations of flame height and color indicated a carbon level of 0.10 pct. Blow times varied from 12 to 17 min and were dependent upon the quantity of scrap added.

RESULTS

An initial series of tests showed that cold scrap could constitute up to 28 pct of the charge. Cold scrap additions above this level resulted in a significantly lower oxygen efficiency and deteriorating furnace operations *(23–24)*.

A second series of experiments were conducted in which preheated scrap charged to the BOF ranged from 22 to 40 pct of the total charge. Data from these tests are shown in table 2. Average preheated scrap temperatures ranged from 1,050° to 1,650° F, with the lower amount of preheated scrap resulting in the highest scrap temperature. Scrap temperatures were dependent upon the quantity of scrap in the preheater and upon the length of the oxygen blowing period. With 40 pct preheated scrap, the average scrap temperature increased as a result of a significantly lengthened blow time with lower oxygen efficiency. At 1,650° F, sufficient heat is stored in the scrap to yield approximately 44 pct of the energy required for melting. Results indicated that a 40-pct preheated scrap charge was the maximum that could be tolerated by the Bureau's BOF to maintain satisfactory oxygen efficiency and sufficient metal temperature for tapping. Therefore, preheating the scrap increases scrap utilization from 28 pct of the charge to 40 pct, an increase of 43 pct. On the basis of these tests, 36 pct of preheated scrap appeared optimum with respect to final steel temperatures (≅3,000° F) and oxygen efficiency. Typical temperatures of preheater entrance and exit gases and scrap under these conditions are shown in figure 3 *(23–24)*.

Scrap preheating was enhanced by the oxidation of the CO, formed in the BOF, to CO_2 before reaching the preheater. This was caused by secondary air infiltration around the BOF hood. Significant scrap oxidation occurred only when scrap bed temperatures exceeded 1,800° F. A tighter fitting hood over the BOF would decrease the air infiltration and perhaps allow higher offgas inlet temperatures in the preheater without excessive scrap oxidation *(23–24)*. However, the heat content of the inlet gas would be lower and the scrap preheat temperature therefore would be lower.

Table 1.—Typical chemical analysis of BOF metallic charge and product, weight percent

Description	C	Cu	Mn	P	Si
Scrap	<0.1	0.12	0.062	0.011	0.32
Hot metal	4.0	.25	.80	.07	1.0
Steel[1]	0.12– .15	.21	≤.1	≤.01	≤.1

[1] Steel product from 33-pct scrap addition.

Table 2.—Average temperature and heat recovery values of preheater scrap charges

Preheated scrap, pct of BOF charge	Av scrap temp, °F	Heat content,[1] Btu/(lb•mol)	Total heat recovered, Btu	Heat recovered, pct required for melting[2]
22	1,650	14,240	25,500	44
27	1,265	9,770	21,000	30
29	1,175	8,630	20,100	27
33	1,045	7,330	19,700	23
36	1,050	7,380	21,100	23
40	1,150	8,380	27,000	26

[1] From BuMines B 476, 1949, p. 85.

[2] Calculated = $\frac{\text{Heat content, Btu/(lb•mol)}}{\text{32,130 Btu/(lb•mol)}} \times 100$.
(Denominator is the heat content of steel at 2,786° F.)

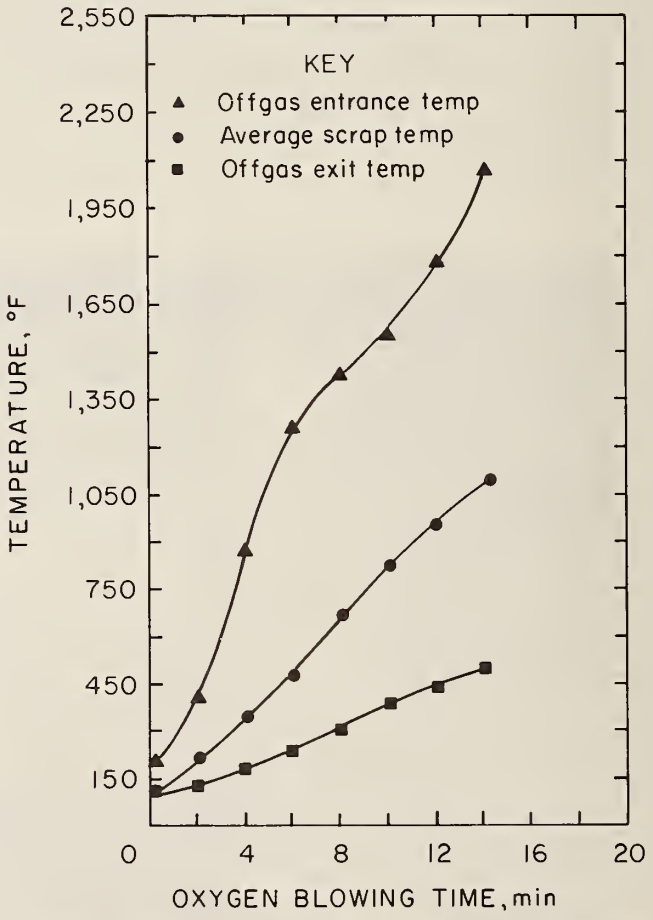

Figure 3.—Effect of oxygen blowing time on preheater offgas and scrap temperatures. Charge condition: BOF = 160 lb scrap + 290 lb hot metal, preheater = 160 lb scrap.

ELECTRIC ARC FURNACE EXPERIMENTS

EXPERIMENTAL EQUIPMENT, MATERIALS, AND PROCEDURES

All tests were conducted in a conventional electric arc steelmaking furnace of 1-st capacity, lined with a basic brick and covered with a rammed-alumina roof, as shown in figure 4. The electrical energy was provided by a 1,200-kV·A transformer through three 4-in-diam graphite electrodes. A stainless steel chute was attached to the furnace. At the opposite end of the chute was a rotating feeder-preheater that consisted of six 12-in-diam sections of stainless steel tubing connected at 90° to each other in a zigzag fashion. Figure 5 shows a schematic diagram of the furnace, scrap feeder-preheater, and furnace offgas ductwork, including gas sampling location and dust removal units. In use, the charge was fed through the chute and preheater, with the hot exhaust gases passing through the preheater **(3)**[4] countercurrent to the direction of the charge, thereby heating the charge and cooling the gases.

The offgases exited directly into a long vertical section of duct that assisted in the removal of those smaller sized dust particles escaping a stainless steel cyclone. The gases then were directed horizontally to a second cyclone **(1)** and an adjacent baghouse for final cleaning before being exhausted to the atmosphere. Gas and particulate samples were taken in this horizontal section **(2)**. This furnace has been described previously in more detail *(5, 25)*. The components in the sampling train for particulate stack sampling, shown in figure 6, included the probe with attached nozzle **(1)**, a particulate filter **(4)**, a cooling and/or gas collector with four impingers **(5)**, flow-measurement devices, and a vacuum pump **(13)**. Other components shown in figure 6 include a cyclone **(2)**, flask **(3)**, thermometers **(6)**, check valve **(7)** connecting cord **(8)**, vacuum gauge **(9)**, coarse adjust valve **(10)**, fine adjust valve **(11)**, oiler **(12)**, filter **(14)**, dry-gas meter **(15)**, orifice tube **(16)**, incline manometer **(17)**, solenoid valves **(18)**, pitot **(19)** thermocouple **(20)** and temperature recorder **(21)**. This equipment and the procedures used for gas sampling also have been described in more detail previously *(25)*.

The shredded scrap used for these tests was purchased from a local scrap processor and consisted of three separate batches, each purchased at a different time and with a different composition. The metal stampings used in the charges were purchased from the same source. Only pieces of scrap with largest dimensions of less than 4 in were used. The chemical analyses of these materials are shown in table 3. The analyses were obtained by a direct-reading spectrograph for cast samples melted in separate 800-lb wash heats without quartz and lime additions to provide a slag cover. Scrap meltdown without a slag cover was conducted to keep the aluminum in the metal phase rather than transfer that constituent to the slag phase.

[4] Bold numbers in parentheses refer to components identified in illustrations.

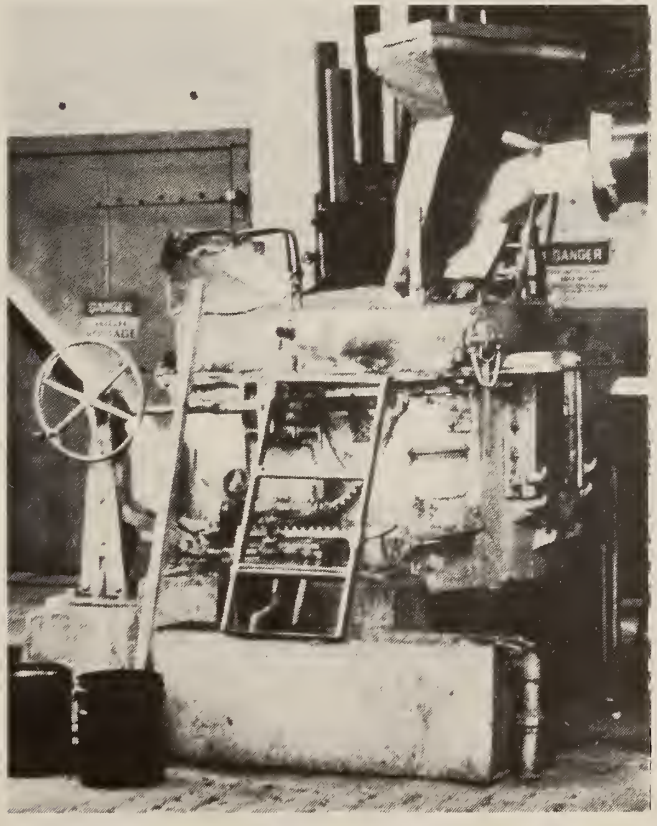

Figure 4.—One-short ton electric arc furnace and feeder-preheater used for steelmaking tests.

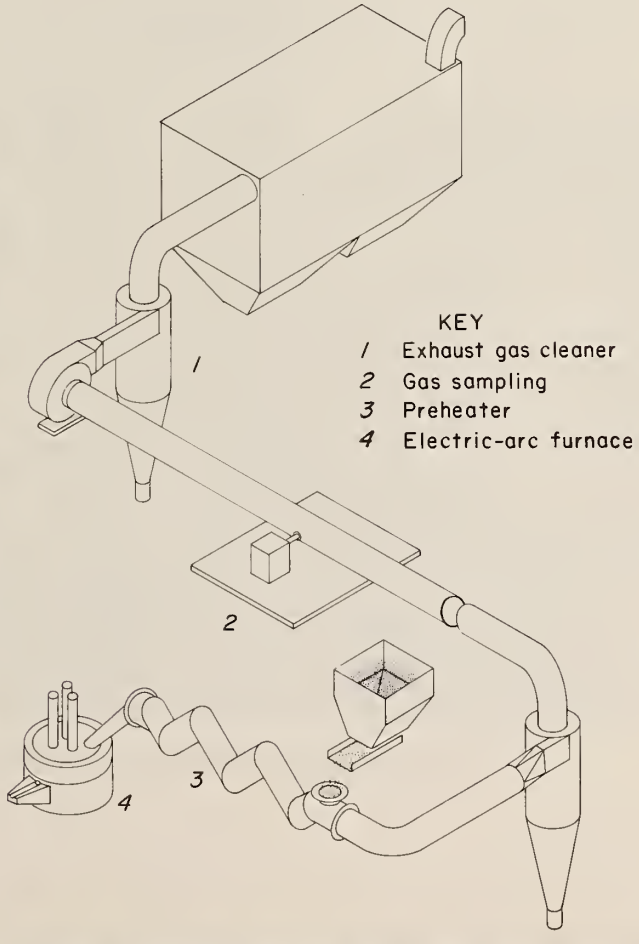

Figure 5.—Schematic diagram of electric arc furnace, feeder-preheater, and offgas ductwork (not to scale).

Table 3.—Chemical composition of shredded automotive scrap[1] and metal stampings used in three types of scrap charging tests in an electric arc furnace, weight percent

	Batch 1	Batch 2	Batch 3		Stampings
			Large	Small	
Al	0.46	0.83	NA	2.15	0.046
C	.41	.56	0.051	1.66	.67
Cr	.16	.40	.050	.47	.49
Cu	.18	.81	.20	1.18	.087
Fe	98.5	95.7	99.5	91.5	97.2
Mn	.12	.43	.036	.69	.41
Ni	.17	.30	.11	.31	.70
P	.008	.034	.011	.070	.013
S	.030	.045	.037	.048	.008
Si	<.01	.85	.011	1.86	.26
Sn	NA	.019	.009	.037	.005
Ti	NA	<.01	<.01	<.01	.003

NA Not analyzed.

[1] Pb and Zn contents of the scrap samples were not analyzed since these constituents volatilized from the furnace during charge meltdown and were recovered in the dust product.

For all tests, the furnace was preheated, and the initial charge of 450 lb of shredded auto scrap, metallurgical coke reductant, and slag formers (pebble lime and quartz) was topcharged to the furnace by means of a charging bucket. After the initial charge was melted, continuous feeding commenced. For the tests in which cold scrap was continuously charged, the feed material was fed into an opening in the side of the feed chute between the furnace and the preheater, as shown in figure 7. The cold scrap to be preheated was fed directly into the preheater shown in figure 8. Preheated scrap temperatures were calculated from data obtained by taking samples of scrap as they entered the furnace from the preheater and immediately immersing the samples into a measured amount of water.

During the backcharging tests, only a portion of the initial 450-lb charge was melted. At that point, the furnace roof was swung aside, and the first backcharge, consisting of 675 lb of shredded scrap, was loaded as shown in figure 9. When this was melted sufficiently to allow another 675 lb of shredded scrap to be added, the same procedure was followed. The remainder of the test was identical to the continuously charged tests.

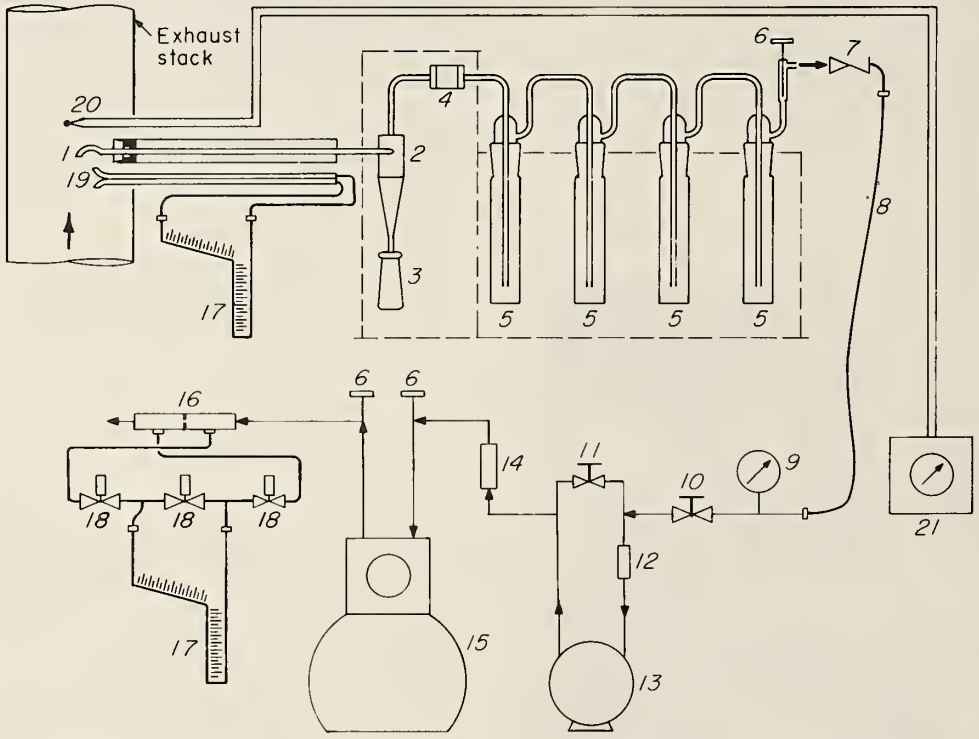

1 Probe *2* Cyclone *3* Flask *4* Particulate filter *5* Impingers *6* Thermometer *7* Check valve *8* Connecting card *9* Vacuum gage *10* Coarse adjust valve *11* Fine adjust valve *12* Oiler *13* Vacuum pump *14* Filter *15* Dry-gas meter *16* Orifice tube *17* Incline manometer *18* Solenoid valves *19* Pitot *20* Thermocouple *21* Temperature recorder

Figure 6.—Schematic diagram of apparatus used for stack gas measurements and sampling.

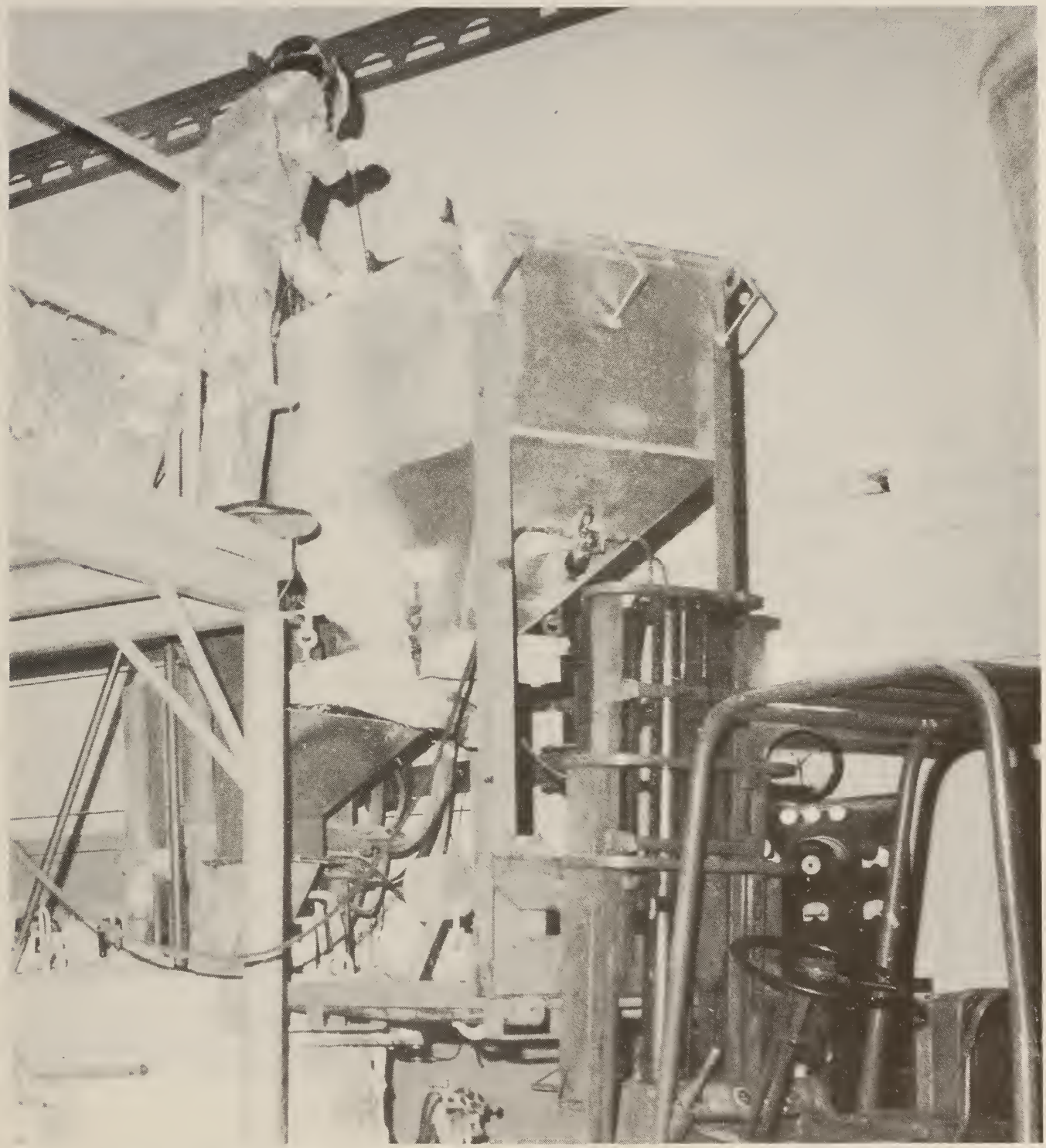

Figure 7.—Continuous feeding of cold scrap into feed chute extending through roof of electric arc furnace.

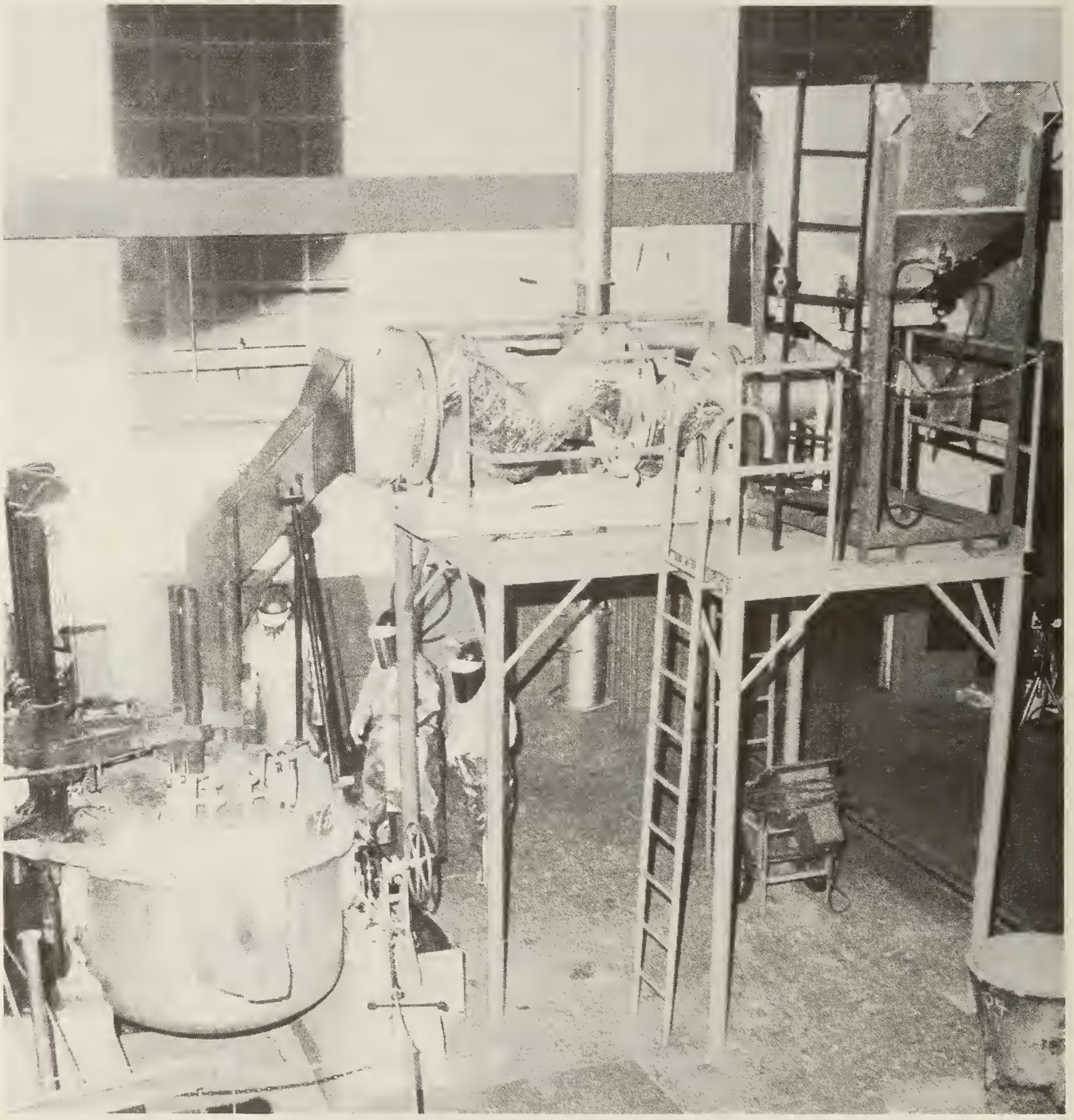

Figure 8.—Continuous charging of preheated scrap into electric arc furnace.

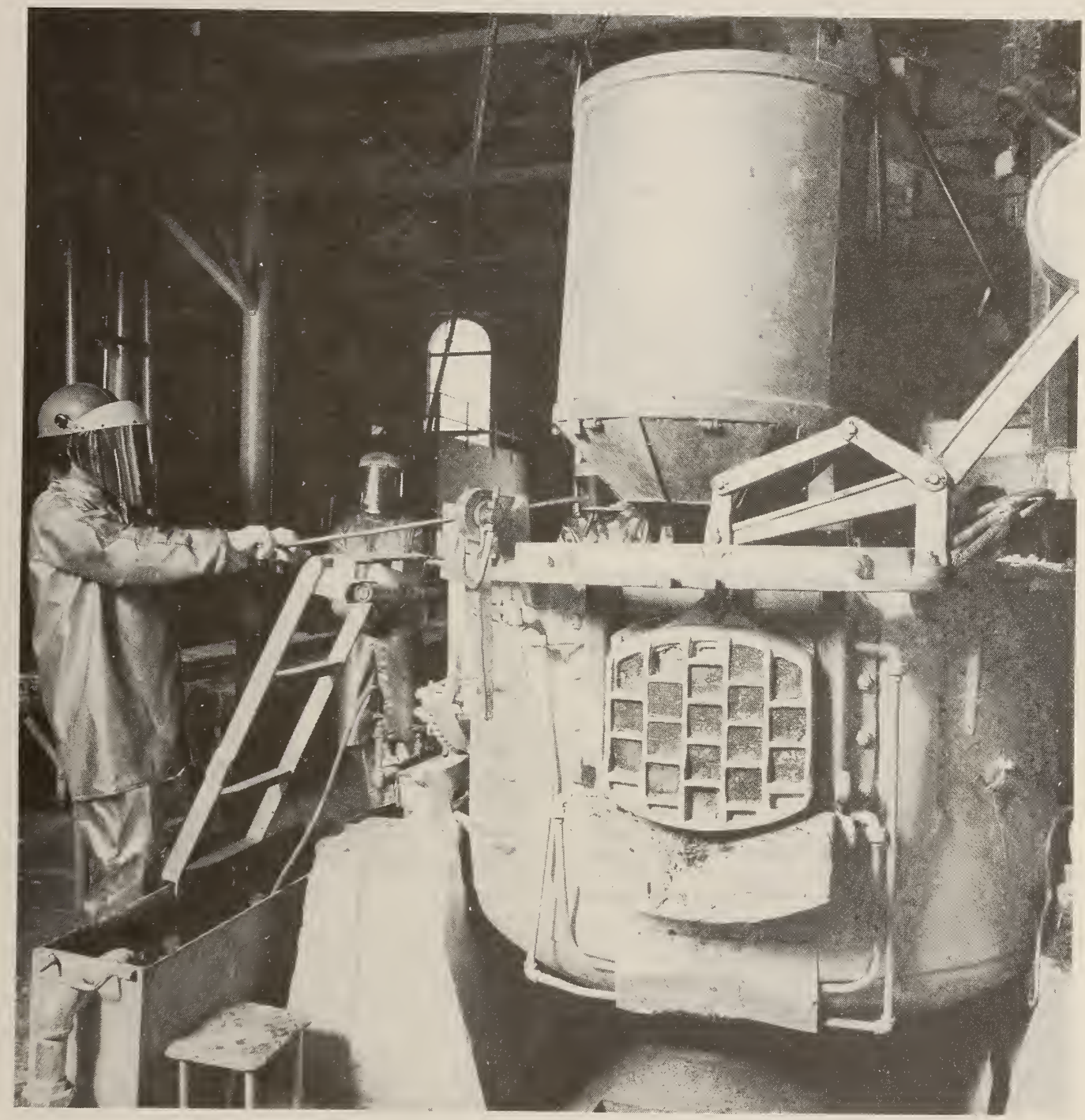

Figure 9.—Backcharging of cold scrap into electric arc furnace.

RESULTS

Continuously Charged Preheated Scrap

Table 4 summarizes the averaged experimental data for 12 tests made with preheated scrap. One standard deviation from the means is shown. The feed rates ranged from 22.9 to 66.2 lb/min, and the power input ranged from 440 to 682 kW. At the feed rates used, no unmelted scrap buildup was noted. For the continuous feeding period, electrical energy consumption ranged from 592 to 810 kW·h/st of charge. Overall energy consumption for these tests ranged from 786 to 924 kW·h/st of scrap. Test-to-test variations in scrap feed rate owing to the fragmented scrap's tendency to hang up in the charge bin primarily were responsible for the range in energy consumption. The temperatures of the furnace offgases introduced into the preheater ranged from 1,020° to 1,200° F. Exit gas temperatures usually were less than 390° F owing to transfer of heat to the preheated scrap and infusion of air into the feed inlet during the continuous charging operation. Preheated scrap temperatures ranged from 840° to 1,110° F. Stack gas temperature ranged from 101° to 135° F, while the flows were 1,382 to 1,783 scfm. The stack gas contained 0.03 to 2.24 gr/dscf of particulate. Moisture contents of the gases ranged from 0.09 to 1.92 wt pct.

Continuously Charged Cold Scrap

The averaged experimental data for 14 tests conducted with continuously charged cold scrap also are shown in table 4. The scrap feedrate ranged from 30.5 to 63.7 lb/min, and the power input ranged from 498 to 657 kW. Electrical energy consumption for the feeding period ranged from 630 to 846 kW·h/st of charge. Overall, the energy consumption was 818 to 1,084 kW·h/st of charge, and the electrode use ranged from 10.5 to 19.1 lb/st of scrap. Stack gas temperatures for 4 of the 14 tests ranged from 191° to 270° F, with flow rates of 1,220 to 1,377 scfm. Particulate concentrations ranged from 0.01 to 0.53 gr/dscf. Moisture contents of the gases ranged from 0.86 to 2.15 wt pct.

Scrap Backcharging Tests

The averaged experimental data for three scrap backcharge tests also are presented in table 4. In these tests, the power input ranged from 533 to 579 kW for the melt down of the 1,800-lb scrap charges. Electrical energy consumption ranged from 612 to 658 kW·h/st of charge. Electrode consumption of 10.2 lb/st of scrap or less was noted in these tests. Stack gases having temperatures of 126° to 146° F flowed at a rate of 1,385 to 1,490 scfm. Particulate concentrations ranged from 0.11 to 0.64 gr/dscf. The moisture content of the gases was 1.31 to 1.75 wt pct.

Comparisons of Melting Techniques

The data indicate that continuously charged preheated scrap consumed 5.3 pct less electrical energy than when cold scrap was continuously charged during meltdown. Tests with continuously fed preheated and cold scrap charges overall consumed 829 and 888 kW·h/st of scrap, respectively. Overall, the preheated scrap charges consumed 6.8 pct less electrical energy than did the cold-charged scrap.

Figure 10 shows the actual electrical energy consumed in the continuous addition, meltdown, and refining periods of the two types of continuous scrap charging tests, along with tests for conventional backcharged scrap. It can readily be seen that both types of continuous charging tests consumed more electrical energy than did

Table 4.—Averaged experimental data for steelmaking tests using continuously charged preheated and cold scrap, and backcharged cold scrap,

	Continuously charged scrap		Backcharged
	Preheated	Cold	cold scrap
Total test time, min	88 ± 10	97 ± 7	80 ± 3
Av power input, kW	577 ± 51	579 ± 31	569 ± 14
Av scrap feed rate, lb/min	44 ± 10	38 ± 9	NAp
Overall energy consumption, kW·h/st scrap	829 ± 43	88 ± 51	637 ± 23
Electrode consumption, lb/st scrap	16 ± 3	15 ± 3	9 ± 1
Tap temperature, °F	2,992 ± 115	3,030 ± 115	2,892 ± 107
Metal, lb/st scrap	1,856 ± 52	1,888 ± 71	1,859 ± 95
Slag, lb/st scrap	245 ± 66	241 ± 78	140 ± 11
Stack dust, lb/st scrap	56 ± 21	[1]89 ± 65	14 ± 7
Metal recovery, pct	93	94	93

NAp Not applicable.

[1] Average of 4 tests. A suitable stack dust collection system was not available for the other 10 tests.

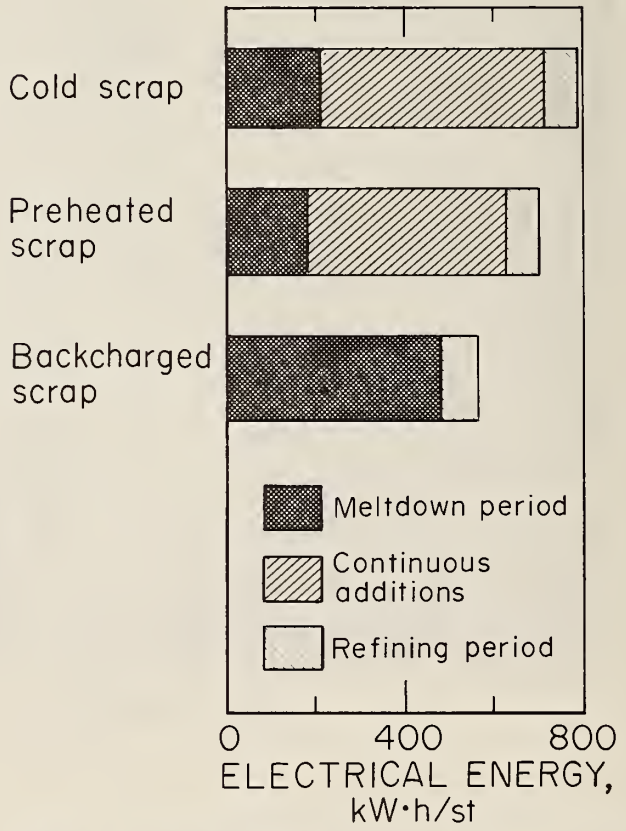

Figure 10.—Actual electrical energy consumption for three types of scrap charging tests.

the tests made with conventional scrap backcharges. Higher energy consumption may be attributed (1) to the inability to continuously charge at a rate fast enough to use all of the available energy, or (2) to less efficient heat transfer using the preheating system. The first hypothesis is supported by the open-bath conditions and the higher bath temperature observed during continuous charging operations. No significant differences were noted in the quantity of metal produced in the three types of tests.

It became apparent that the scrap feed rate was not balanced with the high power input used. The scrap charging and preheating equipment was not large enough to feed the scrap at a rate corresponding to the power input used. One suggested technique to address this problem is choke feeding, whereby the scrap feed rate is sufficient to allow an accumulation of scrap in the furnace to prevent open-bath conditions. The choke feeding technique used for prereduced iron ore pellets resulted in higher melt rates and increased productivity (*26*). Another technique to employ during continuous feeding is use of a foamy slag (*27*). The radiation of arc energy to the sidewalls is reduced since the tips of the electrodes are surrounded by scrap or a foamy slag. In the present case, the equipment and electric-arc furnace were not large enough to permit testing of either technique.

Analytical data from backcharged tests indicated the furnace dust contained less zinc (32.5 wt pct) than the dusts derived from the continuous feeding charges. Both types of continuous-charging tests averaged approximately 100 lb more slag than did tests made with conventional scrap backcharges. This probably was because of dissolved refractory materials since open-bath conditions during the continuous feeding period caused a portion of the arc energy to be radiated to the furnace sidewall. In the case of conventional scrap backcharge practice, the furnace sidewall is shielded most of the time by the unmelted scrap. In the absence of an open bath, less of the arc energy is radiated to the sidewall.

Some differences in stack gas temperatures and flows were observed among the three types of scrap charging tests, as shown in table 5. Stack gas temperature in the preheating tests was lower because heat was absorbed by the scrap fed into the preheater unit. The higher gas flow was attributed to the ingress of air into the scrap feed inlet of the preheater during the continuous addition period. Stack gas from the preheated scrap tests also contained the highest concentrations of particulate (0.97 gr/dscf). A portion of the organic material (such as upholstery), iron oxide scale, and other materials that mechanically separated from the continuously fed scrap as it tumbled in the rotating preheater became entrained as particulate in the furnace offgas stream. In the other type of test, the scrap was charged directly into the furnace, and part of the dirt, glass, etc., reported to the slag phase.

Table 5.—Averaged data for stack gas measurements of the three types of scrap charging tests.

	Continuously charged scrap		Backcharged
	Preheated	Cold	only
Sampling duration, min	21.6 ± 8.4	33.0 ± 8.8	18.3 ± 1.3
Temperature of gas, °F	120 ± 11	220 ± 35	135 ± 10
Gas velocity, ft/s	28 ± 2	26.5 ± 1.4	25.5 ± 1.3
Flow rate, scfm	1,615 ± 132	1,302 ± 73.4	1,433 ± 53.2
Moisture content, wt pct	1.3 ± 0.4	1.6 ± 0.6	1.5 ± 0.2
Particulate conc, gr/dscf	0.97 ± 0.74	0.24 ± 0.24	0.29 ± 0.3

SUMMARY AND CONCLUSIONS

Process offgases generated during oxygen blowing of a scrap-molten iron charge can be used effectively to preheat the next scrap charge in a ¼-st capacity BOF. A maximum of 28 pct unheated scrap can be used in normal BOF operations. When scrap is preheated to 1,150° F, scrap in the charge can be increased to a maximum of 40 pct, representing a 43-pct increase in scrap utilization. Thermal energy recovered using 40 pct scrap represents 26 pct of the heat input required to melt the scrap. Scrap preheating in a BOF decreases energy consumption, allows the use of additional scrap to augment hot metal supplies when scrap is relatively cheap or the demand for hot metal exceeds the supply, and increases scrap utilization.

In electric arc furnace steelmaking operations, continuously fed fragmented scrap preheated by furnace offgases consumed about 5 pct less electrical energy for the meltdown and 7 pct less overall than did similarly charged cold scrap. Data indicated that the preheated and cold charges of fragmented scrap continuously fed into the furnace consumed more electrical energy and electrode materials than did conventional backcharged scrap. The higher energy consumption is not necessarily characteristic of continuous feeding but may be due to the way the testing was conducted. Significant differences in stack gas temperatures, flows, and particulate concentrations were noted among the three types of scrap charging tests. Stack gases from scrap preheating tests exhibited the highest flow rate and the lowest temperature.

REFERENCES

1. Schottman, F. J. Iron and Steel. Ch. in BuMines Minerals Yearbook 1985, v. 1, pp. 553-571.

2. Kotraba, N. L. Technology Alters Steelmaking. Am. Met. Mark,, v. 69, No. 237, Dec. 9, 1981, p. 16.

3. Hale, R. W. Energy Use Patterns in Metallurgical and Nonmetallic Mineral Processing (Phase 8—Opportunity To Improve Energy Efficiency in Production of High-Priority Commodities Without Major Process Changes) (contract S0144093, Battelle Columbus Laboratories). BuMines OFR-117(3)-76, 1975, 80 pp.; NTIS PB 261 152.

4. Hunter, W. L., and J. E. Tress. Preheating Prereduced Briquettes and Development of Continuous Steelmaking. Paper in Proceedings of the 27th Electric Furnace Conference. AIME, v. 27, 1970, pp. 122-125.

5. Tress, J. E., W. L. Hunter, and W. A. Stickney. Continuous Charging and Preheating of Prereduced Iron Ore. BuMines RI 8004, 1975, 10 pp.

6. Kobrin, C. L. Preheating Scrap for the BOF. Iron Age, v. 210, No. 2, 1968, pp. 57-59.

7. Moresco, A. J. Scrap Preheat Operation. Iron Steel Eng., v. 46, No. 6, 1969, pp. 103-105.

8. Laws, W. R. Prospects for Scrap Preheating for the Basic Oxygen Furnace. Steel Times, v. 200, No. 9, 1972, pp. 679-682.

9. Kemner, W. F., The Operating, Economic and Quality Considerations of Scrap Preheating With the Basic Oxygen Process. Blast Furn. Steel Plant, v. 57, No. 12, 1969, pp. 1007-1012.

10. Chatterjee, A. Economics of Preheated Scrap Usage in the LD Process. Iron Steel Int., Aug. 1973, pp. 325-331.

11. Meschter, E. Preheaters in the Cold. Am. Met. Mark., v. 90, No. 187, Sept. 27, 1982, Steelmaking Suppl., p. 6A.

12. Kishida, T. A. Ukai, S. Sugiura, and S. Asano. Scrap Preheating by Exhaust Gas From Electric Arc Furnaces. Iron Steel Eng., v. 60, No. 11, 1983, pp. 54-61.

13. Industrial Heating. Scrap Preheating With Electric Arc Melting Furnace Off Gases Improves Operating Efficiency. V. 50, No. 7, 1983, p. 28.

14. Watanabe, H., M. Iguchi, and T. Maki. Scrap Preheater for Electric Arc Furnace. Iron Steel Eng., v. 60, No. 4, 1983, pp. 45-50.

15. Tomizawa, F. and E. C. Howard. Arc Furnace Productivity in the 1980's. Iron Steel Eng., v. 62, No. 5, 1985, pp. 34-37.

16. Finkl, C. W. Benefits of Pre-Heating Scrap. J. Met., v. 17, No. 1, 1965, pp. 67-70.

17. Einerkjaer, J. Preheating of Electric Furnace Scrap. Iron Steel Eng., v. 47, No. 4, 1970, pp. 51-55.

18. Rudzki, E. M., R. J. Reinbold, and B. K. Pease. Scrap Preheating in an Electric Melt Shop. J. Met., v. 25, No. 2, 1973, pp. 38-43.

19. Remalia, D. L. Scrap Preheating for Increased Productivity. Paper in 37th Electric Furnace Conference Proceedings. AIME, v. 37, 1979, pp. 315-319.

20. Mahony, H. A. Rapid Steel Scrap Melting With Gas-Oxygen Burners. U.S. Pat. 3,234,010, Feb. 8, 1966.

21. _____. Smelting of Fine Iron Ores to Molten Iron in Induction Furnaces. U.S. Pat. 3,235,374, Feb. 15, 1966.

22. Tomizawa, F., and E. C. Howard. Scrap Preheating Within a Clean House Enclosure and Associated Operation Benefits. Paper in 42d Electric Furnace Conference Proceedings. AIME, v. 42, 1984, pp. 79-91.

23. Drost, J. J., C. B. Daellenbach, W. M. Mahan, and W. C. Hill. Thermal Energy Recovery by Basic Oxygen Furnace Offgas Preheating of Scrap. BuMines RI 7929, 1974, 8 pp.

24. Mahan, W. M., C. B. Daellenbach. Thermal Energy Recovery by Basic Oxygen Furnace Offgas Preheating of Scrap. Paper in Procedings of Symposium on Efficient Use of Fuel in the Metallurgical Industries. Inst. Gas Technology, IIT Center, Chicago, IL, Dec. 1974, pp. 457-465.

25. Elger, G. W., R. H. Nafziger, J. E. Tress, and A. D. Hartman. Utilization of Scrap Preheating and Substitute Slag Conditioners for Electric Arc Furnace Steelmaking. BuMines RI 9130, 1987, 26 pp.

26. Nafziger, R. H., J. E. Tress, and W. L. Hunter. Rapid Addition of Charge Materials in Continuous Electric Furnace Steelmaking. Iron Steelmaker, v. 2, No, 5, 1975, pp. 33-37

27. Caine, K. E., Jr. A Review of New Electric Arc Furnace Technologies. Iron Steel Eng., v. 60, No. 10, 1983, pp. 45-47.

FLUORSPAR SUBSTITUTES IN STEELMAKING

By R. H. Nafziger[1] and G. W. Elger[2]

ABSTRACT

One goal of Bureau of Mines research is to establish the potential of abundant domestic resources as substitutes for imported materials. Fluorspar, which is used as a slag conditioner in steelmaking, is one of these materials. The Bureau has conducted research on substitutes for fluorspar such as colemanite ($Ca_2B_6O_{11}\cdot 5H_2O$), fused boric acid, synthetic fluorspar, and used aluminum smelter potlining in basic oxygen furnace (BOF) operations, and on synthetic fluorspar, boric acid, hydroboracite ($CaMgB_6O_{11}\cdot 6H_2O$), used aluminum potlining and anode tailing wastes, and Sorelflux B (ilmenite) in electric arc furnace steelmaking. For BOF slags, colemanite and fused boric acids were superior fluidizers to fluorspar when compared on the basis of boron versus fluorine concentration and were more stable. Synthetic fluorspar and used aluminum potlining provided equivalent slag fluidity to that noted by natural fluorspar. In electric arc furnace steelmaking, the boron-containing conditioners (hydroboracite and boric oxide) fluidized the slags better than those containing fluorine (synthetic fluorspar, used aluminum potlining, and anode tailing wastes) and titanium (Sorelflux B), in that order. The results indicate that substitute fluidizers do not adversely affect the quality of the steel produced.

INTRODUCTION

Fluorspar is a critical mineral. Approximately 81 pct (553,000 st) of domestic fluorspar consumption was imported in 1985 *(1)*.[3] Estimates for 1986, based on 9 months of data, show 94 pct of the domestic needs for fluorspar was imported *(2)*. Approximately 33 pct of the fluorspar consumed domestically is used as a fluidizer in steelmaking. Most steelmaking operations require a slag fluidizer to promote the required reactions, to increase productivity, to improve tapping operations, and to conserve energy. Fluorspar, as an auxiliary flux, promotes the rapid solubility of lime and rapid slag formation, in both the BOF and electric arc furnace. This also improves BOF steelmaking operations by lowering frothing and sparking during the oxygen blowing period. Over 181,000 st of fluorspar was consumed in steelmaking in 1985 *(1)*. In 1985, BOF's used approximately 2.7 lb of fluorspar per short ton of raw steel produced *(1)*. The electric arc furnace consumes approximately 2.1 lb of fluorspar per short ton of raw steel.

If a satisfactory substitute can be found, U.S. dependence on foreign sources of suitable fluorspar would diminish and import costs could decrease. A number of potential fluorspar substitutes that are more readily available from domestic sources than fluorspar are not being used. Several of these potential substitutes are wastes of which the disposal presents environmental problems.

The search for fluorspar substitutes as a flux conditioner began a number of years ago with work conducted at Stelco (Steel Company of Canada). Results indicated that calcium borates and manganese ore were similar to fluorspar in their ability to form a basic slag rapidly in BOF operations. Tests in a 500-st capacity open-hearth furnace confirmed these observations *(3)*. QIT-Fer et Titane, Inc., has been promoting its Sorelflux (ilmenite) as a good fluorspar substitute for several years. Most recently, trials were conducted in a 4-st capacity electric arc furnace using spent aluminum potlining material. All of the heats provided steel within specifications. From a qualitative standpoint, the slags with the potlining fluidizer were more fluid than those obtained when fluorspar was used *(4)*.

The objective of the research reported in this review paper is to evaluate the use of readily available domestic materials or wastes as substitutes for fluorspar slag conditioners in BOF and electric arc furnace steelmaking. Substitute materials were compared with fluorspar on the basis of both viscometry measurements and visual observations made of the molten bath before and after the fluidizer addition. This investigation is part of the Bureau program to develop technology that emphasizes the reuse of recycled materials and to help meet the goal of substituting abundant domestic materials for imported critical materials.

[1] Research supervisor.

[2] Research chemist.

Albany Research Center, Bureau of Mines, Albany, OR.

[3] Italic numbers in parentheses refer to items in the list of references at the end of this paper.

SUBSTITUTE MATERIALS

For BOF steelmaking, colemanite ($Ca_2B_6O_{11}\cdot 5H_2O$), fused boric acid, synthetic fluorspar made from fluosilicic acid at the Bureau's Albany (OR) Research Center, and used aluminum smelter potlining materials were used as conditioning substitutes and were compared with reagent- and ceramic-grade fluorspar. Both the colemanite and the fused boric acid were obtained commercially. The synthetic fluorspar was prepared from fluosilicic acid, a byproduct of the acidulation of fluorapatite ($Ca_{10}(PO_4)_6F_2$), produced in the manufacture of fertilizers *(5)*. The used aluminum smelter potlining material was provided by Alcoa, Pittsburgh, PA. Analyses of these materials are summarized in table 1.

Table 1.—Average chemical composition of slag conditioners used in BOF steelmaking tests *(7, 10)*, weight percent

	Fluorspar		Colemanite	Fused boric acid	Synthetic fluorspar	Used potlining	
	Reagent-grade	Ceramic-grade				Lump[1]	Pellet[2]
Al...	ND	0.01	ND	ND	ND	6.9	6.7
B...	NDt	NDt	12.2	28.2	0.3	ND	ND
C...	ND	.38	ND	ND	2.2	34.8	38.1
Ca..	49.4	49.9	18.3	NDt	39.0	2.1	1.9
F...	48.0	45.0	NDt	NDt	31.7	12.5	11.5
Mg..	NDt	.12	1.4	NDt	.3	.06	.06
Na..	NDt	.04	<.04	.01	.2	7.4	6.6
P...	ND	.12	ND	ND	1.3	ND	ND
S...	ND	.07	ND	ND	.8	.2	.2
Si...	<.05	<.05	3.0	NDt	3.2	2.5	2.9

ND Not determined. NDT Not detected.
[1] Minus ⅜ in plus 10 mesh.
[2] Minus ¾ plus ½ in.

In the electric arc furnace steelmaking tests, three types of slag conditioners were used: fluorine-, titanium-, and boron-containing compounds or materials. The fluorine group included natural fluorspar, synthetic fluorspar, used aluminum smelter potlining, and anode tailing wastes. The natural fluorspar was purchased from a commercial supplier and was the type normally used in steelmaking operations. The synthetic fluorspar was similar to that used in the BOF tests. The used potlining and anode or tailings were obtained from Kaiser Aluminum and Chemical Co., Spokane, WA. Both were from aluminum reduction cells. The linings of aluminum reduction cells must be replaced regularly. The linings are carbonaceous and become impregnated with fluorine and sodium compounds while in service. The material accumulates at a rate of approximately 190,000 st/yr and presents a disposal problem for the aluminum industry *(6)*. The anode tailing wastes were the ends of the carbon anodes.

The titanium-containing material was Sorelflux B. This was furnished by QIT-Fer et Titane, Inc., and was mostly ilmenite and feldspar, with a small amount of hematite.

The boron-containing conditioners included boric oxide and Gerstley borate. Boric oxide was prepared by fusing and grinding boric acid. The Gerstley borate, which consisted of hydroboracite ($CaMgB_6O_{11}\cdot 6H_2O$), is used as a glaze in the ceramics industry. The Gerstley borate was heated to 800° F to drive off the contained water. The chemical analyses of all these slag conditioners are shown in table 2.

Table 2.—Chemical composition of slag conditioners used in electric arc furnace steelmaking tests *(12)*, weight percent

	Fluorspar		Used potlining	Butt tailings	Sorel-flux B	Boric oxide	Gerstley borate
	Natural	Synthetic					
Al...	2.11	0.09	11.3	2.02	1.97	ND	0.50
B...	ND	ND	ND	ND	ND	22.2	9.72
C...	1.27	.71	1.86	63.8	ND	ND	ND
Ca..	40.6	45.3	2.10	.53	.66	ND	12.7
F...	34.8	40.5	21.5	7.5	ND	ND	ND
Fe..	.28	ND	ND	ND	38.8	ND	.23
Mg..	.27	.25	.10	.04	1.79	ND	2.01
Mn..	ND	ND	ND	ND	.12	ND	ND
Na..	ND	ND	25.0	4.1	ND	ND	3.75
P...	ND	ND	ND	ND	.021	ND	ND
Pb..	1.0	.34	ND	ND	ND	ND	ND
S...	<.39	.19	.27	2.85	ND	ND	ND
Si...	3.70	1.77	.81	.31	2.65	ND	4.10
Ti...	ND	ND	ND	ND	20.3	ND	ND
V...	ND	ND	ND	ND	.25	ND	ND

ND Not determined.

BOF EXPERIMENTS

LABORATORY-SCALE VISCOMETRY TESTS

Laboratory-scale viscometry experiments were conducted on boron-containing slags and results were compared with fluorspar determinations at the Bureau's Twin Cities (MN) Research Center *(7)*. Two master slags were prepared in the BOF and ground to minus 100 mesh. Preheated lime was added to the molten slag samples in the viscometer to adjust the basicity or $CaO\text{-}SiO_2$ ratio (usually more than 3:1). The viscometer was of the rotating-concentric cylinder type and has been described in detail by Kilau *(7)*. The wire-wound resistance furnace and viscosity transmitter also have been described *(7)*. The addition of a pressure transducer, X-Y recorder, and temperature programmer allowed continuous viscosity measurements.

Kilau *(7)* found that when 2.2 to 3.1 wt pct fluorine was added as reagent- or ceramic-grade fluorspar, the viscosity increased with increasing slag basicity. At approximately 3 wt pct fluorine, a fluidizing limit was suggested, above which foaming and crusting may occur. Based on analyses of quenched slags, from 5 to as much as 26 pct fluorine was lost at temperatures up to approximately 1,500° C. On the basis of elemental boron and fluorine concentrations, boron added as colemanite is a superior fluidizer to fluorspar for slags with a basicity of 3. This is illustrated in figure 1 *(7)*. Fused boric acid proved to be slightly superior to colemanite as a slag fluidizer. Both colemanite and fused boric acid showed no losses of boron upon heating. No fluidizing limit for fused boric acid was noted by up to 4.4 wt pct boron levels.

For synthetic fluorspars, up to 58 pct fluorine loss was noted at 1,000° C by Kilau *(8)*. However, it was shown that improved synthetic fluorspars only lost up to 14 pct fluorine *(8)*. The improved synthetic fluorspar used limestone in the precipitation of CaF_2 from the fluosilicic acid. Also, pH control was improved. Such synthetic

fluorspars can differ greatly in their stability and ability to fluidize BOF slags, depending upon their method of preparation. As shown in figure 2 *(8)*, the improved synthetic fluorspars are comparable to natural (ceramic-grade) fluorspar. However, Kilau showed that a commercially prepared synthetic fluorspar was somewhat inferior to the natural fluorspar (fig. 2).

TESTS IN THE BOF

Equipment and Procedures

Experiments to evaluate synthetic fluorspars and used aluminum smelting potlining materials were conducted in the Bureau's 500-lb-capacity BOF at the Twin Cities (MN) Research Center.

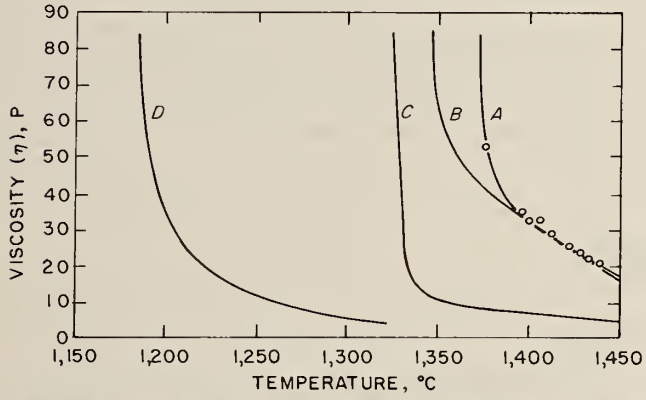

Figure 1.—Viscosity-temperature profiles for fluorspar, colemanite, and fused boric acid additions to BOF slags *(7)*. *A*, 2.0 pct B from added dehydrated colemanite (13.6 pct); *B*, 1.9 pct B from added fused boric acid (6.7 pct); *C*, 2.9 pct F from added ceramic-grade fluorspar (6.4 pct); *D*, 3.1 pct B from added fused boric acid (11.0 pct).

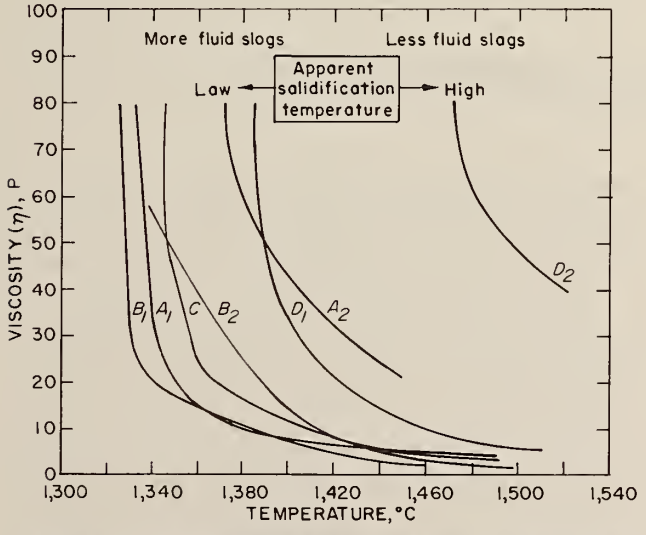

Figure 2.—Viscosity-temperature profiles for natural and synthetic fluorspar additions to BOF slags *(8)*, A_1, Natural fluorspar (ceramic grade), 2.7 pct F; A_2, natural fluorspar (ceramic grade), 2.2 pct F; B_1, synthetic fluorspar (improved product), 3.2 pct F; B_2, synthetic fluorspar (improved product), 2.9 pct F; *C*, synthetic fluorspar (commercial product), 2.9 pct F; D_1, synthetic fluorspar, 2.7 pct F; D_2, synthetic fluorspar, 1.9 pct F.

This furnace has been described previously by Drost *(9)*. Two synthetic fluorspars (the improved and commercial varieties) were compared with natural ceramic-grade fluorspar using identical 300-lb charges of hot metal and 80 lb of shredded automotive scrap *(10–11)*. The synthetic fluorspars were briquetted to decrease dusting losses during BOF operations. Fluidizers were added on an equivalent fluorine basis (2.0–2.6 lb). The charges also consisted of 30 lb lime. All heats were blocked in the furnace using 2 lb of ferrosilicon and 1.5 lb of electrolytic manganese. Blocking deoxidizes the heat to maintain a constant carbon content. Each fluorspar test consisted of three heats. The BOF was blown at 25 scfm oxygen for 10 to 12 min. Offgases were passed through a wet scrubber. The scrubber water and solids were collected and submitted for analyses, along with the metal and slag samples. Additional details were described by Spironello *(10–11)*.

The same furnace was used to evaluate used aluminum smelter potlining material as a substitute fluidizer. Shredded automotive scrap (90 lb) was added to the furnace, followed by hot metal (310±15 lb). The oxygen flow was set at about 24 cfm. Approximately 1 min after ignition, 30 lb lime was charged, followed by the potlining material (4 lb). Ferrosilicon and silicomanganese were added after the oxygen blow to block the heats *(10–11)*.

Results

When synthetic fluorspar slags were used, the furnace operated satisfactorily. Metal and slag analyses are shown in table 3 *(8)*. Kilau found that the steel produced was satisfactory for all of the fluorspars tested, despite relatively high phosphorus levels in the synthetic fluorspar (table 1). MgO concentrations in the slag (table 3) suggested that no excessive refractory consumption resulted from the use of the synthetic fluorspars *(8)*. The resulting slags were subjected to laboratory-scale testing as described previously in this paper. Results are shown in figure 3 *(8)*. It can be seen that the commercial synthetic fluorspar appears greatly inferior to either the improved synthetic fluorspar or to the natural fluorspars.

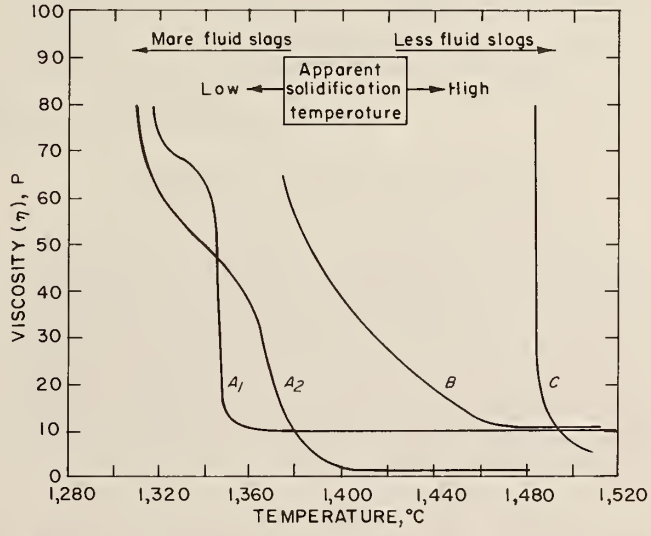

Figure 3.—Viscosity-temperature profiles for pilot-scale BOF steelmaking slags to which natural and synthetic fluorspars were added *(8)*. A_1, Overblown BOF slag with natural fluorspar, 0.7 pct F, 35.9 pct total Fe, 3.6 basicity; A_2, normal practice BOF slag with natural fluorspar, 1.4 pct F, 19.7 pct total Fe, 3.8 basicity; *B*, BOF slag with synthetic fluorspar (improved product) 1.3 pct F, 17.6 pct total Fe, 3.3 basicity; *C*, BOF slag with commercial synthetic fluorspar, 1.4 pct F, 13.3 pct total Fe, 4.4 basicity.

Table 3.—Chemical analyses of BOF slags and metals *(8)*, weight percent

	Natural fluorspar		Bureau synthetic fluorspar		Commercial synthetic fluorspar	
	Metal	Slag	Metal	Slag	Metal	Slag
Al_2O_3	NAp	0.35	NAp	0.35	NAp	0.36
C	0.28	NAp	0.05	NAp	0.07	NAp
CAO	NAp	42.1	NAp	50.5	NAp	53.2
F	NAp	1.5	NAp	1.3	NAp	1.2
Fe^{2+}	NAp	16.8	NAp	12.6	NAp	13.3
MgO	NAp	4.9	NAp	2.6	NAp	2.7
Mn	.23	6.1	.26	4.6	.29	5.5
P	<.01	.28	<.01	.36	<.01	.51
S	.011	.096	.014	.076	.016	.100
Si	.12	NAp	.24	NAp	.12	NAp
SiO_2	NAp	12.8	NAp	15.1	NAp	14.8
Total Fe	NAp	20.7	NAp	16.5	NAp	16.0

NAp Not applicable.

The results of Kilau *(8)* also indicated that a fluidizer substitute need only be effective in the early stages of a blow to solubilize the dicalcium silicate. Toward the end of the blow, increasing iron contents of the slag could serve to provide the required fluidity. Hence, a relatively unstable synthetic fluorspar could be effective in BOF steelmaking. In some cases, a BOF could be operated without fluorspar, especially for low-carbon steels in which the longer blowing time could permit adequate refining and produce sufficient iron oxide in the slag to effect satisfactory fluidization.

Chemical analyses of the steel produced in the BOF using aluminum smelter potlining material and fluorspar are shown in table 4 *(10)*. Spironello found that higher sulfur levels resulted from the use of potlining material because the sulfur content was higher in the hot metal charge. All slags were fluid and permitted satisfactory sampling and tapping. Slag analyses are presented in table 5, also from Spironello *(10)*. Based on the MgO contents of the slags, there were no significant differences in refractory lining attack when potlining was used. The higher Al_2O_3 and Na_2O contents resulted from the aluminum and sodium in the potlining material *(10)*.

Table 4.—Steel analyses from evaluation of used potlining in a BOF *(10)*, weight percent

Heat	Al	C	Mn	P	S	Si
Fluorspar:						
1	0.46	<0.10	0.42	0.006	0.008	0.10
2	.47	<.10	.45	.013	.009	.15
Potlining lump:[1]						
1	.35	<.10	.36	.010	.019	.10
2	.57	<.10	.34	.010	.015	.10
Potlining pellets:[2]						
1	.42	<.10	.46	.010	.023	.10
2	.33	<.10	.58	.010	.017	.18

[1] Minus ⅜ in plus 10 mesh.
[2] Minus ¾ plus ½ in.

Table 5.—Slag analyses from evaluation of used potlining in a BOF *(10)*, weight percent

Heat	Al_2O_3	CaO	F	Fe^{2+}	MgO	Mn	Na_2O	P	S	SiO_2	Total Fe
Fluorspar:											
1	0.44	53.6	1.4	12.4	5.4	4.3	<0.02	0.55	0.063	13.5	17.3
2	.73	56.4	1.8	11.0	5.0	5.0	<.02	.69	.072	17.5	11.1
Potlining lump:[1]											
1	2.8	50.5	.91	11.8	4.7	5.5	.95	.47	.087	14.8	16.2
2	3.2	53.1	.85	14.5	4.5	5.4	.95	.52	.084	13.2	17.5
Potlining pellets:[2]											
1	1.7	56.6	.67	8.6	4.7	4.6	.47	.56	.100	15.1	11.6
2	1.7	53.9	.65	11.6	4.8	5.1	.50	.57	.110	14.2	14.6

[1] Minus ⅜ in plus 10 mesh.
[2] Minus ¾ plus ½ in.

The product steels were hot-rolled and mechanically tested. Spironello found that the results showed yield and tensile strengths comparable to conventionally produced steels *(10)*.

ELECTRIC ARC FURNACE EXPERIMENTS

EQUIPMENT AND PROCEDURES

All tests were conducted in a 1-st-capacity, three-phase ac electric arc furnace at the Bureau's Albany (OR) Research Center. Shredded automotive scrap, lime, and quartz were used as charge materials. After the feed had entered the furnace and the bath was molten, the slag conditioner was added. After about 5 min of heating, the slag was removed from the bath. Then, 10 lb of silicomanganese was added, the bath was adjusted to the proper temperature, and the furnace was tapped. Both metal and slag samples were taken after slag removal and at the tap *(12)*.

RESULTS

Of the three types of slag conditioners evaluated on the basis of visual observations (e.g., stickiness of the slag and ease of slag-metal separation), the Gerstley borate and B_2O_3 group appeared the most effective in increasing the fluidity of the individual slags. The resultant slags contained up to 0.5 wt pct B, while the tapped metal products contained 0.001 to 0.002 wt pct B. Boron at these levels is not considered a harmful constituent in most low- or medium-carbon steels. The constituent markedly increases the hardenability of steels at higher levels approaching 0.007 wt pct.

The fluorine-containing materials were also effective in increasing slag fluidity. In the tests made with natural and synthetic fluorspar slag conditioners, the tapped metal products contained between 0.03 and 0.05 wt pct P. The synthetic fluorspar made from fluosilicic acid obtained from a phosphate plant was not a source of phosphorus contamination in the tapped metal products. The sodium constituent in aluminum potlining waste presented a slight fuming problem during scrap meltdown. In the third group, Sorelflux B was the least effective under the conditions used. Only visual comparisons can be given since slag viscosity data were not obtained. Moreover, the slag compositions varied from test to test owing to erosion of furnace lining material. The furnace refractories suffered considerable damage owing to open-bath conditions *(12)*.

SUMMARY AND CONCLUSIONS

Experiments have shown that boron-containing compounds such as colemanite and fused boric acid fluidize BOF slags better than fluorspar on the basis of laboratory-scale viscosity determinations. The comparisons were made on equivalent amounts of boron and fluorine concentrations in the slags. Kilau demonstrated that the boron-containing slags showed no boron losses, whereas slags containing fluorspar were more unstable and lost fluorine by volatilization, resulting in increased slag viscosities and higher apparent solidification temperatures *(7)*. Increased slag basicity increased the fluorine-containing BOF slag viscosity *(7)*. The stabilities and fluidizing abilities of synthetic fluorspars in BOF slags varied considerably, depending upon their method of preparation, as shown by Kilau *(8)*. Improved preparation methods *(8)* yielded synthetic fluorspars that compared favorably with natural fluorspar with respect to stability and fluidizing ability. On the other hand, a commercially prepared synthetic fluorspar was slightly inferior to natural fluorspar *(8)*.

Tests in a pilot-scale BOF demonstrated that synthetic fluorspar can be used as a substitute for natural fluorspar as a flux fluidizer without decreasing the quality of the metal produced. No excessive refractory wear was evident. Fluorspar fluidizers may need to be added only in the early stages of a blow since increasing iron oxide contents of the slag as the blow progresses in a BOF may provide the required fluidity. Low-carbon steels may require no fluidizer. Use of aluminum smelter potlining material as a substitute fluidizer resulted in fluid slags and acceptable metal quality. Refractory wear was nominal.

Three groups of slag conditioners that contained boron (hydroboracite and fused boric acid), fluorine (natural and synthetic fluorspar and aluminum potlining and butt tailings), or titanium (Sorelflux B) were used as substitutes for natural fluorspar in electric arc furnace steelmaking. The boron- and fluorine-containing additives were effective in increasing the fluidity of the slags, with the boron-containing materials more effective. Use of the boron-containing conditioners did not increase the boron levels in the meltdown metal. The tapped metal products contained 0.001 to 0.002 wt pct B. Open-bath conditions caused refractory lining erosion.

REFERENCES

1. Pelham, L. Fluorspar. BuMines Minerals Yearbook 1985, v. I, 1987, pp. 419–428.

2. _____. Fluorspar. Sec in BuMines Mineral Commodity Summaries 1987, pp. 52–53.

3. Buxton, F. M., and P. A. Sandaluk. Fluorspar Substitutes in Steelmaking. Ind. Heat., v. 40, 1973, pp. 288, 290, 292.

4. Belding, P. C., D. R. Augood, and R. J. Schlager. Making Steel Using Spent Potlining Flux. Trans. Am. Foundrymen's Soc., v. 91, 1983, pp. 493–498.

5. Nash, B. D., and H. E. Blake, Jr. Fluorine Recovery From Phosphate Rock Concentrates. BuMines RI 8205, 1977, 16 pp.

6. Balgord, W. D. Recycle of Potlining in the Primary Aluminum Industry. Opportunities for Technical Improvements. Paper in Proceedings of the Sixth Mineral Waste Utilization Symposium. IIT Res. Inst., Chicago, IL, 1978, pp. 324–333.

7. Kilau, H. W., V. R. Spironello, and W. M. Mahan. Viscosity of BOF Slags Fluidized With Fluorspar, Colemanite, and Fused Boric Acid. BuMines RI 8292, 1978, 25 pp.

8. Kilau, H. W., V. R. Spironello, I. D. Shah, and W. M. Mahan. Evaluation of Synthetic Fluorspar in BOF Slags. BuMines RI 8558, 1981, 28 pp.

9. Drost, J. J., C. B. Daellenbach, W. M. Mahan, and W. C. Hill. Thermal Energy Recovery by Basic Oxygen Furnace Offgas Preheating of Scrap. BuMines RI 7929, 1974, 8 pp.

10. Spironello, V. R., and I. D. Shah. An Evaluation of Used Aluminum Smelter Potlining as a Substitute for Flurospar in Basic Oxygen Steelmaking. BuMines RI 8699, 1982, 11 pp.

11. Spironello, V. R. An Evaluation of Aluminum Smelter Potlining as a Substitute for Fluorspar in Cupola Ironmelting and in Basic Oxygen Steelmaking. BuMines RI 8775, 1983, 18 pp.

12. Elger, G. W., R. H. Nafziger, J. E. Tress, and A. D. Hartman. Utilization of Scrap Preheating and Substitute Slag Conditioners for Electric Arc Furnace Steelmaking. BuMines RI 9130, 1987, 26 pp.

RESEARCH ON BASIC STEELMAKING REFRACTORIES

By T. A. Clancy[1] and J. P. Bennett[1]

ABSTRACT

The Bureau of Mines conducted research studies over a 10-yr period on basic refractories commonly used in steelmaking processes. These studies dealt with properties of refractory raw materials (magnesia, dolomite, and natural flake graphite) and formulations containing these materials. High-temperature properties are reported for periclase (MgO) produced from seawater, brines, and magnesite ($MgCO_3$). Improvements in high-temperature strength and slag resistance properties are described for refractories produced from periclase grain altered by various additions. The properties of 14 calcined domestic dolomites are described. The role of natural flake graphite in dolomite-carbon refractories and the feasibility of substitution by synthetic carbons are discussed.

INTRODUCTION

The Bureau of Mines has conducted extensive research on basic refractories commonly used in steelmaking processes. These laboratory studies have focused on raw materials (periclase, dolomite, and natural flake graphite) and refractory formulations (magnesia and dolomite-carbon). Most of these studies have been directed at conserving natural resources via substitution or by improved materials performance. In the case of the refractory raw materials, laboratory studies generally consisted of chemcal, physical, and mineralogical characterization of materials from domestic sources. Refractory mix formulations, however, involved studies of high-temperature physical properties of new or modified mix formulations. High-temperature tests such as flexural strength, deformation under load, and slag resistance evaluations are the most useful for comparing the high-temperature properties of various refractories.

Basic refractories are the preferred material in most steelmaking operations such as the basic oxygen furnace (BOF), the electric arc furnace (EAF), the argon-oxygen decarburizing process (AOD), and ladles. As mentioned in a 1983 paper by Van Dreser and Neely *(1)*,[2] the BOF produces the greatest tonnage of steel in the United States, as in most of the world. Much attention has been focused on refractories used in this furnace, extending service life of refractory linings from 200 to 300 heats of earlier days to an average of 1,500 heats. The types of materials used with current BOF practice are shown in table 1. Magnesite and periclase in the table distinguish only grades. Over 80 pct of the world's production of steel is produced in BOF's and EAF's *(2)*. The EAF is continually undergoing changes in steelmaking practices, bringing about changes in refractory requirements. These include changes such as scrap preheating, water-cooled panels for sidewalls and roofs, and EAF use as a feed source for AOD vessels. Material usage on EAF sidewalls and slaglines are shown in table 1, roof refractories, being mainly alumina-based materials, are not included.

With the advent of water-cooled panels, the EAF is rapidly becoming a diminishing market for refractories. There is, however, a new market in gun mixes for water-cooled sidewall panels as maintenance mixes, at slaglines and bottoms. At the slagline, the predominant usage is magnesia-carbon (MgO-C) brick. Shop option and performance generally determine the type of MgO-C brick (amorphous graphite or flake graphite) and the carbon level (8–20 pct residual carbon) to be used. As in the BOF, the principal mode of wear is decarbonization of the matrix. Consequently, the major

Table 1.—Basic brick usage in steelmaking

Application area	*Refractory*
Basic oxygen furnace:	
Bottom, cone	Tempered, tar-bonded magnesite.
Barrel	Tempered, tar-bonded periclase.
Trunnion pads	MgO-carbon.
Charge pad	Burned, tar-impregnated MgO.
Electric-arc furnace:	
Sidewall	Direct-bonded periclase-chrome.
Slagline	Rebonded fused periclase-chrome.
Hot spots	MgO-C (flake graphite).
Argon-oxygen decarburizer:	
Barrel, bottom	Periclase-chrome or fused periclase-chrome grain.
Tuyere pad	Fused MgO-Cr_2O_3 grain or dolomite.
Ladle:	
Slagline	Direct-bonded MgO-Cr_2O_3 or tar-bonded dolomite.
Sidewall	Chem-bonded MgO-Cr_2O_3 or tar-bonded dolomite.
Impact pad	Direct-bonded MgO-Cr_2O_3.

[1] Ceramic engineer, Tuscaloosa Research Center, Bureau of Mines, Tuscaloosa, AL. This paper is based upon work done under an agreement between the University of Alabama and the Bureau of Mines.

[2] Italic numbers in parentheses refer to items in the list of references at the end of this paper.

thrust in improving MgO-C brick is directed toward providing oxidation resistance or protection for the matrix.

The AOD furnace is one of the most severe, highly corrosive environments to which refractories are exposed. Lining life has been extended from 20 to 30 heats in the early 1970's to in excess of 100 heats today. The AOD furnace is used in conjunction with the EAF and is the principal means of production of stainless steel. Refractory usage associated with the AOD is shown in table 1.

The last major area of basic refractory usage is the ladle. New refractory demands evolve for ladle refractories as steel processes change to continuous casting and ladle refining. Commonly used basic linings are shown in table 1.

This paper summarizes the research done at the Bureau's Tuscaloosa (AL) Research Center on the refractory raw materials, periclase, dolomite, and natural flake graphite used in basic refractories.

RAW MATERIALS

PERICLASE

Conversion of steelmaking from the open hearth and Bessemer processes to the BOF and EAF, along with the shift to continuous casting, has resulted in the exposure of refractories to the much more hostile conditions associated with these newer processes. For example, the operating temperature of the newer metallurgical furnaces has risen, with considerable changes in the requirements for refractory linings. Recent trends point toward the increased use of higher purity magnesia linings, which have become the most important refractory lining material in steelmaking.

In the early 1950's, basic magnesia plants began producing high-purity-periclase (MgO) material from seawater and well and lake brines that competed economically with periclase from dead-burned magnesite ($MgCO_3$) ores. Today both "natural" (magnesite) and "synthetic" (seawater, brines) magnesias ranging from 93 to 99 pct MgO are available. Although the high-purity magnesias are more expensive than the lower grade magnesias (<93 pct MgO), their improved performance often warrants the higher costs.

Consumption of refractory-grade MgO has declined in the United States and other countries. Bureau of Mines statistics *(2)* show 290,271 st of refractory MgO and 99,517 st of caustic calcined MgO were shipped and used in the United States in 1985. World capacity is estimated to be about 10 million tons, with 80 pct derived from natural $MgCO_3$. Refractories account for greater than 70 pct of the MgO consumed in the United States and the world. The decline in world steel production and improvements in refractory life have resulted in world overcapacity and the closure of several plants.

Periclase is produced by the crystallization of magnesia and the growth and agglomeration of magnesia particles during calcining and sintering of magnesite, brucite, or chemically precipitated hydroxide. These magnesia particles are referred to as grains rather than crystals because they are polycrystalline.

Generally, seawater and brine magnesias are obtained by using suitable alkali materials such as limestone or dolomite to precipitate magnesium hydroxide. However, during precipitation, impurities are inadvertently introduced. For example, seawater magnesias often contain boron, the concentration of which depends on the boron content of the feed stock or bittern. Magnesia produced from brine wells and lake sources generally contains less boron but may contain traces of chloride and/or sulfate anions. However, during calcination to remove water of hydration, many of these impurities are volatilized. Material produced from magnesite ore is usually dead burned in rotary kilns at temperatures exceeding 1,600° C to remove volatile and low-melting-point impurities. Besides impurities in the MgO grain, refractory-grade MgO users are concerned with the crystallite size and density (larger crystallite size and higher density giving greater refractory life) *(3)*.

The Bureau characterized a series of 13 magnesia raw materials (natural and synthetic) as to chemistry and mineralogy of the fired periclase *(4)*. The results of these tests are summarized in tables 2 and 3.

Regardless of the magnesia source, processing variables during precipitation, sizing, pelletization, and calcination often affect the physical properties and the integrity of the refractory grains produced. Several investigators *(5–7)* have reported that modulus of rupture (MOR) data obtained at elevated temperatures gave the most reliable indication of the high-temperature strength and performance of a refractory.

Using the periclase materials, shown in tables 2 and 3, samples of each magnesia grain were evaluated by the Bureau. Hot MOR determinations were made at 1,500°, 1,550°, and 1,600° C on ¼- by ¼- by 2-in samples. The test results indicated that (1) the seawater magnesias generally had the lowest hot strengths while a brine periclase material had the highest hot strength, (2) an optimum $CaO\text{-}SiO_2$ (C-S) ratio with reference to hot strength existed for each periclase material, and (3) B_2O_3 contents over 0.1 pct dramatically lowered the hot strength of periclase grains.

The effect of controlled additions of selected metal oxides, as well as the adjustment of the C-S ratio, on the hot strength of periclase grains was investigated in a followup study *(8)*. Oxides of Zr, Ti, Ta, Sc, Fe, and Mn were added in amounts up to 2 pct to three periclase grains. The C-S mole ratios were adjusted to values of 1.5, 2.0, 2.5, and 3.0. Test results showed that threefold to fourfold increases in hot MOR of some periclase materials were obtained

Table 2.—Chemical analysis of commercial periclase grains, weight percent

Sample type	MgO	B_2O_3	CaO	SiO_2	Al_2O_3	Fe_2O_3
Brine	93.7–99.2	0.0 –0.09	0.6 –2.8	0.1–1.9	0.04–0.26	0.08–0.25
Magnesite	88.2–93.5	.01– .03	2.8 –4.9	1.7–3.2	.23– .34	.36– .82
Seawater	93.3–97.6	.01– .33	.53–1.2	.6–3.3	.26– .38	.27– .7

Table 3.—Mineralogy and physical properties of commercial periclase grains

	Brine	Magnesite	Seawater
Mineralogy, X-ray[1]	M_2S, C_2S, C_3MS_2	C_3MS_2, C_2S, αAl_2O_3, CMS	M_2S, CMS
Bulk density, g/cm³	3.23–3.37	3.11–3.32	3.13–3.41
Average grain size, μm	20–60	30–60	30–60

[1] M_2S = forsterite, CMS = monticellite, C_3MS_2 = merwinite, C_2S = dicalcium silicate.

with additions of ZrO_2 and by adjustment of their C-S ratio to 2.5 to 3.0. Results also showed that for each periclase refractory raw material, there existed a combination of percent ZrO_2 addition and C-S ratio adjustment to attain optimum hot MOR values. Data also indicated that the improved hot strengths can be attributed to the high-temperature secondary phase (dicalcium silicate) formed between the periclase impurities and the additives, resulting in improved intergranular high-temperature bond strength.

The effects of chemical adjustments of periclase grain and adjustments to an $Mg(OH)_2$ slurry prior to grain densification were investigated *(9)* using full-size commercially processed brick samples. Strength values, both hot and cold, for the optimized brick mixes were superior to those for a commercial 98-wt-pct-MgO refractory. The best results were obtained for a natural magnesite with an adjusted C-S ratio of 3.0 and a 1.0-wt-pct addition of ZrO_2, and for a seawater periclase with an adjusted C-S ratio of 2.5 and a 0.5-wt-pct addition of MnO_2. For samples produced from chemically modified $Mg(OH)_2$ slurries, additions of both MnO_2 and ZrO_2 along with an increase in C-S ratios produced significant increases in hot MOR, similar to those resulting from chemical additions made to periclase grains. The most effective modifications were additions of MnO_2 to brine-derived periclases having a C-S ratio adjusted to 3.0. These results on chemically modified magnesia refractories indicated that such material could potentially substitute for magnesia-chrome refractories containing imported chromite.

A study *(10)* was also made to determine if the physical property improvements noted in periclase through metallic oxide additions of powders would occur in fired brick samples impregnated with water-soluble additions of metallic salts. Samples of 90- and 98-pct-MgO brick were soaked in solutions containing Al, Ca, Cr, Co, Fe, Mg, Mn, Mo, Ni, Si, Sr, Sn, Ti, or Zr ions. Additions to 98-pct-MgO brick did not generally result in statistically significant property improvements. Statistically significant improvements were noted in MOR, slag resistance, and spalling resistance of the 90-pct-MgO brick for additions of Al, Mg, or Sn. High-temperature performance of treated 90-pct-MgO refractories was equal to or approached that of 98-pct-MgO brick. The marked improvements due to Sn were obtained with additions of only 1.14 wt pct SnO_2.

DOLOMITE

Dolomite *(11)* ($CaCO_3 \cdot MgCO_3$), identified by Dolomieu in 1791, occurs as sedimentary deposits similar in nature to limestone. Geologically, some dolomites are precipitated directly from seawater, but most dolomites are a result of the alteration of calcium carbonate sediments or rocks by hypersaline brines. Good examples are the almost-pure dolomite Silurian reefs in northern Illinois, Indiana, and Ohio, and in southern Michigan. Other carbonate minerals are found associated with dolomite, but usually not in great quantities.

The Bureau estimated that 31 million st of dolomite was produced by 60 companies in 24 States during 1985. The use of dolomite in refractories is minor compared with the total amount produced. More than three-fourths of the dolomite quarried in the United States is used as an aggregate or a soil conditioner. In 1985 *(12)*, the amount of dead-burned dolomite sold or used by producers was 378,000 st, which was only 2.4 pct of the total volume of lime sold or used by producers.

The only States mentioned by Colby *(13)* as producing refractory-grade dolomites were Alabama, California, Colorado, Illinois, Michigan, Nevada, Ohio, Pennsylvania, Utah, and West Virginia. Impurities in refractory-grade dolomite are typically less than 2 pct *(14)*. Worldwide occurrence of dolomite deposits with good commercial value (good chemical and physical properties located close to the consumer) for refractories or flux usage are rare *(15)*.

Dolomite used as refractories has the CO_2 driven off and the grain densified (called dead burning) to increase the calcium stability. For high-purity, low-iron dolomite, this requires heating to 1,800° C. Lower purity dolomite for fettling purposes (the process of repairing furnace bottoms with loose dolomite grain) is generally sintered in the 1,400° to 1,600° C range. Dead-burned dolomite is generally purer than fettling grades. Iron oxide is sometimes intentionally added to the fettling grade to meet the special use requirements. As open-hearth steelmaking decreases worldwide, the need for fettling grades of dolomite will decline to zero. The open hearth was once the most important use area for refractory-grade dolomite.

The main applications of dolomite brick in the steel industry are in BOF furnaces, ladle linings, AOD vessels, and some EAF use. Ladle use of dolomite brick is not the largest consumption area in steelmaking, but it has the most promising future. Cleaner, higher quality, and more cost-effective steel is claimed to be produced by dolomite brick in ladles as more secondary steel processing occurs there. The output of dead-burned dolomite refractories, however, suffers from reduced steel output.

Dolomite bricks have a stability problem (the CaO reacts with water or CO_2, causing brick degradation) that can be overcome by special handling procedures or by coating the material with tar or pitch. Impurities such as silica can also react at high temperatures with lime in dolomite to produce beta-dicalcium silicate. On cooling, this converts via a large volume expansion to gamma-dicalcium silicate, which can cause dusting of a brick.

The overall chemistry as well as the ratio of accessory oxides to the combined MgO and CaO content affect the physical and the chemical resistance of dead-burned dolomite grains. Since the majority of dolomite grains are used in the form of organically bonded brick or specialty mixes, this is the logical form in which to measure hydration resistance. Hubble *(16)* devised a hydration test that led to the establishment of a standard test, ASTM C492-66 *(17)*.

The American Society for Testing and Materials *(18)* classifies dolomite refractory raw materials as (1) raw refractory dolomite, (2) calcined refractory dolomite, and (3) dead-burned refractory dolomite. This classification is based primarily on MgO content, loss on ignition, and impurity contents.

Samples of 14 different raw dolomites from sources in Alabama, Ohio, Pennsylvania, Missouri, Michigan, California, and Wisconsin were evaluated *(19)*. Prior to this study there were no published data on the refractory properties of domestic dolomite even though it was receiving serious consideration as a substitute for periclase. Eight of these samples were obtained from suppliers of refractory-grade dolomites; the other six were representative of dolomites that were used for nonrefractory applications. The raw materials were characterized as to chemical, physical, and thermal properties. These test results are summarized in table 4. All of the materials contained at least 49 wt pct combined MgO and CaO. Raw apparent specific gravities ranged from 2.81 to 2.87 and the raw bulk densities ranged from 2.55 to 2.80 g/cm^3. The major accessory minerals associated with these dolomites were calcite and quartz.

The thermal analyses of the materials were characterized by two endothermic peaks, one occurring between 780° and 820° C and the other occurring between 860° and 920° C. Examination of thin section photomicrographs of the raw dolomites indicated that the average crystallite grain size ranged from around 100 μm up to about 750 μm. The microstructures of two Pennsylvania dolomites that are suitable for calcining to high-density dead-burned grain in a single firing were characterized by the largest average crystallite grain sizes and by a large number of twinned grains. It is possible that the large grain sizes and occurrence of twinned grains

Table 4.—Properties of raw domestic dolomites

State of source	Chemical analysis, wt pct					Loss on ignition	Apparent specific gravity
	MgO	CaO	SiO_2	Al_2O_3	Fe_2O_3		
Alabama	20.1–20.8	30.1–30.5	1.1 –1.5	0.4–0.8	0.2–0.3	46.5–47.3	2.85–2.87
Ohio	19.5–21.2	29.6–30.6	.02–1.7	.1– .8	.1–3	45 –47.5	2.84–2.87
Pennsylvania	21 –21.3	27.6–30.8	.1 – .3	.1– .2	.2– .4	46.4–47.1	2.81–2.86
Michigan	21 –21.2	30.3–30.6	.5	.1	.1– .2	47.2–47.4	2.84
Missouri	19.2	31.2	.3	.1	3.6	45.4	2.84
Wisconsin	21.2	30.8	.3	.04	.2	46.9	2.86
California	21.7	31.1	.5	.1	.1	45.9	2.82

has some influence upon the calcination and densification of these dolomites. These Pennsylvania dolomites, along with materials from Missouri, California, and Ohio, were found to be suitable for refractory use.

FLAKE GRAPHITE

Continuous casting of steel combined with increased operating temperatures and demands for longer refractory life have focused attention on carbon-containing refractories *(20–21)*. Carbon, in the form of natural flake graphite, imparts a high degree of oxidation resistance, reduces the level of wettability by slag, and increases the thermal conductivity of the refractory. Graphite-base refractories are used in BOF, EAF, and transfer ladles, as well as pouring tubes and nozzles. The carbon-base refractories typically contain MgO, Al_2O_3, or dolomite bonded by pitch or resin with up to 30 wt pct natural flake graphite. The natural flake graphite used in refractories is totally imported. Deposits of natural flake graphite are available in the United States, but they are not economical to mine.

Flake graphite occurs as flat, platelike particles occurring in layers of metamorphosed silica-rich sedimentary rock such as quartz and mica schists, felspathic and micaceous quartzites, gneisses, and marble. Commercial importance varies considerably, depending upon flake size and carbon content *(22)*. Import of natural flake graphite for refractory consumption has held fairly constant and was about 1,000 tons in 1980, the last year the Bureau of Mines reported this figure.

Graphite, because of its unique properties, makes substitution of other materials difficult. Although carbon blocks are used in blast furnaces, synthetic graphite is considered too expensive to be substituted for graphite use. For many uses, graphite from different origins is not considered interchangeable. Many consumers use blends of graphites from different sources to eliminate supply problems.

Mag-carbon bricks, developed in the United States, were applied to a large number of EAF furnaces in Japan. The current trend is for EAF steelmakers to replace chemically bonded magnesia brick with more durable resin-bonded mag-carbon brick with carbon contents of 15 to 20 pct. Furnace service life is about 500 heats. EAF operating temperatures can be raised to over 2,000° C utilizing water-cooled sidewalls. In BOF's, brick linings containing up to 20 pct natural flake graphite have a lining life of around 750 casts. Mag-carbon bricks are also used in ladles, with a carbon content of about 10 pct. Lining life, because of the oxidizing atmosphere, is approximately 50 heats.

The optimum ash content for graphites used in mag-carbon brick is 2 pct, although graphites with ash contents as high as 10 pct are used. Research has shown that silica, alumina, and iron impurities in graphite form low melting compounds that shorten brick life. Flake size in mag-carbon refractories ranges between 150 and 710 μm. The relationship of flake length to width should be greater than 20:1 in order to minimize oxidation.

Table 5.—Natural flake graphite properties

Graphite grade	85	90	95	100	RG
Screen analysis, wt pct retained:					
Plus 18	0	0	0	0.2	0.1
Minus 18 plus 30	1.7	14.4	9.8	11.9	12.6
Minus 30 plus 40	23	26.4	25.9	27.7	31.2
Minus 40 plus 60	59.7	44.3	48.1	48.1	47.9
Minus 60 plus 80	14.3	12.1	13.8	10.7	7.6
Minus 80 plus 100	1.2	1.5	1.6	1.1	.5
Minus 100	.2	1.3	.9	.3	.1
Ash, wt pct	13.7	10.6	6	0	.8
Ash chemistry, wt pct:					
SiO_2	55.9	45.2	43.8	NA	23.4
Fe_2O_3	11.8	23.7	26.1	NA	21.9
Al_2O_3	26.2	22.8	25.7	NA	.9
MgO	1.1	6.8	4.3	NA	.7
CaO	1	1.3	1.2	NA	2.2
B_2O_3	ND	ND	ND	NA	43.75
Ash, PCE	14–15	6–7	6	NA	NA

NA Not analyzed. ND Not detected.

The need to develop a substitute material for natural flake graphite in basic refractories has been recognized *(23)*. However, fundamental high-temperature engineering data, such as are available on mag-carbon systems, does not exist for dolomite-carbon refractories. A study at the Bureau's Tuscaloosa (AL) Research Center *(24)*, in cooperation with the J. E. Baker Co., on the properties of several flake graphites (listed in table 5) was initiated. The grade 100 is a thermally purified material, and the grade RG is a material treated with boron to increase oxidation resistance.

The five grades of natural flake graphite were used to evaluate the effects of different amounts of graphite on the physical and thermal properties of dolomite-carbon refractories containing 4 pct phenolic resin binder. Refractory formulations were mixed as 150-lb batches in a high-speed countercurrent mixer. Brick of 6- by 9- by 3½-in dimensions were pressed at 20,000 psi and cured on a commercial schedule. One set of samples contained 10-wt-pct additions of the five different graphites, and another set contained increasing quantities (0, 5, 10, 15, 20, and 30) of a grade 90 graphite. Changes in oxidation resistance at 1,093° C, hot strength from 260° to 1,510° C, and deformation under load at 1,500° C were determined.

Results indicated that carbon purity of 10-wt-pct-graphite additions did not influence hot strength or deformation under load. When the quantity of grade 90 natural flake graphite addition varied between 0 and 30 wt pct, hot MOR was highest and deformation under load lowest with 10-wt-pct additions. As the hot MOR test temperature was increased from 260° to 1,510° C, the strength difference observed between 0- and 30-wt-pct additions of a grade 90 graphite became less. Additions of a boron-treated graphite caused significantly higher strength and lower deformation under load at high temperatures, while an addition of ball clay significantly reduced strength and increased deformation.

A subsequent study is being conducted to evaluate substitute synthetic carbon materials for natural flake graphite in dolomite-carbon refractories. Polyacrylonitride and pitch-carbon fibers of ⅛- and 1/16-in length and carbon flakes punched out of synthetic graphite paper were tested. Commercial-grade refractory mixes were prepared and pressed into bricks. Carbon fiber additions above 2 pct resulted in rebound or springback during pressing. Two-percent carbon fiber additions resulted in hot strengths of 260 psi versus 600 psi for samples with natural flake graphite additions.

REFERENCES

1. Van Dreser, M. L., and J. E. Neely. Refractories for Steelmaking in the U.S.A . . . Current Practice and Future Trends. Pres. at First International Conference on Refractories, Tokyo, Japan, Nov. 15, 1983, 28 pp.; available upon request from T. A. Clancy, BuMines, Tuscaloosa, AL.

2. Kramer, D. A. Magnesium Compounds. Ch. in BuMines Minerals Yearbook 1985, v. 1, 1987, pp. 661–667.

3. Coope, B. Magnesia. Sec. in "IM" Refractories Survey 1986—Raw Materials for the Refractories Industry, ed. by E. M. Dickson, 1986, pp. 28–42.

4. McLendon, J. T., N. S. Raymon, and H. Heystek. Relationship of Mineralogical and Chemical Composition of Refractory Periclase to Modulus of Rupture at 1,500° to 1,600° C. BuMines RI 8386, 1979, 18 pp.

5. Buist, D. S., A. Hatfield, and H. Pressley. Modulus of Rupture as an Index of Potential Refractory Performance in Service. Trans. J. Br. Ceram. Soc., v. 68, 1969, pp. 45–47.

6. Gilpin, W. C., and D. R. F. Spencer. New Developments in Dead-Burnt Magnesite and Dead-Burnt Dolomite. Refrac. J., v. 47, No. 4., Apr. 1972, pp. 4–16.

7. Jackson, B., and J. Laming. The Significance of Mechanical Properties of Basic Refractories at Elevated Temperature. Trans. J. Br. Ceram. Soc., v. 68, 1969, pp. 21–28.

8. Raymon, N. S. Influence of Selected Additives and $CaO:SiO_2$ Ratio on High Temperature Strength of MgO Refractories. BuMines RI 8732, 1982, 8 pp.

9. Bennett, J. P., and T. A. Clancy. Magnesia Refractories Produced From Chemically Modified Periclase Grains and $Mg(OH)_2$ Slurries. BuMines RI 8848, 1984, 14 pp.

10. Bennett, J. P. High-Temperature Properties of Magnesia-Refractory Brick Treated With Oxide and Salt Solutions. BuMines RI 8980, 1985, 11 pp.

11. Carr, D. D., and L. F. Rooney. Limestone and Dolomite. Ch. in Industrial Minerals and Rocks. AIME, 1975, 1360 pp.

12. Pelham, L. Lime. Ch. in BuMines Minerals Yearbook 1985, v. 1, 1987, pp. 635–644.

13. Colby, S. F. Occurrence and Uses of Dolomite in the United States. BuMines IC 7192, 1941, 21 pp.

14. Hopkins, D. A. Dolomite. Am. Ceram. Soc. Bull., v. 66, No. 5, 1987, pp. 759–760.

15. Dickson, T. Dolomite. Sec. in "IM" Refractories Survey 1986—Raw Materials for the Refractories Industry, ed. by E. M. Dickson, 1986 pp. 44–46.

16. Hubble, D. H., and W. J. Lackey. Hydration Test for Dead-Burned Dolomite. Am. Ceram. Soc. Bull., v. 41, No. 7, 1962, pp. 442–446.

17. American Society for Testing and Materials. Standard Test Method for Hydration of Granular Dead-Burned Refractory Dolomite. C492-66 in 1981 Annual Book of ASTM Standards: Part 17, Refractories, Glass, Ceramic Materials; Carbon and Graphite Products. Philadelphia, PA, 1981, pp. 404–405.

18. _____. Standard Classification of Granular Refractory Dolomite. C468-70 in 1981 Annual Book of ASTM Standards: Part 17. Refractories. Glass Ceramic Materials; Carbon and Graphite Products. Philadelphia, PA. 1981, pp 383–384.

19. Clancy, T. A. Dolomite Refractories, and Their Potential as Substitutes for Imported Chromite. BuMines IC 8913, 1983, 18 pp.

20. Brown, A. The Properties of Ceramic Graphite Bodies. Refrac. J., No. 2, Mar./Apr. 1985, pp. 7–10.

21. Cooper, C. F. Refractory Applications of Carbon. Trans. J. Br. Ceram. Soc., v. 84, 1985, pp. 48–53.

22. Kenan, W. M. Graphite. Am. Ceram. Soc. Bull., v. 66. No. 5, 1987, pp. 762–763.

23. Hayashi, T. Recent Trends of Refractory Technologies in Japan. Taikabutsu Overseas. v. 4, No. 1, 1984, pp. 3–19.

24. Bennett. J. P. The Effect of Different Natural Flake Graphite Additions on the High-Temperature Properties of a Dolomite-Carbon Refractory. BuMines RI 9111, 1987, 12 pp.

BASIC RESEARCH ON CORROSION OF IRON-BASED MATERIALS

By David R. Flinn[1]

ABSTRACT

The Bureau of Mines has conducted corrosion-related research at a significant level for the past three decades. Much of this research consisted of exposure testing to evaluate commercially available metals and alloys for use in minerals and metals processing environments and to determine the corrosion behavior of newly available metals such as Ti, Nb, Ta, and Zr in selected environments. In recent years a significant portion of the research has been redirected toward the development of a fundamental understanding of the roles of alloy composition and microstructure and of the process environment in determining corrosion behavior. This paper discusses the importance of this understanding to the efficient utilization of mineral resources and examples are given of research designed to accomplish these objectives.

INTRODUCTION

Corrosion is the degradation of the mechanical, physical, and chemical properties of materials resulting from chemical-electrochemical processes and the interaction of these processes with mechanical and wear processes. The cost of corrosion to the U.S. economy was estimated to be $70 billion in 1975, or about 4.2 pct of the gross national product *(1)*.[2]

With current technology, approximately 15 pct of that cost could have been avoided and the opportunity for even greater savings exists with the development of new and improved corrosion control and prevention measures. The benefits of corrosion-related research and development activities are well recognized in terms of the savings in energy and materials to reduce excess capacity, enhance production, reduce product losses, lower maintenance, and improve safety. In a recent report by the National Materials Advisory Board *(2)*, the value of corrosion control was estimated ". . . to have an economic impact from fifty- to a hundred-fold greater than its dollar value." A further benefit to be expected from the development of corrosion control technologies is the conservation of critical and strategic materials by substitution of more abundant and domestically available materials and by improving service life in environments used in existing technologies and the more severe environments of new and emerging technologies.

In a recent report *(3)* published by Battelle Columbus Laboratories and based on a conference of materials engineers, corrosion scientists, and electrochemists on corrosion control and prevention, 60 pct of the highest priority research needs applied to corrosion problems experienced in the minerals and materials processing industries. The same report *(3)* pointed out that, for the primary metals industry, corrosion problems are usually sidestepped by operating processes at reduced energy efficiency.

An important aspect of the Bureau of Mines mission is the development and assessment of technological alternatives in mineral processing and related materials development to support the security and economic well-being of the Nation with regard to mineral and material processing, performance, utilization, and recycling. The Bureau conducts long-range and generic basic research on corrosion phenomena important to all minerals and materials processing industries. The objective of this research is to provide a scientific understanding of corrosion processes, including the roles of material composition and structure as well as the role of the environments to which the material is likely to be exposed. Through this understanding it is possible to determine cost-effective corrosion control strategies that may involve such options as materials substitution or materials protection. This research has the goal of providing the underpinning for the development of improved and new technology for the minerals and materials processing industries. A further goal is the promotion of conservation of critical and strategic materials throughout the industrial community. These goals are reflected in the many accomplishments of the Bureau in corrosion research achieved over the past three decades *(4)*. Most of this research has been concerned with aqueous environments. The work discussed here will be limited to aqueous environments and to iron-based alloys.

---

[1] Supervisory research chemist, Albany Research Center, Bureau of Mines, Albany, OR.

[2] Italic numbers in parentheses refer to items in the list of references at the end of this paper.

ROLE OF ALLOY COMPOSITION AND STRUCTURE

Except for comparatively rare instances, most metals and alloys are not thermodynamically stable with respect to even the most common environments. Fortunately, some of these metals and alloys can be used in many environments because they corrode at low rates. The chemical composition of an alloy strongly influences its corrosion resistance. Tomashov *(5)* has reviewed the mechanisms by which different alloying elements can affect corrosion resistance. Some elements increase thermodynamic stability, some retard cathodic reactions (hydrogen evolution, oxygen reduction) that are required to support the anodic alloy dissolution, while others retard the anodic dissolution reaction itself *(5)*.

This latter mechanism, which usually involves the formation of a protective (''passivating'') surface film, is the most common, and scientifically most interesting, way that alloys resist dissolution. Reviews of the processes thought to be involved in the formation of protective passive films on alloys are widely available in the literature (as examples, see references 6 through 8). Even with this knowledge, there remains a very incomplete understanding of how the elemental composition and the structure (homogeneity, degree of crystallinity, defect structures, etc.) of an alloy influence the formation of protective passive films. An important research area of continuing interest in the Bureau is to gain a fundamental understanding of how the composition and structure of an alloy influence the formation of corrosion films that can provide resistance to aggressive environments.

BUREAU OF MINES FUNDAMENTAL CORROSION RESEARCH[3]

EFFECTS OF ENVIRONMENT

Corrosion is an electrochemical process involving species from the alloy and from the environment. For this reason, meaningful research on corrosion processes can only be accomplished when the chemistry of both the alloy and the environment are controlled and/or characterized. The importance of a controlled environment was demonstrated for electrochemical polarization studies of iron in sulfuric acid *(9)*. The electrochemical corrosion behavior of iron in solutions made from distilled water and reagent-grade sulfuric acid was shown to be irreproducible. For some tests, a potential range where the iron was passive would be observed, while no passivation was observed in other, apparently identical, tests. When special precautions were taken to use high-purity deionized water and special high-purity acid, the polarization studies yielded very consistent results. In the same study *(9)*, solution purity was found to have much less influence on the electrochemical corrosion behavior of Fe-18Cr.

In a later study *(10)*, the electrochemical behavior of Fe-18Cr was investigated in an even higher purity environment. Very carefully purified solutions and gases, gastight cells, and a special high-purity Fe-18Cr alloy wire were used. In this ultra-high-purity system, the Fe-18Cr alloy did not corrode in a 1*N* H_2SO_4, H_2 saturated solution. but instead attained a potential very near that for a reversible hydrogen electrode. This potential was maintained for months in the solution.

It was determined *(10)* that the alloy could be caused to corrode by cathodically polarizing the electrode; the Fe-18Cr alloy could be returned to the noncorroding state by a brief anodic polarization of the electrode. Specially developed electrochemical techniques were used in this study *(10)* to prove that metal-oxygen species were not present in significant amounts on the electrode surface and could not be the cause of the behavior observed.

These two studies *(9–10)* are examples of why it is important to characterize and/or control the materials and the environment being used. Although such extreme purification procedures do not represent realistic situations, they do provide important baseline information that can be used to evaluate the effects of controlled additions of species, such as oxygen gas or chloride ion, that could be expected to be present in many important aqueous environments.

A more recent study was conducted to determine the effect of oxygen on the formation of passive films on stainless steel at open circuit conditions *(11)*. An Fe-18Cr alloy was selected for the study because it does not spontaneously passivate from a state of corrosion when oxygen is added to the environment, but it can be passivated by electrochemical polarization. Because of these characteristics it was possible to determine the amount of dissolved oxygen needed in 1*N* H_2SO_4 to maintain passivity following controlled potential passivation. In addition, the composition of the passive film as a function of potential was determined using surface analytical techniques. The effect of solution oxygen partial pressure on the potential-time relationship of Fe-18Cr was examined by first passivating the alloy for 80 min at 0.6 V versus the normal hydrogen electrode (NHE) potential in nitrogen-saturated (1*N*) H_2SO_4, and then simultaneously releasing the potential to open circuit and substituting various O_2-N_2 gas mixtures for the nitrogen.

The results of these tests are shown in figure 1. For solution oxygen partial pressures below 0.045 atm (1.7-ppm O_2 solution concentration) the potential of the passivated alloy was observed to fall into the range of active corrosion after about 2×10^3 min. For solution oxygen partial pressures above this value, the open circuit potential of the alloy was observed to decrease to a minimum and then increase again. At times in excess of 10^4 min (not shown), the potential leveled off near 0.6 V. The 1.7-ppm oxygen concentration appears to be the minimum amount required to maintain the alloy in the passive state under the experimental conditions used *(11)*. The mechanism for breakdown of these passive films probably involves trace impurities, so that the exact level of oxygen required to maintain the passive film will differ for various solutions purities.

Also discussed in this paper *(11)* were the effect of time and potential on the composition of the passive film as determined by Auger electron spectroscopy (AES). Fe-18Cr was electrochemically passivated at 0.6 V for 80 min in oxygen-saturated solution (approximately 29-ppm O_2 concentration) and released to open circuit. The chromium atomic fraction compared to iron in the corrosion film was found to remain at approximately 0.45 over the potential-time region shown in figure 1 up to approximately 10^3 min. At longer times and higher potentials, the chromium fraction in the film increased rapidly, approaching 0.65 at longer times. These findings were also supported by X-ray photoelectron spectroscopy (XPS) analyses *(11)* that showed a decrease in the iron content of the film with increasing potential and a simultaneous

[3] As will be demonstrated in the examples that follow, the understanding of corrosion processes cannot be separated from the environments and materials involved. For this reason, the fundamental corrosion research effort in the Bureau is multidisciplinary, involving chemists, physicists, engineers, metallurgists, and materials scientists.

decrease in film thickness. These results demonstrate the dynamic nature of the passive film on chromium-containing iron-based alloys. They indicate that the behavior of many stainless steels in acidic environments may well be as dependent on such variables as solution oxygen content and impurity levels as on any chemical or electrochemical treatment of the alloy.

The effect of chloride ion on the passive state of Fe-18Cr and of AISI Type 430 stainless steel (430SS) was determined in a study *(12)* similar to that described previously. The alloys were electrochemically passivated at 0.6 V NHE for 80 min in oxygen saturated 1*N* H_2SO_4. After the period of passivation the alloy was released to open circuit, and a behavior similar to that shown in figure 1 was observed. At selected times chloride ion (as NaCl), in amounts ranging from 5 to 44 ppt Cl^-, were added and the potential-time response was observed. The time difference between adding the chloride ion and reaching a state of corrosion is defined as the induction time. These times are shown schematically in figure 2, where t_B and t_C are the induction times for the addition of chloride ion in the minimum potential region and in the increasing potential region, respectively. It was found, as expected, that increasing amounts of chloride ion decreased the induction times. However, very significant increases in induction time were observed in cases where the chloride ion was added after approximately 100 min. In the previously mentioned study *(11)* it was found that passive film became thinner and richer in chromium at times in solution of 100 min or longer. Investigations of the type reported here *(11–12)* provide significant insight into the roles that environmental species play in the formation and breakdown of protective passive films.

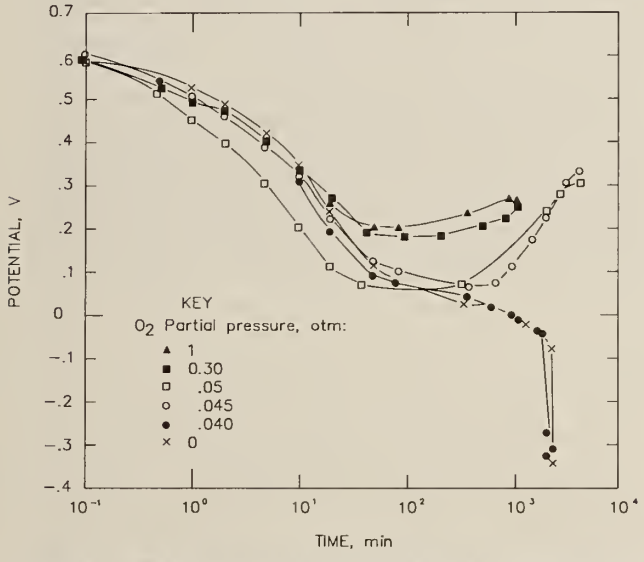

Figure 1.—Effect of oxygen partial pressure on potential vs time behavior of Fe-18Cr samples released to open circuit after being passivated for 80 min at 0.6 V in 1*N* H_2SO_4 at 30° C. Data from Covino *(11)*.

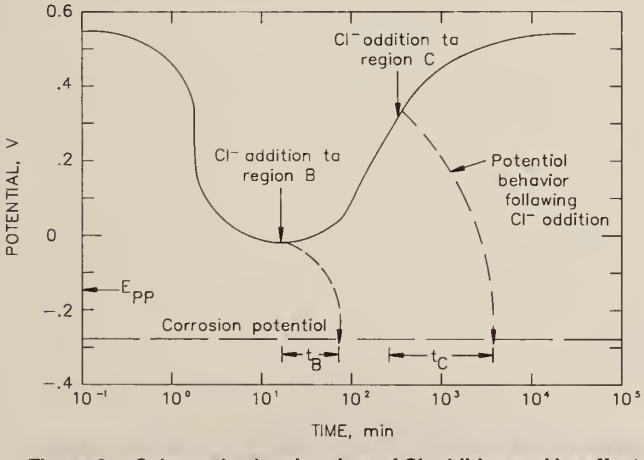

Figure 2.—Schematic showing time of Cl addition and its effect on potential-time behavior of passivated Fe-18Cr and 430SS. E_{PP} is the primary passivation potential. Data from Covino *(12)*.

EFFECTS OF ALLOY COMPOSITION AND STRUCTURE

The Bureau has conducted detailed studies of the effects of alloying elements on the corrosion behavior of steels. Ion implantation was one method used extensively for preparing iron-based alloys containing preselected amounts of the desired alloying element *(13–18)*.

Ion implantation is a process whereby ions of the desired alloying element are accelerated in a vacuum to energies in the range of 20 to 100 keV and allowed to impact a target of the base metal *(13)*. The ions penetrate this target to a mean depth on the order of a few hundred angstroms, with an approximately Gaussian depth distribution. This technique offers numerous advantages over other alloy preparation methods, including speed of preparation and relatively low cost for small amounts of experimental alloys, the very small amount of alloying element required, the wide range of alloy concentrations that can be formed, the preparation of alloys with optimum surface and bulk properties for a given application, and the preparation of certain metastable alloys that cannot be formed by conventional techniques. These attributes make ion implantation a very useful tool for preparation of model alloys for corrosion research.

In the 1970's the Bureau conducted pioneering studies on the use of ion implantation as a technique for the preparation of alloys for corrosion studies. It was proven *(14–15)* that nickel or chromium implanted into iron produced Fe-Ni or Fe-Cr alloys having corrosion properties identical to those of bulk alloys of similar composition. Because of the thinness of the ion implanted layer, these "surface" alloys obviously would lose their corrosion resistance if exposed to aggressive environments for extended times. Even so, for the period of time that this alloy layer is intact, it can be expected to behave in a manner similar to that of a bulk alloy of the same composition.

In another study *(16)*, it was shown that chromium-implanted iron exposed to air at 320° C oxidized at a rate identical to an equivalent bulk alloy for times as great as 1,000 h, and that the oxide thickness was identical on the two alloys. In the same study *(16)* it was shown that aluminum implantation into titanium produced an alloy that, when coupled to aluminum in a NaCl solution, greatly reduced the galvanic corrosion loss of aluminum compared to that produced when aluminum was coupled to unimplanted titanium. The implanted aluminum was found to reduce the rate of oxygen reduction on the titanium by as much as a factor of 40.

The effects of ion implantation on stress corrosion cracking *(17)* and on corrosion fatigue *(18)* of iron-based alloys have also been examined. Very significant effects were noted on the stress corrosion cracking (SCC) behavior of AISI Type 316 stainless steel (316SS) in boiling $MgCl_2$ by implanted Si, N, or Ar. Argon implantation reducted the time to failure by 30 to 40 pct compared to unimplanted samples for a total implant dose of 3×10^{16} ions/cm (approximately equivalent to 20 at. pct in the implanted volume). This detrimental effect of argon was caused by ion damage to the

surface region during implantation (approximately 40 nm in depth). Implantation of nitrogen into the 316SS resulted in a similar decrease in time to failure by SCC.

Examination of the nitrogen-implanted surface by scanning electron microscopy (SEM) following these tests showed that portions of the surface had been ruptured along slip planes by an explosive escape of gas from below the surface. An elemental depth profile. obtained by AES, of the surface of a nitrogen-implanted sample after SCC failure is shown in figure 3. A significant amount of nitrogen remained in the sample following the test, indicating that much of the nitrogen must have been present within the alloy rather than just in grain boundaries.

Implanted silicon had a much different effect on the SCC behavior of 316SS. As shown in figure 4, the resistance to SCC increased approximately linearly with the fluence (atoms/cm^2) of implanted silicon. Examination of the silicon-implanted samples following exposure to the $MgCl_2$ showed that the surface was covered by a film that was rich in silicon and magnesium. This film passivated the surface, reducing the general corrosion rate. Silicon also reduced the SCC crack propagation rate. This effect was not anticipated because of the very thin implanted region.

In another study *(18)*, the effects of implanting Ti or a combination of Mo and Ta on the corrosion fatigue behavior of 1018 carbon steel were examined. The Mo plus Ta implanted steels behaved no differently from unimplanted steel in the 0.1*N* H_2SO_4 solution, with apparently identical corrosion potentials and surviving about the same number of cycles in a rotating beam test prior to failure. The steels were adversely affected by the titanium implantation, however. The corrosion rate of the steel was approximately doubled, and the fatigue life decreased linearly with the titanium implant dose. An approximate 15 at. pct concentration of titanium decreased the cycles to failure by about 50 pct compared to the unimplanted steel. Examination by SEM of the surface of the titanium-implanted steel following failure revealed the presence of a film containing titanium and iron, with small iron crystallites penetrating this film. The reduced fatigue resistance is thought to be caused by an accelerated corrosion at these small crystallites.

Another technique that has been used in Bureau research to prepare experimental alloys with controlled composition and structure is vapor deposition *(19)*. This technique involves sputtering a target (or targets) composed of the elements to be incorporated in the desired alloy. Energetic inert gas ions are used to remove atoms from the target by impact. The sputtered atoms are quenched onto a substrate to form the alloy of interest. This quenching process is equivalent to cooling a molten alloy so rapidly that virtually no movement of the deposited atoms occurs following deposition when the substrate is cold. Depending on such factors as the substrate temperature and the rate of deposition, the alloy produced may be either crystalline or amorphous.

One alloy system produced by vapor deposition that showed extremely good corrosion resistance for a wide range of compositions was Fe-Zr *(19)*. Vapor deposited Fe-Zr alloys were determined to be amorphous (no long-range crystalline ordering) over the range of composition from $Fe_{90}Zr_{10}$ through $Fe_{33}Zr_{67}$. Electrochemical polarization studies showed the $Fe_{90}Zr_{10}$ to be approximately as corrosion resistant as Fe-18Cr in 1*N* H_2SO_4.

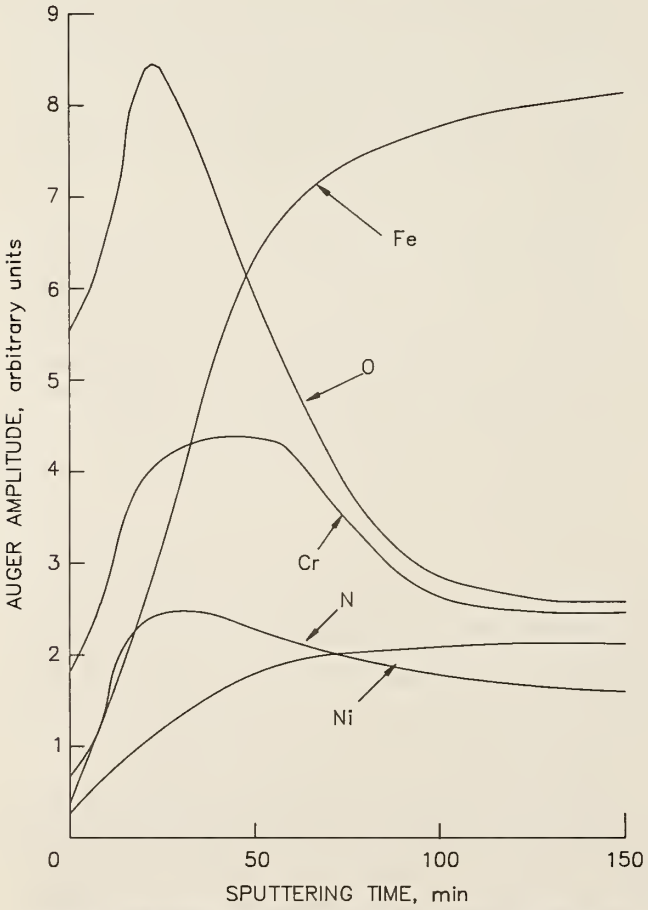

Figure 3.—Elemental depth profile as obtained by Auger electron spectroscopy for nitrogen-implanted 316SS indicating retained nitrogen after exposure to boiling $MgCl_2$. Data from Walters *(17)*.

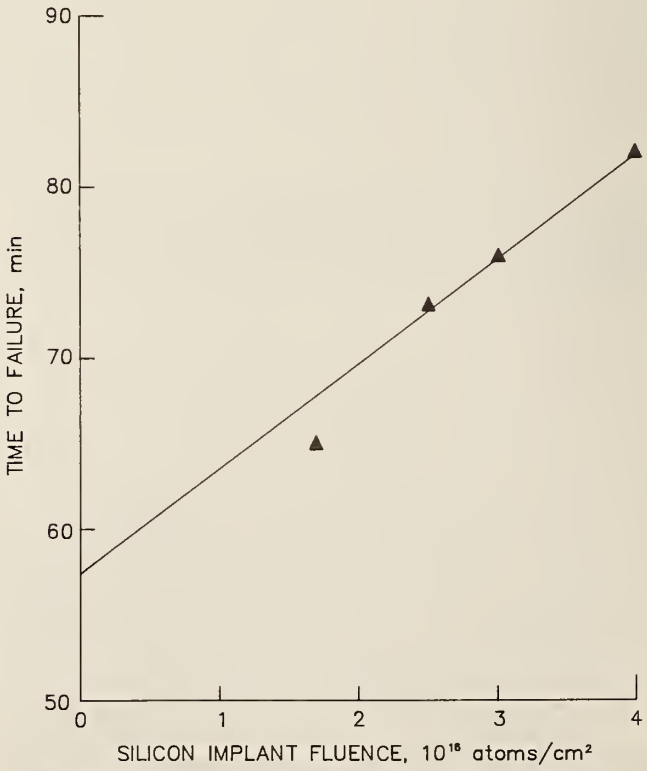

Figure 4.—Relationship of time to failure of 316SS in boiling $MgCl_2$ as a function of amount of silicon implanted. Data from Walters *(17)*.

The electrochemical polarization response for the $Fe_{33}Zr_{67}$ alloy is compared in figure 5 to that of Fe, Fe-18Cr, and Zr in 1*N* H_2SO_4 *(19)*. Over the range of potentials from open circuit corrosion (ca. -0.2 V) to the high positive potentials where oxygen evolution occurs (ca. 1.2 V), the $Fe_{33}Zr_{67}$ alloy has approximately the same corrosion resistance as zirconium. AES analysis of the Fe-Zr alloys subsequent to the polarization studies showed that the surface corrosion film is composed predominately of zirconium and oxygen, with the iron to zirconium ratio in the film being significantly reduced compared to its value in the interior of the alloy.

An additional technique that has been applied to the preparation of experimental alloys is laser processing, in which a laser is used to melt a thin layer of a surface. When a thin coating is present on the material being processed, the laser beam can provide a means of melting and mixing the coating into the surface of the substrate. The electrochemical behavior of a series of Fe-Cr alloys prepared using a Nd-YAG pulsed laser has recently been reported *(20)*. The electrochemical behavior of these alloys exhibited small, but important differences from those observed for similar bulk alloys. Some, but not all, of these differences were found to be caused by the presence of a very protective oxide film on the surface resulting from the incomplete exclusion of oxygen during the laser processing.

A three-dimensional chromium concentration plot, obtained by electron microprobe measurements of a cross section of the laser processed region, is shown in figure 6. The original bulk material was a Fe-5Cr alloy. Laser mixing of a thin coating with the substrate produced an approximately Fe-15Cr alloy to a depth of from 25 to 30 μm. On top of this alloyed region is a chromium-rich oxide film, approximately 5 μm thick that was produced during processing. This oxide layer is clearly visible by optical microscopy or SEM examination. Based on the microprobe resolution on the order of 1μm, only slight variations in chromium concentration are observable within the laser-alloyed region. However, chemical etching of the cross-sectioned sample resulted in the upper portion of the laser alloy, equivalent to the region in figure 6 from approximately 5 to 15 μm on the depth axis, becoming extremely roughened. From approximately 15-μm depth within the alloy and continuing into the unalloyed substrate, the etched surface was very smooth, with only minor grain boundary dissolution. Because of the large amount of irregular dissolution that occurred within grains in the upper portion of the laser-alloyed region, with features having dimensions of the order of 0.1 μm, it was determined that an elemental analysis method having better resolution than the electron microprobe (fig. 6) was required to establish whether the laser-alloyed regions were compositionally homogeneous.

Scanning transmission electron microscopy combined with energy dispersive X-ray spectroscopy (STEM-EDS) was utilized to investigate at high resolution the microstructure and microchemistry within the laser-alloyed region. For this study a second alloy, also prepared by the laser processing technique, was used. This alloy contained approximately 18 wt pct Cr in the laser-processed region and the substrate contained 9 wt pct Cr. The alloy and substrate regions were analyzed as a function of depth into the sample for a thinned cross section. For these STEM-EDS analyses, a 200-nm analysis interval was used with a 50-nm electron beam (probe) size. The results of these analyses are shown in figure 7.

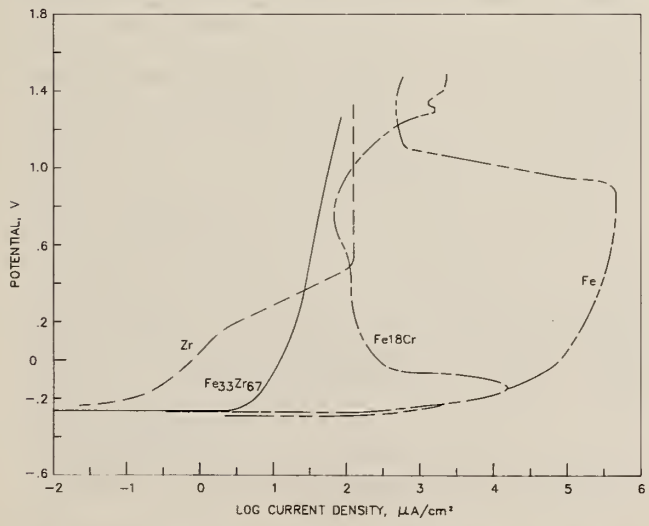

Figure 5.—Polarization curves in deaerated 1*N* H_2SO_4 for $Fe_{33}Zr_{67}$ amorphous alloy compared to Fe, Fe-18Cr, and Zr. Data obtained at polarization rate of 60 V/h. Data from McCormick *(19)*.

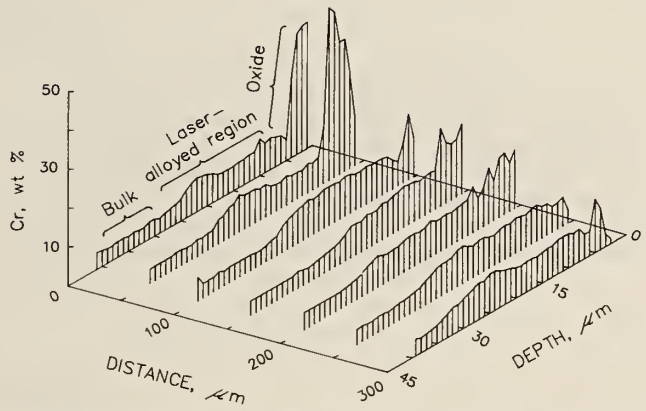

Figure 6.—Three-dimensional chromium concentration plot of a typical laser-processed alloy showing surface oxide, laser-alloyed region, and bulk substrate. Chromium concentrations in bulk and laser-processed region are approximately 5 and 15 wt pct, respectively. Data from Molock *(20)*.

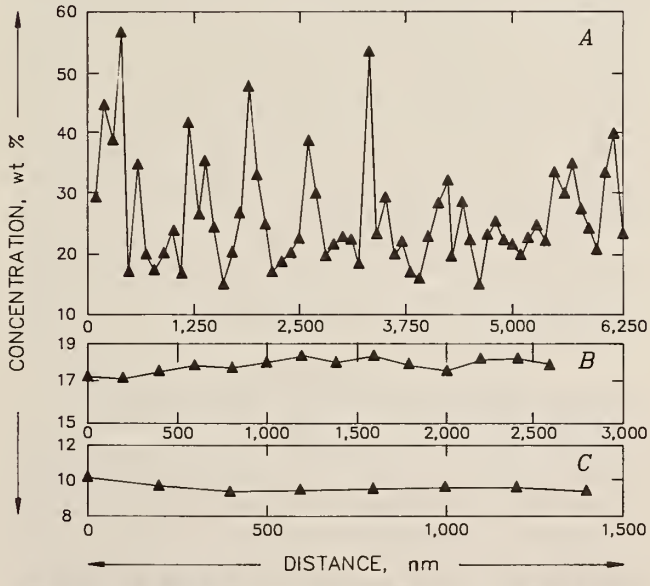

Figure 7.—STEM-EDS chromium concentration profiles. A, Profile typical of upper portion of laser-processed region, indicating extensive microsegregation; *B*, profile typical of lower portion of laser-processed region; C, profile of Fe-9Cr substrate. Data from Molock (*20*).

By using this very small probe size it was possible to detect inhomogeneities in elemental concentration of a few percent over a distance as short as 100 nm. The chromium concentration in the upper portion of the laser processed region is shown in figure 7*A*. Referring to figure 6, this analysis trace was taken in a region corresponding on the depth scale from about 7 to 13 μm. It is evident that the chromium concentration is highly erratic in this region, and is the cause of the unusual electrochemical polarization and chemical etching behavior mentioned earlier. It should be pointed out that if the data shown in figure 7*A* were grouped in sets of 10 points and the average concentration was plotted, the result would be an apparently uniform chromium level of about 18 wt pct for the six calculated averages, similar to what was measured by the microprobe method. For the lower portion of the laser processed region (fig. 7*B*) and the substrate (fig. 7*C*), the chromium concentration appears to be uniform based on the STEM-EDS analysis using the 50-nm probe diameter and 200-nm sampling interval.

The cause of the microsegregation of chromium shown in figure 7*A* was attributed *(20)* to impurities migrating in the liquid ahead of the solidification front subsequent to the laser processing, and to supercooling and formation of nonequilibrium phases in the last of the liquid that solidifies. Whatever the cause of this microsegregation, its effects on the corrosion properties were much more significant than would have been expected considering the scale of variation.

CONCLUSIONS

During the past few years, several new techniques have become available for preparing new alloys with interesting and potentially useful properties. There also is an increasing availability of analytical instruments having much greater sensitivity and spatial resolution capabilities. This combination has already resulted in an improved understanding of the roles of composition and structure in controlling alloy properties and will be of increasing importance in the future. These techniques are just as applicable to the improvement in properties of existing classes of alloys as they are for development of new materials.

Examples of how the improved understanding of corrosion processes and materials performance have been applied to real problems are given in reference 4.

REFERENCES

1. Bennett, L. H., J. Kruger, R. L. Parker, E. Passaglia, C. Reimann, A. W. Ruff, H. Yakowitz, and E. B. Berman. Economic Effects of Metallic Corrosion in the United States, Part I. NBS Spec. Publ. 511-1, 1978, 65 pp.

2. National Materials Advisory Board—Commission on Engineering and Technical Systems—National Research Council. New Horizons in Electrochemical Science and Technology (U.S. Dep. of Energy contract B-M44SS-A-Z). NAS, Publ. NMAB 438-1, 1986, 147 pp.

3. Battelle Columbus Laboratories. Research Needs for Corrosion Control and Prevention in Energy Conservation Systems (U. S. Dep. Energy contract DE-AC06-76RL01830/MPO-B-F6814-A-K). Feb. 1985, 74 pp.

4. Flinn, D. R. Optimization of Materials Selection Through Corrosion Science. Paper in Chromium-Chromite: Bureau of Mines Assessment and Research. Proceedings of Bureau of Mines Briefing Held at Oregon State University, Corvallis, OR, June 4-5, 1985, comp. by C. B. Daellenbach. BuMines IC 9087, 1986, pp. 115–124.

5. Tomashov, N. D. Corrosion-Resistant Alloys and Prospects for Their Development. Protection of Metals (Engl. Transl. of Z. Metallov), v. 17, No. 1, 1981, pp. 11–25.

6. Uhlig, H. H. Passivity in Metals and Alloys. Corros. Sci., v. 19, No. 11, 1979, pp. 777–791.

7. Sato, N., and G. Okanoto. Electrochemical Passivation of Metals. Ch. in Comprehensive Treatise of Electrochemistry, ed. by J. O'M. Bockris, B. E. Conway, E. Yeager, and R. E. White. Plenum (New York), v. 4, 1981, pp. 193–245.

8. Hashimoto, K. Passivation of Amorphous Metals. Paper in Proceedings of Fifth International Symposium on Passivity: Passivity of Metals and Semiconductors, ed. by H. Froment (Proc. Conf. Bombannes, France, May 30-June 3, 1983). Elsevier, 1983, pp. 235–246.

9. Driscoll, T. J., B. S. Covino, Jr., and M. Rosen. Electrochemical Corrosion and Film Analysis Studies of Fe and Fe-18Cr in 1*N* H_2SO_4. BuMines RI 8378, 1979, 33 pp.

10. Rosen, M. Electrochemical Corrosion of Iron-Chromium Alloys Under Ultra-High-Purity Conditions. BuMines RI 8425, 1980, 66 pp.

11. Covino, B. S., M. Rosen, T. J. Driscoll, T. C. Murphy, and C. R. Molock. The Effect of Oxygen on the Open-Circuit Passivity of Fe-18Cr. Corros. Sci., v. 26, No. 2, 1986, pp. 95–107.

12. Covino, B. S., and M. Rosen, Induction Time Studies of Fe-18Cr and 430SS Under Open Circuit Conditions in Chloride-Containing Sulfuric Acid. Corros., v. 40, No. 4, 1984, pp. 141–146.

13. Sartwell, B. D., A. B. Campbell III, B. S. Covino, Jr., and P. B. Needham, Jr. Characterization of Alloys Formed by Ion Implantation. BuMines RI 8434, 1980, 29 pp.

14. Covino, B. S., B. D. Sartwell, and P. B. Needham. Anodic Polarization Behavior of Fe-Cr Surface Alloys Formed by Ion Implantation. J. Electrochem. Soc., v. 125, No. 3, 1978, pp. 366–369.

15. Covino, B. S., P. B. Needham, and G. R. Conner. Anodic Polarization Behavior of Fe-Ni Alloys Fabricated by Ion Implantation. J. Electrochem. Soc., v. 125, No. 3, 1978, pp. 370–372.

16. Sartwell, B. D., A. B. Campbell, B. S. Covino, and T. J. Driscoll. Applications of Ion Implantation to Metallic Corrosion. IEEE Trans. Nucl. Sci., v. NS-26, No. 1, 1979, pp. 1670–1676.

17. Walters, R. P., N. S. Wheeler, and B. D. Sartwell. The Effects of Surface Modification on the Stress Corrosion Cracking Behavior of 316 Stainless Steel. Corros., v. 38, No. 8, 1982, pp. 437–445.

18. Sartwell, B. D., R. P. Walters, N. S. Wheeler, and C. R. Brown. The Effect of Ion-Implanted Alloy Additions on the Linear Polarization and Corrosion Fatigue Behavior of Steel. Paper in Corrosion of Metals Processed by Directed Energy Beams, ed. by C. R. Clayton and C. M. Preece. Trans. Metall. Soc.-AIME, Warrendale, PA, 1982, pp. 53-73.

19. McCormick, L. D., N. S. Wheeler, C. R. Molock, and C. L. Chien. Corrosion Properties of Amorphous Iron-Zirconium Films in 1*N* Sulfuric Acid. J. Electrochem. Soc., v. 131, No. 3, 1984, pp. 530–534.

20. Molock, C. R., R. P. Walters, and P. M. Fabis. Effect of Laser Processing on the Electrochemical Behavior of Fe-Cr Alloys. J. Electrochem. Soc., v. 134, No. 2, 1987, pp. 289–294.

FUNDAMENTALS OF STAINLESS STEEL ACID PICKLING PROCESSES

By Bernard S. Covino, Jr.[1]

ABSTRACT

Research on the pickling of stainless steels has been conducted by the Bureau of Mines in cooperation with the American Iron and Steel Institute (AISI). The objectives of the research were to reduce the loss of the strategic and critical metals chromium and nickel, to reduce the use of HNO_3 and HF acids, and to reduce the quantity of waste pickling solutions generated. The model used to design the research consisted of removal of scale (pickling) from the stainless steel by undercuttlng (dissolving) the metal beneath the scale. The dissolution behavior of AISI Type 304 stainless steel (304SS) and of three experimental alloys (Fe-4Cr-13Ni, Fe-12Cr-12Ni, Fe-12Cr-17Ni) representative of the chromium-depleted metal beneath the scale was studied as a function of temperature and the concentrations of HNO_3, HF, and dissolved Fe, Cr, and Ni. Results indicated that the dissolution process was activation controlled, linearly dependent on HF, Fe, and Cr concentrations, and nonlinearly dependent on HNO_3 concentration. A comparison of the behavior of 304SS to that measured for the experimental alloys indicated that it was possible to optimize the pickling of 304SS in terms of metal lost, acids used, and waste generated. A pickling liquor composition of 0.8*M*-1.3*M* HNO_3 plus 0.5*M* HF at 50° C can optimize the pickling of 304SS.

INTRODUCTION

Some of the basic steps used in the formation of stainless steel sheet are given schematically in figure 1. The hot- and cold-forming operations used in this process leave the steel in an unusable work-hardened state. A short-term high-temperature annealing operation is used to soften the metal to allow further rolling of the metal. The effects of annealing are that the bulk microstructure is altered, the surface is oxidized to form a thick scale, and the region just below the oxidized surface is compositionally altered thus forming the chromium-depleted region. While the first effect is desirable and controllable, the final two effects are not and result in the loss of metal. The oxide scale and chromium-depleted region formed during annealing must be totally removed during the pickling operation and the metal removed is usually not recovered. In fact, the metals lost end up concentrating in the pickle liquor, making it difficult to use for further pickling operations, and necessitating the disposal of the spent pickle liquor. An in-depth understanding of the pickling process and of all of the factors affecting it could help to minimize the loss of metals from the stainless steel, the use of pickling acids, and the generation of spent pickle liquor. To accomplish this, a cooperative program between the Bureau of Mines and the American Iron and Steel Institute (AlSI) was initiated. The AISI member companies aided research by providing materials and background information.

Pickling is defined here as the act of soaking in a solution for the purpose of cleaning or conditioning. For stainless steels, the surface that is eventually pickled has already been influenced by the annealing and scale-conditioning processes. The first process, annealing, determines the initial state of both the surface and of the chromium-depleted region. Temperature, time at temperature, and oxygen partial pressure during the annealing operation affects the thickness, structure, composition, and adhesion of the oxide scale to the stainless steel. All of these factors affect the ease of pickling and if left uncontrolled may cause a variability in the pickling process.

The depth and composition of the chromium-depleted region are interrelated with the scale formation. That is, the chromium that's depleted from the bulk metal goes to form the oxide scale. Temperature, time at temperature, and oxygen partial pressure, the same factors that affect the annealing scale, affect the chromium-depleted region. This depleted region has to be removed during pickling to assure full corrosion resistance and it may, in fact, play a key role in the pickling process.

Conditioning of the scale prior to pickling, which is not always done commercially, is the second process that affects the pickling of stainless steel. This consists usually of mechanical (shot blasting), chemical (acid), electrolytic (sulfate), or molten salt treatments that are aimed at facilitating the pickling process. Each of the conditioning techniques has in common the alteration of the chemical or physical structure of the oxide scale. While it is easy to recognize the usefulness of such conditioning techniques it may be that a proper understanding of the annealing and pickling processes would make them unnecessary.

The actual process of pickling stainless steels is complex because of the environment that is usually used. The environment

[1] Supervisory research chemist, Albany Research Center, Bureau of Mines, Albany, OR

consists of solutions of nitric and hydrofluoric acids at temperatures of 50° to 80° C containing large quantities of dissolved Fe, Cr, and Ni. To truly understand the process of pickling, and thus to control it, it is necessary to understand the chemistry of this complex environment. This is an environment where HF, a weak acid and a strong complexing agent, is combined with a strong oxidizing acid that can be relatively easily converted into diverse other oxidized or reduced forms. The dissolved metals tend to tie up the HF, making it necessary to continually add more HF, while the high-temperature and chemical dissolution reaction tend to expel the nitric acid from solution as a nitrogen oxide. The knowledge that is needed consists of activity coefficients, solubilities, and stability constants for a large number of stable and metastable compounds and complexes.

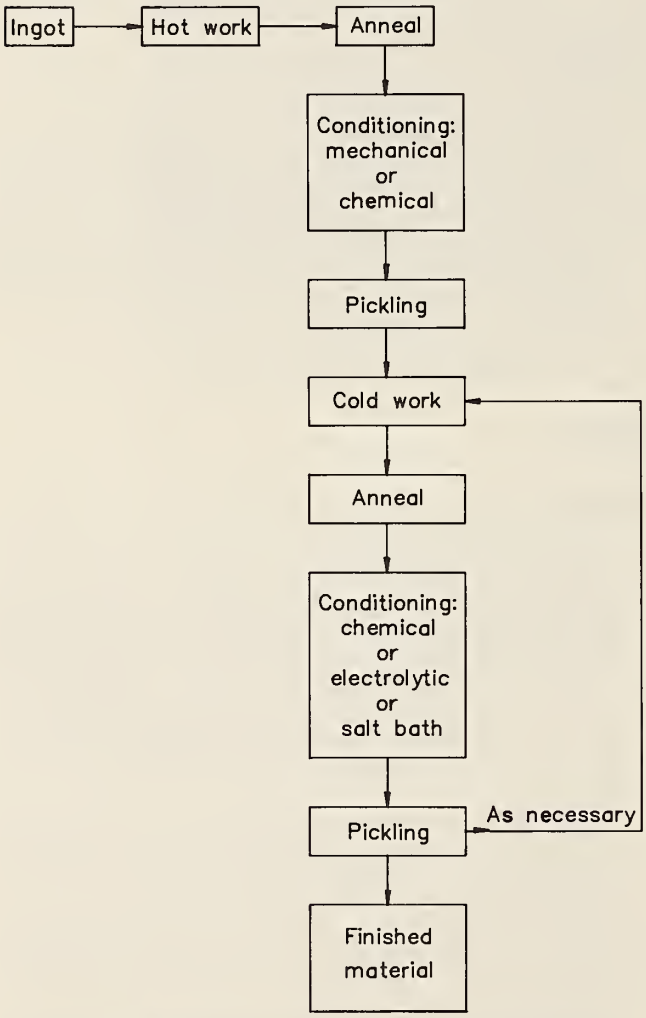

Figure 1.—Steps used in processing stainless steel strip.

Some studies in most of the areas relevant to the pickling of stainless steels have been done. These include studies by the AISI members on the effects of annealing and conditioning on the pickling of stainless steels. Some basic properties of HNO_3-HF solutions and methods to remove dissolved metals from these solutions are being studied at the Mackay School of Mines. The work to be reported in this paper consists of the effect of temperature, acid, and dissolved metal concentrations on the pickling of 304SS.

The model of the pickling process used to design the experimental approach consisted of an undercutting of the scale through dissolution of the chromium-depleted region beneath the scale. This is shown schematically in figure 2. The chromium-depleted region on 304SS, which formed because of a short high-temperature anneal, has been characterized *(1)*.[2] On the basis of this characterization, alloys were developed and used in the test program that is being reported here. Pickling was thus assumed to occur by dissolution of the chromium-depleted region as represented by three experimental alloys described in the following section. Optimization of the pickling process would occur when the chromium depleted region dissolved at its fastest rate and the bulk 304SS dissolved at its slowest rate. Under these conditions optimization would result in the minimum amount of Fe, Cr, and Ni dissolved, the minimum amount of acids used, and the minimum amount of spent pickle liquor generated.

[2] Italic numbers in parentheses refer to items in the list of references at the end of this paper.

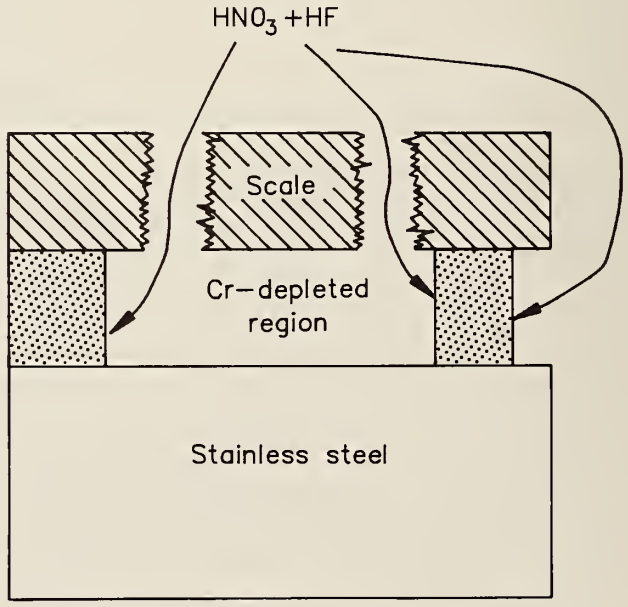

Figure 2.—Schematic of assumed pickling process.

EXPERIMENTAL

The commercial alloy used in all experiments was 304SS supplied by the Allegheny Ludlum Steel Corp., Leechburg, PA, and having the nominal composition Fe-18Cr-9Ni. The three experimental alloys were nominally Fe-4Cr-13Ni, Fe-12Cr-12Ni, and Fe-12Cr-17Ni.

All of the alloys were exposed to the HNO_3-HF solutions which were made from reagent grade HNO_3 and HF and high-purity (18 MΩ-cm) water. Only the 304SS was exposed to solutions containing dissolved Fe, Cr, and Ni. These solutions were made using reagent grade $Fe(NO_3)_3 \cdot 9H_2O$, $Cr(NO_3)_3 \cdot 9H_2O$, and $Ni(NO_3)_2 \cdot 6H_2O$. All solutions were deaerated using ultra-high-purity (UHP) nitrogen for 4 to 16 h prior to running a test.

All weight-loss tests were conducted by exposing the sample for a period of time, removing from solution, rinsing with high-purity water, and drying with UHP nitrogen. Samples were subsequently weighed to determine the weight loss, and then reexposed to the solution for additional periods up to a total of 90 min exposure time. All corrosion rates were determined by fitting the linear weight loss versus exposure time data to a linear equation.

Auger electron spectroscopy (AES) measurements were taken using a Physical Electronics[3] model 10-155 cylindrical mirror analyzer. The Auger electrons were induced by a 5-keV electron beam incident at 60° with respect to the sample normal, and a 2-V peak-to-peak modulation signal was applied to the analyzer. To obtain element depth profiles, a 2.5-keV Ar^+ beam incident at 10° with respect to the sample normal was used to sputter away small increments of oxide thickness.

RESULTS

Data for 304SS are plotted in figures 3 through 6 to show the general effects of temperature, nitric, and hydrofluoric acid concentrations, and dissolved iron, chromium, and nickel concentrations on the dissolution of 304SS. Buildup of dissolution products during the 90-min exposure had no effect on any of the dissolution rates reported here. This was based on the fact that the metals lost weight linearly with time. If dissolution products affected the dissolution process then the data would tend to deviate from linearity. The activation energy necessary for dissolution of 304SS as calculated from curves similar to figure 3 appeared generally to range from 5 to 10 kcal/mol in solutions with 1.3*M* nitric acid and from 9 to 14 kcal/mol in solutions with lower concentrations of nitric acid. These categories applied also when dissolved metals were present.

The data in figure 4 show that the dissolution rate of 304SS at constant temperature and nitric acid concentration varies approximately linearly with hydrofluoric acid concentration. This was the same relationship observed for the three experimental alloys. Neither nitric acid nor dissolved iron affected this linear relationship. The data in figure 5 show that the dissolution rate of 304SS at constant temperature and hydrofluoric acid concentration passes though a maximum as a function of nitric acid concentration. This maximum occurs at approximately 0.4*M* to 1.5*M* nitric acid. Hydrofluoric acid concentration affected only the magnitude of the dissolution rate and not the shape of this curve. For the three experimental alloys, the shape of this curve was the same but the location of the maximum was shifted to higher concentrations compared to that for 304SS and the overall height of the curve increased with decreasing chromium concentration.

A typical pickling solution usually has large quantities of dissolved iron, chromium, and nickel, but because of the composition of the stainless steels the dissolved iron is always more concentrated than either dissolved chromium or nickel. A comparison of the effect of dissolved iron, chromium, and nickel on the dissolution rate of 304SS in HNO_3-HF solutions is shown in figure 6. Both iron and chromium cause a decrease in dissolution rate. Iron was the most effective in reducing the dissolution rate of the 304SS, dissolved chromium was less effective than iron, while dissolved nickel had no apparent effect. Iron was also the only dissolved metal species to shift the intercept of the curve.

Films formed as a result of exposure to HNO_3-HF were analyzed using AES. Profiles were obtained by alternately doing AES analyses and argon ion sputtering at a rate of 1.5 Å min (calibrated using Ta_2O_5). Profiles of 304SS samples exposed to different HNO_3-HF solutions show an enrichment in Cr in the film compared to the metal substrate, and a small quantity of fluorine in the region of the film-environment interface. The fluorine level was

[3] Reference to specific products does not imply endorsement by the Bureau of Mines.

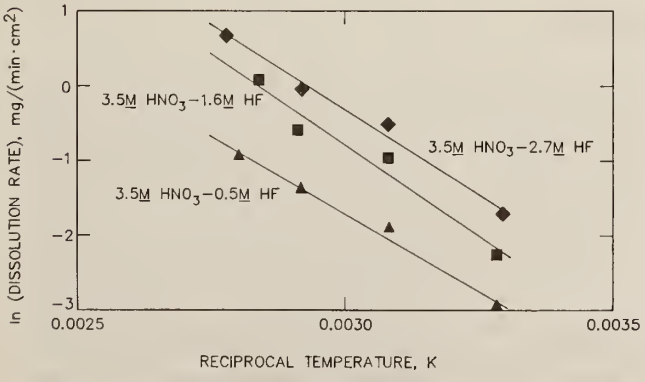

Figure 3.—Arrhenius plots for the dissolution of 304SS in HNO_3-HF solutions.

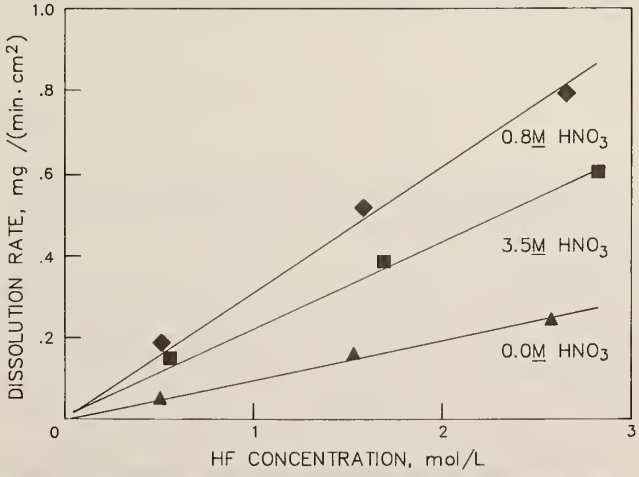

Figure 4.—Effect of HF concentration on dissolution rate of 304SS in HNO_3-HF solutions at 50° C.

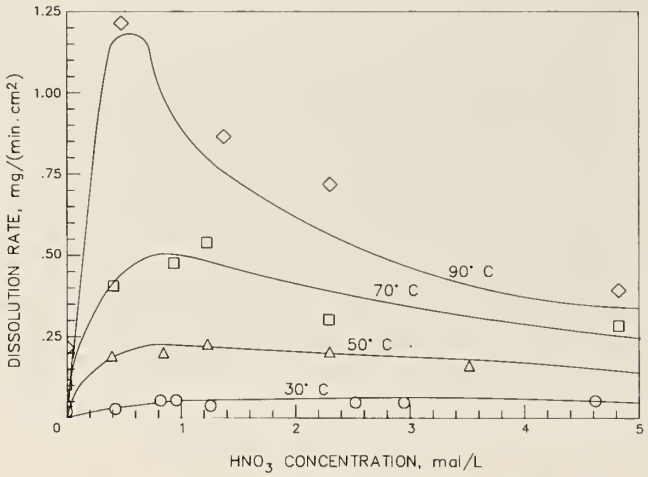

Figure 5.—Effect of temperature and HNO_3 concentration on dissolution rate of 304SS in HNO_3-HF solutions with approximately 0.5*M* HF concentration.

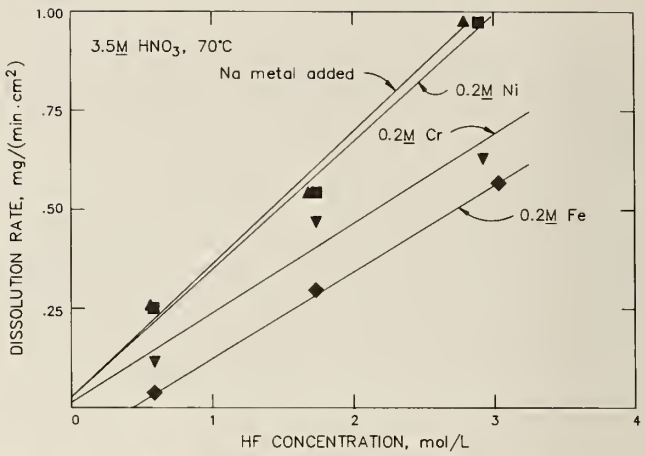

Figure 6.—Effect of equimolar concentrations of dissolved Fe, Cr, and Ni on dissolution rate of 304SS in HNO_3-HF solutions at 70° C containing approximately 3.5*M* HNO_3.

independent of HF concentrations between 0.5*M* and 1.5*M* HF. There was some evidence that the level of fluorine was dependent on the solution at concentrations below 0.5*M* HF. The main difference was a variation in film thickness by about a factor of 2 between the thickest and thinnest films. This variation in thickness was not correlated with any of the test parameters such as temperature or concentration.

The fluorine profile in figure 7 shows that a fraction of a monolayer of fluorine exists on the oxide surface below the carbon surface contamination. The surface carbon consists primarily of hydrocarbons picked up from exposure to the atmosphere following the HNO_3-HF treatment. The conclusion that the fluorine exists on the oxide surface is based on many profiles identical to that shown in figure 7. There was a general correlation between the time required to sputter away the carbon surface contamination and the fluorine. It appeared that the fluorine was rapidly removed only after most of the surface carbon was removed. The relatively flat portions of the fluorine profiles represent regions where only surface contamination was being removed. If all of the fluorine was concentrated at the film surface (i.e., at the film-carbon contamination interface), then the fluorine could represent as much as one-quarter to one-half a monolayer of fluorine at that surface.

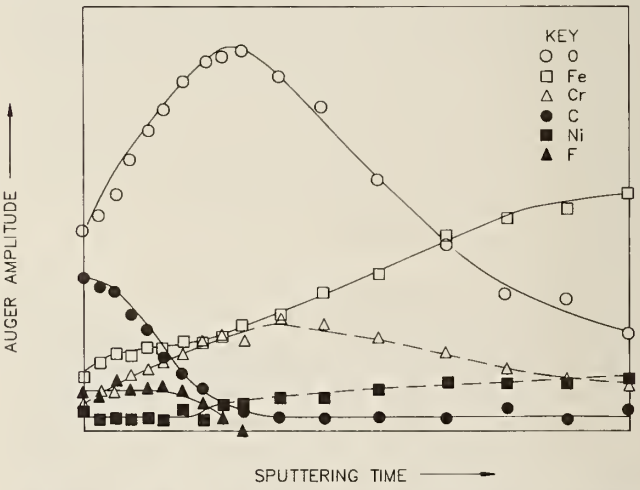

Figure 7.—AES sputter depth profile of film formed on 304SS exposed to 3.5*M* HNO_3-0.5*M* HF-0.2*M* Fe solution for 90 min at 70° C. The sputter rate was approximately 1.5 Å min.

DISCUSSION

The first part of this discussion will be applied to understanding the mechanism of dissolution of metals in HNO_3-HF solutions. The second part will concentrate on applying the data to optimizing the pickling process.

The range of activation energies (5-14 kcal/mol) measured here are similar to those reported *(2–8)* for the dissolution of rapidly corroding metals in solutions other than HNO_3-HF. This is in contrast to those activation energies (15-22 kcal/mol) reported *(7–8)* for the dissolution of metals that passivate. It therefore appears that 304SS in the HNO_3-HF solution is not inhibited from dissolving by a passive film.

The evidence obtained from the AES measurements suggests that there is a film on the surface of the metal in solution and that this film is not a passive or protective type of film. Research *(9)* done elsewhere on 304SS in similar solutions supports the conclusion that this is not a passive film. A truly passive film in HNO_3 solutions would exhibit a more intense chromium peak than that shown in figure 7. The presence of the fluoride on the outer surface of this film suggests that fluoride is intimately involved in the dissolution mechanism. This is supported also by the observed linear increase in dissolution rate with increasing HF concentration.

The dissolution rate vs HF curves for HNO_3-HF solutions were extrapolated to zero dissolution rate at an HF concentration of zero. This is in agreement with the reported *(10)* zero dissolution rate of 304SS in low-temperature HNO_3. The HNO_3-HF-Fe solutions do not, however, pass through zero dissolution rate at a zero concentration of HF. This is probably related to the formation of iron-fluoride complexes. These complexes are reported *(11)* to be very

stable and would be able to tie up the available fluoride. The intercept of the curves in figure 6 corresponds to approximately a 3:1 molar ratio of F to Fe, which suggests the formation of FeF_3

The iron, chromium, and nickel additions to the HNO_3-HF solutions cause various degrees of reduction of the dissolution rate of the 304SS. Dissolved iron has the greatest inhibiting effect, followed by dissolved chromium, which is less effective, and dissolved nickel, which has little effect on the dissolution rate. The effectiveness of these metal ions in inhibiting the dissolution of 304SS appears to be due to the specific cation's ability to tie up the available fluoride anions. This can be seen by considering the stability constants for the metal-fluoride ligand involving one metal and one fluoride ion. The stability constants *(12)* are 1.5×10^5 for FeF^{2+}, 2.3×10^4 for CrF^{2+}, and 6.3 for NiF^+. Thus, the order of effectiveness of the metal ions is the same as the order of the stability constants. The negligible effect of the dissolved nickel is reasonable because the stability constant *(11)* of 6.3 for NiF^+ is very similar to the value of 3.9 for the most prevalent *(12)* ionized fluorine species, HF_2.

The role played by dissolved metals in reducing the dissolution rate of 304SS appears to be one of reducing the amount of fluoride available for participation in the dissolution reaction. These dissolved metals do not participate directly in the dissolution reaction, but rather they alter the solution chemistry. This emphasizes the importance of the fluoride component of the pickling bath. The finding, by AES measurements, of the fluoride on the surface of the metal's film becomes a key to the mechanism of dissolution of the metal. Others *(13–14)* have suggested that HF has a catalytic effect in the formation of metal-fluoride complexes at the film-solution interface. It is postulated that HF allows a more rapid transfer of these complexes into solution as compared to species formed in non-fluoride-containing solutions.

The data in figure 5 provide evidence of the catalytic nature of the dissolution reaction. The shape of the dissolution rate versus nitric acid concentration curve is characteristic of a reaction that proceeds through heterogeneous catalysis. In such a case the catalyst typically adsorbs to the surface where the reaction occurs and the catalyst remains unchanged. For the dissolution of 304SS in HNO_3-HF solutions it appears that the fluoride ion adsorbs to the nearly passive film formed in solution, enhances the dissolution of this film, and then complexes with the dissolved metal species. For this mechanism to continue it is necessary for the film to continually reform and this can more than adequately be done by the reaction of the nitric acid with the metal.

The data shown in figure 5 make it possible to consider optimizing the pickling process. The maximum and minimum represent two areas where dissolution can be very fast or very slow. It was already noted that a similar type of behavior was observed for the three alloys representative of the chromium-depleted region. Thus to optimize the pickling process in terms of HNO_3 concentration it is only necessary to superimpose the graphs for 304SS and one or more of the experimental alloys. This has been done schematically in figure 8 for 304SS and the Fe-12Cr-17Ni alloy. The other alloys had basically the same shape but a greater height. The region on figure 8 labeled as optimum represents the range of nitric acid concentrations over which the pickling of 304SS should be optimized. At 50° C that range is 0.8*M* to 1.3*M* HNO_3 in solutions with 0.5*M* HF. It is in this range that the dissolution of the chromium-depleted region will be maximized and the dissolution of bulk 304SS will be minimized. It can be seen that being to the left of this region would sacrifice base metal for dissolution (pickling) speed while being to the right will result in a very slow pickling.

The other factors to consider are temperature and HF concentration. The HF concentration should linearly increase pickling rate and loss of base metal so that it is best to use as low a concentration as practical. Choice of temperature is another variable that is determined somewhat by practicality. For the activation energies reported here, there is an order of magnitude increase in dissolution (pickling) rate of 304SS for approximately each 20° to 40° C rise in temperature.

The dissolution rate data can also be used to develop an equation describing the overall response of dissolution rate to time, temperature, and acid concentrations. The equation would take the form of a heterogeneous catalysis rate equation and be similar to the following equation:

$$\text{Dissolution rate} = \frac{k\,[HF]^a\,[HNO_3]^B}{1 + [HF]^a\,[HNO_3]^B}\exp(-\triangle H/RT),$$

where k, a, B, and R are constants, $\triangle H$ is the activation energy, T is the absolute temperature, and [HF] and $[HNO_3]$ are acid molarities. Such as equation will help to give a better insight into the dissolution mechanism (depending on the fitted values of a, B, and $\triangle H$) and can also be used to predict dissolution (pickling) rates for acid concentrations and temperatures between those actually measured.

Equations such as that described for 304SS and for the three experimental alloys can be used further to model the amount of metal lost during the pickling reaction. This would be accomplished in terms of the overall basic assumption made in this paper. That is, that pickling occurs by a dissolution of the chromium-depleted region, undercutting the scale and thus removing it. The modeling would proceed by assuming a thickness of chromium depletion, an amount of scale formed during annealing, a preset pickling time, and the number of pickling-working-annealing steps in the life of a coil of stainless steel. The result would be the minimum amount of time needed to remove the chromium-depleted region (and thus the scale) and the minimum amount of metal lost (and metal lost unnecessarily).

There are certain quantities that would make this predictive model more accurate. The quantities that are relatively unknown at present are represented by the chromium-depleted region and the annealing scale. The needed information would be in the form of equations expressing the effect of annealing time, temperature, and oxygen content of the environment on both the chromium-depleted region and the oxide scale composition and thickness. These would be rewarding areas in which to conduct research.

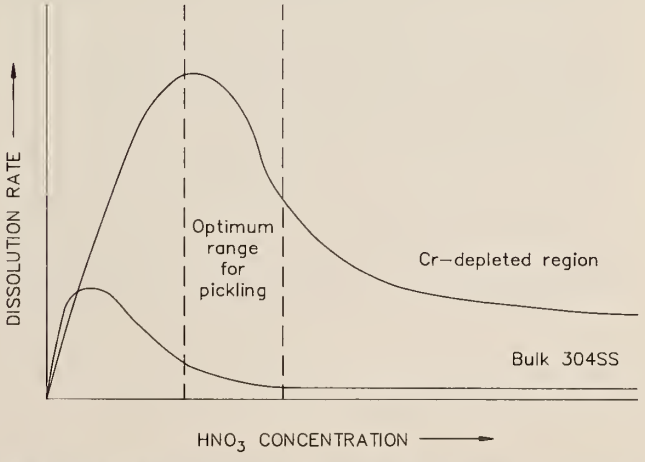

Figure 8.—Schematic of optimum range of HNO_3 concentrations for pickling 304SS in HNO_3-HF solutions.

FUTURE WORK

Additional work in this area at the Bureau's Albany (OR) Research Center will consist solely of data analysis. Data analysis will be completed and equations developed to model the dissolution rate as a function of acid concentrations and temperature. These will then be used to model the loss of metals during pickling with the hope of being able to best predict optimum conditions for pickling stainless steels. This will also include completing the analysis of work on 430SS and experimental alloys used to represent its chromium depleted region.

CONCLUSIONS

1. Increasing hydrofluoric acid concentration causes a linear increase in the dissolution rate of 304SS.
2. Increasing nitric acid concentration up to 0.4*M* to 1.5*M* HNO_3 causes an increase in the dissolution rate of 304SS, and a decrease in the dissolution rate for higher HNO_3 concentrations.
3. Dissolved iron and chromium reduce the dissolution rate of 304SS in HNO_3-HF solutions. Dissolved nickel has little or no effect.
4. The surface films present on 304SS in HNO_3-HF solutions did not change as a function of dissolution rate and contained a fraction of a monolayer of fluoride on the outer surfaces of the films.
5. Optimum pickling conditions exist at nitric acid concentrations of 0.8*M* to 1.3*M* HNO_3 at 50° C in solutions with 0.5*M* HF.

REFERENCES

1. Fabis, P. M., and B. S. Covino, Jr. Near Surface Elemental Contration Gradients in Annealed 304 Stainless Steel as Determined by Analytical Electron Microscopy. Oxid. Met., v. 25, Nos. 5/6, 1986, pp. 397–407.
2. Muralidharan, V. S., and K. S. Rajagopalan. Kinetics and Mechanism of Corrosion of Iron in Phosphoric Acid. Corros. Sci., v. 19, 1979, pp. 199–207.
3. Alexander, B. J., and R. T. Foley. Anion Dependence of the Activation Energy for Iron Corrosion. Corrosion, v. 31, No. 4, 1975, pp. 148–149.
4. Altura, D., and K. Nobe. Activation Energy for the Corrosion of Iron in Sulfuric Acid. Corrosion, v. 20, No. 11, 1973, pp. 433–434.
5. Makrides, A. C., and N. Hackerman. Solution of Metals in Aqueous Acid Solutions. II Depolarized Solution of Mild Steel. J. Electrochem. Soc., v. 105, 1958, pp. 156–162.
6. Riggs, O. L. Activation Energy from Carbon Steel Corrosion in Phosphoric Acid. Corrosion, v. 24, No. 5, 1968, pp. 125–126.
7. Covino, B. S., Jr., J. P. Carter, and S. D. Cramer. The Corrosion Behavior of Niobium in Hydrochloric Acid Solutions. Corrosion, v. 36, No. 10, 1980, pp. 554–558.
8. Ishikawa, T., and G. Okamoto. Potentiostatic Response of Passive Metals to the Rate of Temperature Change. Electrochimica Acta, v. 9, 1964, pp. 1259–1268.
9. Asami, K., and K. Hashimoto. An X-ray Photoelectron Spectroscopic Study of Surface Treatments of Stainless Steels. Corros. Sci., v. 19, 1979, p. 1007.
10. Wilding, M. W., and B. E. Paige. Survey on Corrosion of Metals and Alloys in Solutions Containing Nitric Acid. Allied Chemical Corp., ICP-1107, 1976, 56 pp.
11. Smith, R. H., and A. E. Martell. Critical Stability Constants, Volume 4—Inorganic Complexes. Plenum (New York), 1976, pp. 96–103.
12. Pourbaix, M. Atlas of Electrochemical Equilibria in Aqueous Solutions. Pergamon (New York), 1966, p. 587.
13. Lochel, B., and H. H. Strehblow. Breakdown of Passivity of Iron by Fluoride. Electrochim. Acta, v. 28, No. 4, 1983, pp. 565–571.
14. Lochel, B. P., and H. H. Strehblow. Breakdown of Passivity of Nickel by Fluoride. II Surface Analytical Studies. J. Electrochem. Soc., v. 131, 1984, p. 713.

DECREASED ACID CONSUMPTION IN STAINLESS STEEL PICKLING THROUGH ACID RECOVERY

By G. L. Horter[1] and J. B. Stephenson[2]

ABSTRACT

Acid pickling of stainless steel annually generates approximately 30 million gal of spent nitric acid-hydrofluoric acid solutions as a byproduct. Disposal of these acid solutions significantly increases the cost of manufacturing stainless steel and results in the loss of the acid, Cr, and Ni values. Recent advances in ion-selective membrane technology have opened new avenues to regenerate these acid solutions as an alternative to disposal. Experimental work by the Bureau of Mines has indicated that an electrodialysis cell utilizing ion-selective membranes has potential for separating dissolved metals from spent pickling acid solutions, while regenerating the acids for return to the pickling process.

INTRODUCTION

The Bureau of Mines is conducting research to conserve mineral values and reduce waste generation from spent nitric acid-hydrofluoric acid pickling solutions. The stainless steel industry annually generates approximately 30 million gal of these solutions, which currently have to be neutralized and sent to waste disposal *(4)*.[3]

Hot working and annealing of stainless steels cause a stratified scale to form on the surface of the steel. The scale consists of metal oxides in the top layer, an intermediate layer of spinel oxide [$FeO \cdot (Fe_{(2-x)}Cr_x)O_3$, where $0 \leq \times \leq 2$)], and a layer of steel, which has been depleted of Cr and Ni. The concentration of Cr and Ni in the oxide scales may be four to six times their respective concentrations in the bulk alloy *(2–3, 16)*.

Scale removal relies on a variety of conditioning and pickling steps *(1)*. The commonly used acid pickling solutions contain 5 to 25 vol pct nitric acid and 0.5 to 8 vol pct hydrofluoric acid *(1)*. Evidence suggests that the chemical pickling solution does not dissolve the oxide scale but dissolves the underlying metal, allowing the scale to fall away *(15)*.

The pickling acids become ineffective as the concentration of dissolved Fe increases, after which the solutions are discarded. This necessitates the disposal of the pickling solutions. Disposal according to the required environmental standards has been estimated to increase the total operating cost of the steel industry by 8 to 10 pct.

Several processes have been developed for reclaiming HNO_3 and HF from pickling solutions but the complexity of these methods has limited their acceptance by domestic steel producers. Most notable of the available reclamation processes rely on distillation-crystallization or solvent extraction technology *(14)*.

Preliminary Bureau research focused on adapting a Bureau-developed *(6, 11–12)* electrolytic process for regenerating chromic acid solutions. Electrolytic processing of stainless steel pickling solutions would be attractive because initial capital costs are generally lower than for solvent extraction or chemical processing. In addition, energy requirements are usually less for electrolytic processes than for distillation or evaporation processes. This paper reports on research in progress on the electroregeneration of spent stainless steel pickling solutions in a Bureau-developed three-compartment membrane cell.

---

[1] Chemical engineer.

[2] Research chemist.

Rolla Research Center, Bureau of Mines, Rolla, MO.

[3] Italic numbers in parentheses refer to items in the list of references at the end of this paper.

BACKGROUND

PICKLING CHEMISTRY

The oxide scale formed during hot working and annealing of stainless steel is enriched in Cr and Ni. Chromium and nickel diffuse from the bulk steel to the oxides, changing the alloy composition at the steel surface to a high Fe, low Cr-Ni alloy. The Cr content in this surface alloy is insufficient to provide a protective, passive oxide film for adequate corrosion resistance. To regain suitable corrosion resistance, the oxides and Cr-deficient surface alloy must be removed from the steel.

Heavy oxide scale produced during hot rolling typically is treated and removed prior to acid pickling by shot blasting. Cold-rolled and annealed material have thinner oxide layers. However, in both situations, the Fe-enriched surface alloy is the principal material dissolved by acid pickling. Iron is the predominant metal in solution because of this enrichment, as shown in table 1 *(1)*.

Table 1.—Typical concentrations in spent pickling solutions

Component	Concentration	
	g/L	*M*
Nitrate	144	2.32
Fluoride	46	2.42
Iron	34	.61
Chromium	6	9.34
Nickel	6	.10

Literature review indicates that mechanisms and kinetics for metal dissolution in this acid system are complex and not fully understood. Research has shown that both HNO_3 and HF play a role in dissolving metal *(2)*. It is believed that nitric acid reacts with the surface to convert metals to oxides. This is consistent with the oxidizing behavior of nitric acid. Hydrofluoric acid reacts with the oxides to form soluble fluoride salts. Fluoride is a strong ligand, which readily complexes Fe in solution. The equilibria relationships for iron fluoride salts, given in table 2, indicate that an iron fluoride salt should be the principal metal species in solution. The relative abundance of fluoride in relation to Fe in typical spent pickling solutions indicates that the predominant specie would be the cation FeF_2^+ *(7, 9, 13)*.

Table 2.—Formation constants for iron fluoride salts *(9)*

$Fe^{3+} + F^- \rightarrow FeF^{2+}$	$K = 1.58 \cdot 10^5$
$Fe^{3+} + 2F^- \rightarrow FeF_2^+$	$K = 1.26 \cdot 10^9$
$Fe^{3+} + 3F^- \rightarrow FeF_3$	$K = 1.00 \cdot 10^{12}$
$Fe^{3+} + 4F^- \rightarrow FeF_4^-$	$K = 1.00 \cdot 10^{14}$
$Fe^{3+} + 5F^- \rightarrow FeF_5^{2-}$	$K = 3.16 \cdot 10^{14}$

Increasing the hydrofluoric acid content of the bath results in speciation changes toward higher fluoride salts. A solubility limit for FeF_3 and CrF_3 salts occurs at a total metal content of approximately 50 g/L. Adding HF to a solution at this metals content dramatically increases the danger of salt crystallization. Therefore, the pickling solution is usually discarded before the 50-g/L metal content is reached.

THE ELECTRODIALYSIS PROCESS

Before applying an electrolysis process to HNO_3-HF pickling solutions, the possible electrode reactions that can occur must be considered. An applied electromotive force provides a strong separation driving force by attracting cations to the cathode. Metal removal by electrolytic deposition from the pickling solutions would not be expected because of the presence of HNO_3; therefore, a receiving solution should be provided as a sink for the dissolved metals. HNO_3 reacts with the metallic anodc to liberate NO_x; therefore, it would be desirable to avoid contacting the pickling solutions with the anode. Hydrogen ions generated as an electrolysis product at the anode must be allowed to migrate into the pickling solution in order to regenerate nitric and hydrofluoric acids. Physically separating the solutions in an electrolysis cell, therefore, requires the use of permeable barriers that allow transport of the dissolved metals and hydrogen ions, while retaining the acids in the pickling solution.

Perfluorinated sulfonic acid (PFSA) cation exchange membrane was the most suitable permeable barrier commercially available when the research was initiated. The PFSA membranes are prepared from long-chain fluorinated polymers with material characteristics similar to Teflon[4] fluorocarbon polymer. Sulfonic acid groups incorporated in the polymer matrix act as exchange sites, allowing migration of cations across the membrane while rejecting anions *(5)*.

The type of electrolysis cell incorporating all the above requirements was an electrodialysis cell (fig. 1). The PFSA membranes separate the pickling solution from the electrodes, the anolyte provides a source of hydrogen ions, and the receiving solution (catholyte) provides a sink for the dissolved metals.

The movement of ions in the electrodialysis cell is regulated by the PFSA membranes and the current flux in the cell. The charged ions attempt to move to the oppositely charged electrode. The anions (A^-) are attracted to the positively charged anode; however, movement is blocked by the PFSA membrane. Therefore, the majority of anions should be retained in the pickling solution. The cations (C^+) are attracted to the negatively charged cathode and are accepted for transport by the PFSA membrane. Hydrogen ions are produced at the anode and migrate to the cathode. As the hydrogen ions pass through the central compartment, they will replace the metal cations that have been removed, generating HNO_3 and HF. However, part of the hydrogen ions generated at the anode will pass through the pickling solution to the cathode where they are reduced to hydrogen gas.

[4] Reference to specific products does not imply endorsement by the Bureau of Mines.

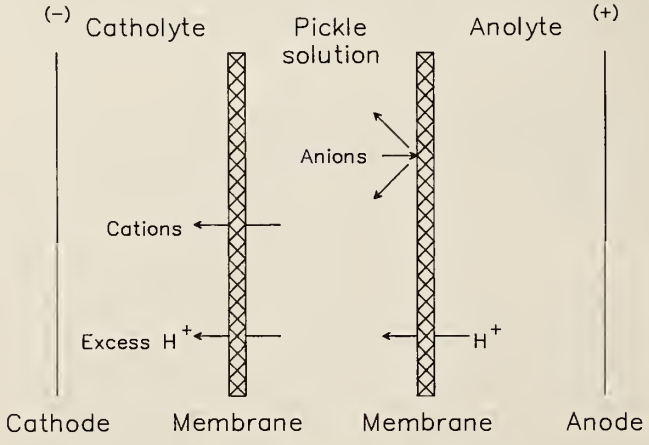

Figure 1.—Electrodialysis cell.

EXPERIMENTAL METHOD AND RESULTS

LABORATORY CELL DESIGN

The laboratory cell design utilized a plate and frame construction to allow flexibility in size and configuration of the cells *(8)*. The design was based on use of U-shaped frames to form the liquid-holding compartments and plates on the outer ends to seal the compartments. Capacity of the cells ranged from 300 mL to 1 L per compartment. The working dimensions of each compartment were 10.2 cm wide by 27.9 cm high by 1.3 cm deep for the small frames and 5.0 cm deep for the large frames. A seal between the frames was obtained with neoprene gaskets. The frames were held together by stainless steel bolts placed on 2.5-cm centers around the perimeter of the cell. A 316 stainless steel cathode and a Pb-Sb anode were used; each with working dimensions of 9.21 cm by 25.4 cm for a working area of 2.34 dm^2. The membrane window was 10.2 cm by 25.4 cm for an effective area of 2.59 dm^2. Circulation was provided by means of an input pump and a simple overflow incorporated into the compartment outer wall.

CELL PERFORMANCE

The effectiveness of the electrodialysis cell was initially determined on two synthetic pickling solutions. A statistically designed experiment utilizing Plackett-Burman screening methodology was performed as an initial investigation of the electrodialysis regeneration process *(10)*. This method involves selecting maximum and minimum values for the system parameters of interest and performing a series of trials using combinations of the parameter values. Statistical analysis of the system responses indicates which of the parameters had an effect on the system performance.

The system parameters selected for study were the form of the dissolved metal complex in either a high HNO_3 or a high HF solution, H_2SO_4 concentration in the anolyte and catholyte, and the applied current density. The maximum and minimum values for these parameters were selected according to available industrial data and the physical constraints of the system (table 3) *(8)*.

The fluoride and nitrate levels in the pickling solution were varied to control the complex species present and determine its effect on Fe transport across the membrane. Iron complexes with fluoride in preference to nitrate, therefore, adjusting the abundance of fluoride in the system ensured the predominance of either monovalent or divalent iron fluoride salts (table 4). The HF-based stock should contain predominantly FeF^{2+} in equilibrium with the nitrate in solution. The HNO_3-based stock should contain predominantly FeF_2^+.

The selected system responses were the quantity of Fe, F, and nitrate extracted from the pickling solution. To regenerate the pickling solution, the Fe must be extracted in greater quantity than the nitrate and fluoride. Failure to achieve this would indicate that the electrodialysis would have little potential for regenerating the pickling solution.

Table 3.—Parameters used in Plackett-Burman designed experiment

Parameter	Minimum	Maximum
Pickle type, 1*M*	FeF_3, HNO_3	$Fe(NO_3)_3$, HF
Concentration, vol pct H_2SO_4:		
Catholyte	1	10
Anolyte	1	10
Current density, A/dm^2	1.1	5.4

Table 4.—Pickling solution analyses

Pickle type	Molar concentrations			Molar ratios	
	Fe	F	NO_3	F-Fe	NO_3-Fe
HF-based	0.82	1.04	2.45	1.3:1	3.0:1
HNO_3-based	.92	2.90	1.10	3.2:1	1.2:1

DISCUSSION

Statistical analysis of the system responses showed a response dependency on two of the four varied parameters (table 5). Note that the type of pickling solution had no effect on Fe extractions but did affect extractions of fluoride and nitrate. Current density had a significant effect on iron extraction since it was related to the driving force for ion transport in the cell. The PFSA membrane rejects anions: therefore, the dependency of fluoride extraction on current density indicates transport of a cationic iron-fluoride complex. It is significant that anolyte and catholyte concentrations had no effect on Fe extraction. Iron transport independent of the sulfuric acid concentration in the anolyte and catholyte allows greater flexibility for optimizing the efficiency of the cell.

The extractions achieved during the experiments indicate that current density had the most notable effect on Fe extraction (table 6). Note that the fluoride extraction was also greatest for the experiments performed at high current density. The difference in nitrate

Table 5.—Parameter effects

Ion extracted	Pickle type	Concentration		Current density
		Catholyte	Anolyte	
Iron	No	No	No	Yes.
Fluoride	Yes	No	No	Yes.
Nitrate	Yes	No	No	No.

Table 6.—Extractions

Parameter	Runs	Extraction, pct			Molar ratio	
		Fe	F	NO_3	F-Fe	NO_3-Fe
Average	12	35.09	26.46	11.35	1.7:1	0.7:1
HF-based	6	34.09	28.38	15.43	1.1:1	1.4:1
HNO_3-based	6	36.01	24.54	7.26	2.2:1	.2:1
5.4 A/dm^2	6	52.99	37.37	12.76	1.6:1	.5:1
1.1 A/dm^2	6	17.68	11.73	9.94	1.5:1	1.2:1

extractions for the 5.4-A/dm² runs and the 1.1-A/dm² runs may be significant, since the higher current density represents a stronger driving force; however, the statistical analysis of the responses (table 5) indicated no relationship between current density and nitrate extraction.

Comparing the molar ratios of the anions to Fe in the extracted fractions provides a clue as to the mechanism of anion extraction. The molar ratios for the HNO_3-based pickling solution indicated that FeF_2^+ was the predominant specie transported across the membrane (fig. 2). Transport of nitrate from the HNO_3-based pickling solution was not indicated. The experimental runs with the HF-based pickling solution showed that fluoride was extracted unimolar with Fe, indicating that FeF^{2+} was the predominant specie transported. The fluoride extractions from both pickling solution types were consistent with the equilibria constants for iron-fluoride complexes.

The current density had a dramatic effect on the extraction of Fe. This was due to the electromotive driving force in the cell, the higher current density representing the higher flux and hence the strongest driving force for transport of Fe. The range of Fe transport rates during the test series was 0.0093 to 0.0372 g-mol/dm²·h, where the area term relates to membrane area *(7)*.

The variation in current density had little effect on transport of fluoride relative to Fe, supporting the theory that the fluoride was transported with the Fe as a complex species. The extraction of nitrate was almost equivalent for both current density levels indicating that loss of nitrate was only slightly affected by current density, which is consistent with table 5. This indicates that the cationic membrane is effective but does not totally reject transport of nitrate ions.

The desired separation should remove Fe while retaining nitrate and fluoride in the regenerated solution. Comparison of the anion to Fe ratios for the unprocessed pickling solutions (see table 4) and the retained species in the processed pickling solutions (table 7) indicates that the separation is occurring. An increase in the molar ratios of anions to Fe after processing would indicate that Fe was being separated from the nitrate and fluoride (fig. 3).

Except for the experimental runs at 1.1 A/dm², the molar ratios indicated that nitrate and fluoride were being concentrated with respect to Fe; that is, more fluoride and nitrate were being retained in the pickling solutions than Fe. The results for the 1.1-A/dm² runs showed no significant change from the initial solution, indicating that the chemical driving force of the system was stronger than the electromotive driving force in this case.

Table 7.—Retention in pickling solution

Parameter	Runs	Retention, pct			Molar ratio	
		Fe	F	NO_3	F-Fe	NO_3-Fe
Average	12	64.91	73.94	88.65	2.6:1	2.8:1
HF-based	6	65.91	71.62	84.57	1.4:1	3.8:1
HNO_3-based	6	63.91	75.46	92.74	3.8:1	1.7:1
5.4 A/dm²	6	47.02	62.64	87.25	3.0:1	3.8:1
1.1 A/dm²	6	82.32	88.26	90.07	2.4:1	2.2:1

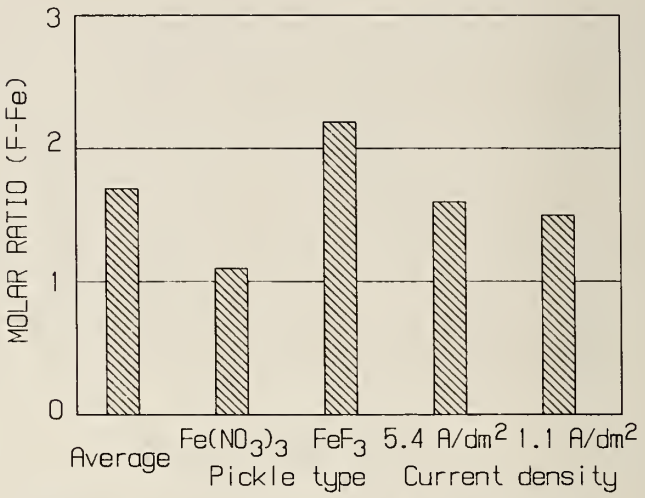

Figure 2.—Fluoride-to-iron ratios in extracted fractions.

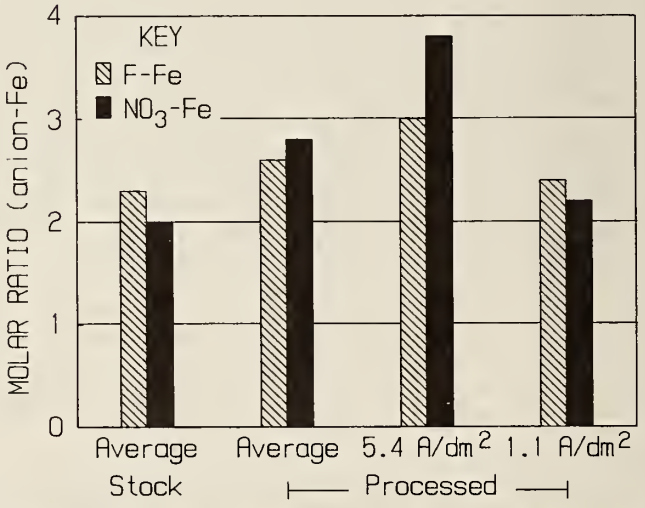

Figure 3.—Anion-to-iron ratios in stock and processed solutions.

CONCLUSIONS

Results of the series of experiments indicate that Fe can be separated from nitrates and fluorides in spent stainless steel pickling solutions using an electrodialysis cell. Extraction of fluorides from the pickling solutions show that a cationic iron fluoride complex was the most likely specie being transported across the membrane. FeF_2^+ and FeF^{2+} were the inferred species. Current density had a significant effect on Fe extraction, which indicates that current density is a controlling parameter for the process. Iron transfer rates ranged from 0.0093 to 0.0372 g-mol/dm^2·h. PFSA membranes withstood exposure to the highly corrosive pickling solutions without a significant loss of selectivity.

Nitrate losses from the pickling solutions indicate that the PFSA membrane does not completely reject nitrate transport. However, the nitrate extractions experienced during these tests were not believed to be detrimental. The overall results indicate the electrodialysis cell can transfer Fe from the pickling solutions and regenerate HNO_3 and HF in the pickling solutions. Development of a technique to control the fluoride transfer may result in a viable regeneration process.

REFERENCES

1. American Society for Testing and Materials. Cleaning and Descaling Stainless Steel Parts, Equipment, and Systems. A380-78 in 1982 Annual Book of ASTM Standards: Part 3, Steel-Plates, Sheet, Strip, Wire; Metallic Coated Products; Fences. Philadelphia, PA, 1982, pp. 274–276.

2. Bombara, G. Potentiostatic Anodic Pickling of Stainless Steel. J. Electrochem. Soc., v. 118, No. 4, Apr. 1971, pp. 676–681.

3. Clark, F. H. Metals at High Temperatures. Reinhold Publ. Corp., New York, 1950, 372 pp.

4. Desy, D. H. Iron and Steel. Ch. in Mineral Facts and Problems, 1980 Edition. BuMines B 671, 1981, pp. 455–480.

5. Eisenberg, A., and H. L. Yeager. Transport Properties of Perfluorosulfonate Polymer Membranes. Ch. in Perfluorinated Ionomer Membranes. ACS, 1982, pp. 41–63.

6. Horter, G. L., and L. C. George. Demonstration of Technology To Recycle Chromic Acid Etchants at Gould, Inc. Paper in Proceedings, 4th Recycling World Congress and Exposition, New Orleans, LA, Apr. 5–7, 1982, pp. M/3/5/1—M/3/5/13.

7. Horter, G. L., and J. B. Stephenson. Recycling Stainless Steel Pickle Liquors by Metathesis With an Electromembrane Cell. Pres. at 41st Ann. Purdue Ind. Waste Conf., West Lafayette, IN, May 13–15, 1986, 16 pp; available from G. L. Horter, BuMines, Rolla, MO.

8. Horter, G. L., J. B. Stephenson, and W. M. Dressel. Permselective Membrane Research for Stainless Steel Pickle Liquors. Paper in Proceedings of the International Symposium on Recycle and Secondary Recovery of Metals (Ft. Lauderdale, FL, Dec. 1–4, 1985). Metall. Soc. AIME, 1985, pp. 467–475.

9. Kragten, J. Atlas of Metal-Ligand Equilibria in Aqueous Solution. Halsted Press, 1978, 779 pp.

10. Plackett, R. L., and J. P. Burman. The Design of Optimum Multifactorial Experiments. Biometrika, v. 33, 1946, pp. 305–325.

11. Soboroff, D. M., J. D. Troyer, and A. A. Cochran. Regeneration of Waste Metallurgical Process Liquor. U.S. Pat. 4,337,129, June 29, 1982.

12. Spotts, D. A. Economic Evaluation of a Process To Regenerate Waste Chromic Acid-Sulfuric Acid Etchants. BuMines IC 8931, 1983, 7 pp.

13. Stephenson, J. B., G. L. Horter, and H. H. Dewing. Iron Removal and the Complexity of Stainless Steel Pickling Liquors. Ch. in Iron Control in Hydrometallurgy, ed. by J. E. Dutrizac and A. J. Monhemius. Halstead Press, Div. Wiley (New York), 1986, pp. 571–581.

14. Stephenson, J. B., R. S. Kaplan, and J. C. Hogan. Recycling and Metal Recovery Technology for Stainless Steel Pickle Liquors. Environ. Prog., v. 3, No. 1, Feb. 1984, pp. 50–53.

15. Vicentini, B., and G. Bombara. On the Mechanism of Scale Removal in the Acid Pickling of Austenitic Stainless Steels. Electrochim. Metall., v. 3, 1968, p. 313.

16. Whittle, D. P., and G. C. Wood. Complex Scale Formation on an Iron—18% Chromium Alloy. J. Electrochem. Soc., v. 114, No. 10, Oct. 1967, pp. 986–993.

RECYCLING OF STAINLESS STEELMAKING DUSTS AND OTHER WASTES

By L. A. Neumeier[1] and M. J. Adam[2]

ABSTRACT

There are significant amounts of Cr, Ni, and other metals contained in furnace dusts, mill scale, and swarfs produced as wastes annually by the domestic specialty steelmaking industry. Bureau of Mines research has led to development of a process for the in-plant recovery of about 90 pct of the Cr and Mo and well over 90 pct of the Ni and Fe from stainless steelmaking electric furnace dusts, argon-oxygen decarburization (AOD) vessel dusts, mill scale, and oily swarf. In the process, the mixed wastes are blended with coke breeze reductant and binder, pelletized, and furnace smelted to recover the contained metals. Although all-pellet heats can be smelted, the recommended procedure is to charge the pellets to the production electric arc furnace to replace up to 20 pct of the scrap charge. A number of industrial-size (19-st) commercial heats have been successfully made with pelletized wastes representing 14 to 19 pct of the furnace charge. Cost evaluation indicates the process is economically attractive.

INTRODUCTION

For technical and economic reasons, the scrap market has traditionally concentrated on metallic materials, with the low-grade dusts, fumes, solutions, and sludges being normally destined for landfills or other available means of disposal. Until recent years, producers of such wastes have had little incentive to treat them for metals recovery.

In the domestic specialty steelmaking industry, for instance, it is estimated that over 20 million lb Cr and 8 million lb Ni, plus other valuable metals, are contained in flue dusts, mill scale, and grinding swarfs in a typical year.

Traditional waste handling and disposition has undergone a significant change over the past decade as a result of the passage in 1976 of the Resource Conservation and Recovery Act (RCRA) and related legislation, which is concerned with the "cradle-to-grave" generation, transportation, and disposal of hazardous waste. Chromium-bearing electric arc furnace dust has been categorized by the U.S. Environmental Protection Agency (EPA) as a hazardous waste. Other particulates are deemed hazardous if they fail the EPA's Extraction Procedure (EP) toxicity test *(1)*.[3] Companies that generate hazardous wastes are faced with much-increased costs of complying with regulatory standards for storing, transporting, and disposing of the wastes. Even costly landfilling may not remain an option as regulations banning land disposal of hazardous wastes and directives dictating utilization of best available treatment technology are being considered seriously by EPA *(2)*.

One alternative to disposal of such wastes is to develop improved recovery and recycling technology, which can augment domestic supplies of critical metals such as Cr and Ni, as well as associated metals such as Fe and Mo.

The Bureau of Mines has conducted research on steelmaking and other wastes over a number of years. Much of the research *(3–6)* involved various schemes to remove Zn and Pb from carbon steelmaking furnace dusts, using combinations of techniques such as sulfation, pelletization, reduction roasting, and specialized furnacing.

Bureau recycling research *(7)* was also conducted on stainless steelmaking baghouse dusts, mill scale, and grinding swarf. Physical separation and leaching tests proved impractical for segregating the metal values. The constituents were too intimately mixed for beneficiation separations and too refractory and complex for selective leaching. Acid-soluble constituents resulted in a high acid consumption. The only method showing promise involved pelletizing the wastes with coke breeze reductant and smelting to produce a master alloy. Encouraging laboratory results in this earlier research led to the making of a 1-st trial heat in an industrial plant *(8)*.

These earlier heats involved all-pellet charges and production of master alloy ingot. Overall metal recoveries were deemed promising, with Cr recoveries being consistently somewhat lower than the recoveries of Ni and Fe. A preliminary economic evaluation was favorable. Further research involved initial tests of adding the pelletized wastes to the electric furnace in lieu of part of the conventional scrap charge *(9–11)*.

As an alternative to in-plant recycling, a master alloy can be produced by a centralized waste processing facility. An example of this type of facility is the Inmetco plant of the International Nickel Co. (INCO), which has in recent years been processing part of the

[1]Supervisory metallurgist (research supervisor).

[2]Metallurgist.

Rolla Research Center, Bureau of Mines, Rolla, MO.

[3]Italic numbers in parentheses refer to items in the list of references at the end of this paper.

stainless steelmaking dusts, mill scale, and grinding swarf being generated *(12)*. The treated and smelted compositions are adjusted with higher grade materials to produce recyclable Fe-Cr-Ni ingot.

Fosnacht *(13)* has compiled a comprehensive bibliography of the state-of-the-art of the processing of particulate steelmaking wastes.

The results reported herein represent efforts of Bureau research during the past decade to find technically and economically feasible recycling technology for specialty steelmaking wastes—to permit return of otherwise lost metal values to the steelmaking circuit. An in-plant reduction technique has been developed that results in the consistent recovery of about 90 pct of the Cr and Mo and well over 90 pct of the Ni and Fe from particulate stainless steel wastes. Description is given of the work, which began with small laboratory arc furnace melts, as it progressed through a number of approximately 19-st demonstration heats at Joslyn Stainless Steels, Fort Wayne, IN, under a Bureau-industry cooperative effort. Discussion of a cost evaluation is included.

PROCEDURE AND RESULTS

RAW MATERIALS

Waste products evaluated in the research included electric furnace (EF) baghouse dust, AOD vessel baghouse dust, oily grinding swarf, and mill scale. The majority of the material was supplied by Joslyn Stainless Steels; partial representative analyses are shown in table 1. Samples of baghouse dust and mill scale also were obtained from several other companies. Variations noted in composition of the wastes reflect variations in the feed to the furnaces, operating procedures, waste collection, and product mix.

Table 1.—Partial chemical analyses of typical stainless steelmaking waste products, percent

Waste material	Fe	Cr	Ni	Mo	Mn	Pb	Zn
EF dust	27.8	9.3	2.2	1.1	3.6	0.8	4.9
AOD vessel dust	40.5	11.1	3.8	.7	5.5	.6	.8
Grinding swarf	61.6	11.7	6.8	1.2	1.0	.1	<.1
Mill scale	54.8	8.6	3.9	.5	.8	.1	<.1

Arc furnace and AOD vessel baghouse dusts are typically about 90 pct minus 400 mesh. They consist essentially of complex oxides involving metals such as Fe, Cr, Ni, Mo, Mn, and Zn, with a number of other constituents involving elements such as Ca, Mg, K, Na, Si, S, C, etc. Mill scale, which is produced during blooming of heated billets, also is composed principally of metal oxides. Mill scale is mostly powder, but it is typically much coarser than baghouse dusts. Some larger chunks of mill scale commonly are present.

Swarfs are generated by the surface grinding of billets, slabs, and bars. Some of the dry swarf resulting from billet grinding, which is less oxidized than baghouse dusts and mill scale, is recycled directly back to the electric furnace. The oily swarf used in these experiments was specifically from the centerless grinding of various sized rods. It consisted of many small, partially oxidized fragments containing entrained oxide and carbide particles from the grinding wheels. It was often still wet from cutting oils used as a coolant during the grinding. The particle size of swarf is typically somewhat coarser than the finer fractions of mill scale.

The coke breeze obtained from a steel plant ranged downward in size from about ¼ in; it was about 85 pct C. The portland cement used as a binder typically has a very fine particle size.

LABORATORY EXPERIMENTS

Laboratory experiments were conducted in which various waste mixtures pelletized with coke breeze provided approximately 100-lb charges for smelting in an arc furnace.

Pelletizing

Pelletizing was selected as the most practical and economic means for agglomeration of the wastes. The four steelmaking wastes (table 1), in proportions consistent with their rates of generation, were mixed with coke breeze reductant and cement binder and blended into a composite mixture. For a plant that is collecting all four wastes, this composition might typically represent some 15 pct of AOD dust, 15 to 25 pct each of EF dust and mill scale, and about 40 pct grinding swarf. Substantial variation can, of course, be expected. Coke breeze, added as about 10 wt pct to this waste blend, was selected as a logical carbon reductant because it is essentially in a powdered condition and is an accessible carbon source in the steelmaking industry. With a wide particle size range for steelmaking wastes, a binder may be necessary, particularly if proportions of coarser sizes are relatively high. An addition of about 4 pct cement was found to be an effective binder for the waste mixes evaluated. The fine particle size of the cement aids pellet formation prior to the hardening reaction.

When raw, somewhat caked coke breeze is used, it must be dried and crushed to pass an intermediate size screen, such as 35 mesh, before adding it to the mixture. The mill scale was also dried, and then passed through crushing rolls until >70 pct passed a 35-mesh screen—usually two passes through the rolls. Only the minus 35-mesh fraction was blended into the pellet mix used in smelting tests; the oversize fraction was saved and added with the pellets as furnace charge. A flow diagram of this procedure is presented in figure 1.

The four-waste mixture was pelletized in a 36-in-diam drum pelletizer. The blended mix required the addition of about 12 pct water in order to form ⅜- to ¾-in-diam pellets. The pellets produced were first air dried for 24 h and then oven dried at 250° F for 6 h. Drying at higher temperatures tended to result in spalling. The pellets had 5- to 30-lb crushing strength, which was sufficient for the limited amount of handling required. When the wastes listed in table 1 were mixed in the indicated proportion and pelletized, the resultant pellets plus oversize mill scale analyzed roughly, in percent, 10 Cr, 4 Ni, 1 Mo, and 2 Mn.

Experience showed, however, that it is not always necessary to oven dry the pelletized waste mix. Most of the laboratory heats made in the latter part of the testing program were made using pellets that were air dried only. The experiments included adding pellets to the furnace that were only 2 h old and very wet. These were rolled at a uniform rate down a conveyor and dropped through the furnace top onto the melt surface. As much as 13 pct of the melt charge (the most tried) was added in this manner without problem.

Other efforts were made to simplify the pelletizing procedure. For some trials, the cement binder was completely eliminated from the pellet mix (could decrease slag volume). No difficulty was

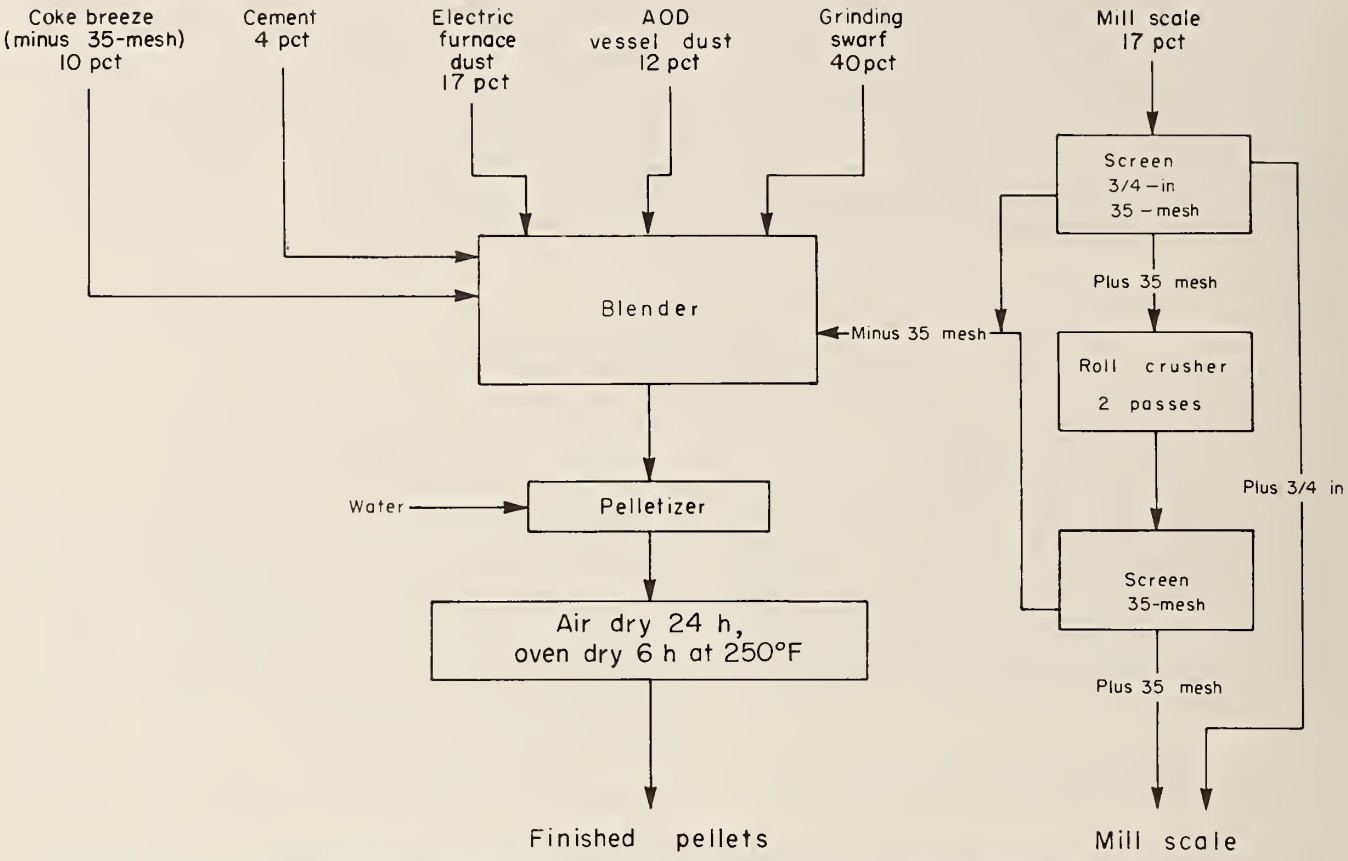

Figure 1.—Flow diagram for laboratory agglomeration of four stainless steelmaking wastes by pelletizing with coke breeze reductant and cement binder. Pellets of somewhat reduced but generally adequate strength can also be produced by air drying only.

encountered in making pellets; however, after storage for several weeks, the pellets tended to spall and powder. For extended storage, some binder appears necessary. Adding 1 to 2 pct bentonite resulted in acceptable pellets that were stable for longer periods than when no cement was added, although not as stable as when the binder was cement. It was also found that the mill scale could be crushed and screened through 20- or even 10-mesh (rather than 35-mesh) screens with no apparent effect on pellet properties.

Laboratory Smelting of Stainless Steelmaking Wastes

Earlier tests in an induction furnace *(7)* indicated that numerous combinations of pellet compositions could be smelted, with the carbon in the coke breeze reducing essentially all the oxides of Fe and Ni and a considerable part of the Cr oxide, roughly about one-half. The Mn oxide present was also readily reduced. It was observed that ferrosilicon could then be added to the molten bath to scavenge much of the remaining Cr from the slag.

The procedure for 100-lb arc furnace melts began with preheating the furnace refractories for 1 h, followed by the charging of 90 to 95 lb of pellets over a 45-min period. The 5- to 10-lb portion of loose (plus 35-mesh) mill scale was then added, and the furnace temperature was brought to at least 2,950° F. At this point, 3.0 pct Si, as ferrosilicon (75 pct Si), was added to the melt, which was stirred vigorously to enhance mixing and effect additional reduction of Cr oxide from the slag. The melt was heated to a temperature of 2,950° to 3,100° F before tapping (fig. 2). The ingots accounted for about 60 pct metal yield from the wastes charged. The slag represented some 10 to 15 pct of the original charge weight.

Further experiments indicated that 0.3 pct Al (as percentage of charge weight), added as shot, accomplished roughly the same amount of Cr and Ni reduction as the 3.0-pct Si addition. Table 2 shows results of the tests comparing the use of Fe-Si, Fe-Si-Al, and Al. The increased reduction associated with the use of Al shot may be due to the lower melting point or the higher thermodynamic activity of pure Al; the same nominal Al addition as the Al-bearing ferrosilicon was less effective, even in combination with the contained Si. For the 3-pct Si addition, most of the Si reported to the ingot.

Table 2.—Recovery of chromium and nickel from pelletized wastes after the smelting addition of various reductants[1]

Reductant added, pct	Ingot content, pct			Recovery, pct	
	Cr	Ni	Si	Cr	Ni
3 [2]Si	14.2	71.	6.9	91.5	99.3
0.6 Si, 0.3 [3]Al	15.1	6.9	2.3	84.7	90.5
0.3 [4]Al	15.5	7.1	.7	93.4	97.8

[1] In addition to 10 pct coke breeze in pellets.
[2] As ferrosilicon (75 pct Si).
[3] As aluminum ferrosilicon (20 Al-40 Fe-40 Si).
[4] As aluminum shot.

Other heats were made without Si or Al reductants. These melts were held similarly for 20 to 30 min before tapping, within the range 2,850° to 3,050° F. Only those held 30 min at 3,050° F showed improved Cr recovery relative to that for the lower temperatures. The reduction of the Cr oxide is related to time and temperature, as well as the type and amount of reductant.

Figure 2.—Laboratory arc furnace being tapped after smelting a charge of pelletized stainless steelmaking wastes.

Some stainless steel producers had indicated that they had been stockpiling mill scale. Samples were obtained from five companies. Partial analyses are shown in table 3. The scale from company C originated from ferritic stainless steel production; the others were from austenitic stainless steel production. The mill scales were mixed with other wastes and pelletized in two approximate compositions, as shown in table 4.

Although arbitrary, the proportions for the low-scale composition are intended to represent an approximate generation rate in a plant producing and segregating all four wastes. The high-scale composition reflects a situation whereby stockpiled mill scale would be used up at a faster-than-generated rate. Small-scale pelletizing tests indicated that pellets containing as much as 55 pct mill scale could be made, but 35 pct was a more practical value from the standpoint of a higher proportion of fines present and better pellet formation and strength.

The mixtures were prepared, blended to the compositions shown for low and high mill scale, and arc furnace melted as described previously. The slag was reduced with ferrosilicon. The results obtained for the group representing low mill scale (17.4 pct) pellets are shown in table 5. Manganese recoveries were 85 pct or more.

The smelting experiments with the low mill scale pellets indicated that 82 to 92 pct of the Cr could be readily recovered. Additional reductant and/or additional heating would increase the recoveries. Nickel recovery was, as expected, higher than the Cr recovery. The results of the smelting trials on high mill scale (35.0 pct) mixtures indicated a Cr recovery 5 to 10 pct lower than for low (17.4 pct) mill scale mixtures. This was believed due, in part, to the fact that the higher mill scale content resulted in a somewhat increased slag volume. That is, even with the same Cr slag solubility per unit volume, more total Cr partitioned to the higher volume slag.

Table 3.—Partial analyses of stainless steel mill scale samples, percent

Company designation	Fe	Cr	Ni	Mo
A	54.8	8.6	3.9	0.48
B	51.9	11.2	7.0	.47
C	62.7	7.6	.5	.22
D	49.4	8.4	3.7	.16
E	56.2	9.1	3.0	.66

Table 4.—Composition of pellets with low and high mill scale content, percent

Component	Low mill scale	High mill scale
Mill scale	17.4	35.0
EF dust	17.4	12.6
AOD dust	13.0	9.5
Grinding swarf	39.1	28.0
Coke breeze	8.7	10.5
Cement	4.4	4.4
Total	100.0	100.0

When other factors are held constant, the Cr solubility in slag decreases with increased slag basicity *(14)*, with slag basicity being defined as the ratio of percentage CaO plus MgO to SiO_2. The increased slag volume and weight brought about by the increased lime addition needed to increase the basicity may, however, offset any gain in reduced Cr solubility when considering the total Cr in the slag.

It should be noted that the laboratory smelting tests involved a charge consisting of 90 to 95 pct pellets and 5 to 10 pct loose mill scale. Some producers might have furnace capacity available to intermittently melt all-pellet charges for metering of hot metal to production heats. This method could also help reduce large backlogs of wastes. However, in normal industrial practice, it is anticipated that only 10 to 20 pct of the furnace charge would consist of pelletized wastes, to replace a portion of the scrap charge. This is the most economical and least energy-intensive approach and can readily match or exceed waste generation rates. Excess reductant normally available in production heats can also assist metal recoveries from the wastes. Under these circumstances, the slag generation would not be as much as indicated for the heats in table 5 but should be near to, although perhaps toward the high end of, normal ranges.

It remains to be conclusively demonstrated to what extent some of the minor metals such as Zn and Pb in the EF dust will build up in the baghouse dust with repeated pelletizing and refurnacing. The longer term concentration of minor elements (rate and extent) in recycled furnace dust will not be clarified until results are reported for campaigns extending over a substantial number of heats, with careful analysis of all charge and product materials.

There have been some extended campaigns to recycle baghouse dusts to the furnace without added carbon or other reductant. For these, the main objective has been to decrease the volume of hazardous waste requiring disposition, rather than gaining metal recovery. One firm has been recycling pelletized minimill carbon steelmaking furnace dust in this manner *(15)*. Even without reductant added with the pellets, some increased Fe yield has apparently been realized in these instances, evidently by supplying some "equilibrium" slag iron oxide requirements from the furnace dust rather than by Fe oxidation from the melt. Some limited reduction may be expected from excess reductant (Si and C) present in the melt. Furnace dusts generated from heats to which pelletized furnace dusts have been recycled are characteristically enriched in Zn and other metals that are volatile or form volatile species at steelmaking temperatures. For further information on the composition and nature of carbon and stainless steelmaking furnace dusts, the interested reader is directed to the final report resulting from the

Table 5.—Results of smelting pelletized waste mixtures containing mill scale[1] obtained from five stainless steel producers

Company designation	Ingot analysis, pct			Recovery, pct			Ingot as percent of charge	Slag as percent of charge
	Cr	Ni	Mo	Cr	Ni	Mo		
A	16.0	7.2	1.00	92.6	100.0	74.5	60.0	14.0
B	16.1	7.7	.80	87.7	90.7	91.9	47.9	13.0
C	14.5	5.9	.79	86.1	97.9	91.5	56.9	16.9
D	14.9	7.1	.83	82.3	93.2	63.6	55.9	19.3
E	14.9	6.2	.92	93.0	99.0	100.0	63.4	19.0

[1]17.4 pct mill scale in the pellets; other ingredients were (in percent) 17.4 EF dust, 13.0 AOD dust, 39.1 grinding swarf, 8.7 coke breeze, and 4.4 cement.

comprehensive arc furnace dust program conducted for the U.S. Department of Commerce by Lehigh University and the Bureau of Mines, with AISI collaboration and coordination *(16)*.

LARGE-SCALE DEMONSTRATION HEATS

All-Pellet Heats

The procedures derived in the laboratory experiments were tried on a larger scale in the form of a 1-st heat of the pelletized waste mixture *(8)*, which was made by Union Carbide Corp., Niagara Falls, NY. When it was evident that recoveries from this heat were sufficiently good, plans were formulated for substantially larger scale industrial trials.

The first of these large-scale demonstration trials was an all-pellet heat of approximately 12.5 st made in the production plant of Joslyn Stainless Steels. The wastes, generated during normal operations at Joslyn, were pelletized by a contractor in accordance with specifications developed at the Bureau's Rolla (MO) Research Center. The pellets ranged from ⅜- to 1-in diam and represented the mixture indicated earlier as low (17.4 pct) mill scale. The pellets analyzed, in percent, 42.5 Fe, 9.6 Cr, 4.0 Ni, and 0.7 Mo.

The charge to the furnace consisted of approximately 20,900 lb of pellets and 1,100 lb of oversize mill scale along with 0.5 st of lime. Several hundred pounds of steel punchings had been added at the outset to help strike an arc. When the charge was fully molten, the melt was sampled over a 30-min period. An addition of 1,320 lb of ferrosilicon (50 pct Si) was made to reduce chromium oxide remaining in the slag. Improved contact between the ferrosilicon and slag was achieved by stirring with an argon lance. The melt was tapped through the slag into a ladle from which it was poured into 14- by 14-in molds. The master alloy ingot produced weighed 12,300 lb and analyzed, in percent, 76.7 Fe, 11.8 Cr, 6.5 Ni, 0.8 Mo, 0.9 Mn, 4.3 Si, and 3.2 C. These values represented recoveries of 86.1, 68.7, and 92.0 pct of the Fe, Cr, and Ni, respectively. As shown in table 6, power consumption was 1.05 kW·h/lb of metal tapped.

The Cr recovery was lower than that experienced in smaller scale tests but was considered good for a single-heat experiment. Temperature was probably responsible for the lower recovery. After the ferrosilicon addition, the bath temperature of 2,750° F was some 200° F below the temperature of most of the laboratory heats. Nevertheless, Ni, the metal of highest total value, reported to the ingot as expected.

An 8,000-lb portion of the master alloy ingot from the all-pellet heat was incorporated into a commercial 19-st heat (heat 2, table 6) of AISI Type 316 stainless steel. The master alloy was completely compatible with the balance of the charge, principally stainless scrap. The heat was completed within the expected time, power consumed was normal, and there were no problems in either the arc furnace melting or AOD refining. The remainder of the ingot material was used in another commercial heat with equally good results.

Table 6.—Comparison of charge weight, metal tapped, and energy requirements for Joslyn demonstration heats 1 and 2

Heat	Type of heat	Charge, lb		Waste, pct	Metal tapped, lb	Power consumption,[1] kW·h
		Total	Waste			
1	All pellet	25,385	22,010	86.7	12,320	1.05
2	Scrap plus heat 1 master alloy	42,025	7,980	19.0	39,700	.254

Pellet-Plus-Scrap Heats

At this point, rather than optimizing the making of all-pellet heats, it was decided to go directly to the overall simpler and more economical introduction of waste pellets into the production arc furnace in lieu of part of the normal scrap charge. It was judged that the advantages of this approach would be (1) lower energy consumption, (2) simpler processing without producing intermediate master alloy ingots requiring remelting, and (3) variation of the quantity and composition of waste pellets as dictated by needs. It was realized that careful attention would have to be given to the furnace charge to accommodate the pellet waste ingredients and their products. However, since the makeup of furnace charges is commonly computer calculated, programs can be readily adjusted to account for this unconventional raw material.

Five Type 316 stainless steel heats were made in a 19-st production furnace, in which pelletized wastes (high or low scale) constituted 14 to 19 pct of the nominal charge. The remaining pellets from the Joslyn all-pellet heat, hereafter referred to as low-scale pellets, were used for two of these heats. Tonnage quantities of pellets also were produced by a contractor with substantially augmented percentage of mill scale. This high-scale composition added in the last three heats was tested to simulate consumption of substantial quantities of stockpiled mill scale. The makeup of the high-scale pellets was as follows, in percent: mill scale, 30; EF dust, 13; AOD dust, 9; grinding swarf, 33; coke breeze, 11; and cement, 4. The pellet composition (including oversize mill scale) was, in percent, 39.2 Fe, 8.9 Cr, 3.7 Ni, and 0.5 Mo.

The pellets were added to the arc furnace concurrently with the stainless scrap, making it unnecessary to backcharge. For all heats, only that quantity of ferrosilicon normally added to "quiet" such scrap melts was added. This ranged from 0 to 300 lb. The slag volume in each case was considered within the normal range for production heats. (With an extended campaign, some increased slag volume can be expected when partly replacing relatively clean scrap with pelletized wastes—other factors equal.) The pertinent statistics for the five heats are presented in table 7. All of the heats

Table 7.—Comparison of charge weight, metal tapped, and energy requirements for Joslyn demonstration heats 3 through 7 (pellets partly replace scrap)

Heat	Type of heat	Charge, lb		Waste, pct	Metal tapped, lb	Power consumption,[1] kW·h	Tap temp, ° F
		Total	Waste				
3	Scrap plus low-scale pellets.	41,790	5,970	14.3	38,500	0.244	2,920
4	...do	41,600	7,870	18.9	36,500	.260	2,960
5	Scrap plus high-scale pellets.	41,940	6,300	15.0	38,000	.263	3,000
6	...do	43,490	6,250	14.4	36,600	.259	2,950
7	...do	42,900	8,200	19.0	36,300	.261	2,940

[1] Per pound of metal tapped.

met required specifications after processing through the AOD vessel and were marketed as commercial bar, rod, or forging ingot. Table 8 gives the recoveries of Cr, Ni, and Mo, which, on the average, were considered equivalent to the customary values for all-scrap heats. Iron recoveries were consistently substantially >90 pct.

Metal Value of Pelletized Wastes

Technically and mechanically, this recycling scheme has been shown to work well. The question naturally arises as to whether it is also economical. The Bureau's Process Evaluation Group conducted internal studies of capital and operating costs for a plant addition producing pellets from wastes such as flue dusts, mill scale, and/or oily swarf. The estimated fixed capital cost for a 15-st/d pelletizing capacity was approximately $974,000 for oven drying of pellets and approximately $560,000 for air drying. Estimated annual operating costs per ton of pellets based on one-shift-per-day, 5-day-per-week operation (20-yr life) was approximately $117/st for oven drying and $40/st for air drying.

This can be contrasted to the contained value of the Cr, Ni, Mo, and Mn in the pellets. In addition to the particular proportions of the metals in the wastes, the value depends on the current price of ferroalloys or of appropriate scrap for which the pellets may substitute, particularly stainless steel (18 Cr-8 Ni) scrap. In some periods, a charge is also added for Fe units; this has not been the case when the scrap market is relatively depressed. On the basis of the Cr, Ni, Mo, and Mn for a waste mixture similar to those described for low-scale pellets (in percent, 9.5 Cr, 4.0 Ni, 0.8 Mo, and 2.0 Mn), with approximate contained metal values of $0.42/lb for Cr, $2.10/lb for Ni, $3.20/lb for Mo, and $0.33/lb for Mn (mid-1987 ferroalloy contained-metal values), the pellets would have a value of over $310/st. Deducting the approximate net operating cost of $117/st for oven drying or $40/st for air drying indicates a net gain of some $0.10 or $0.14/lb, respectively—a significant economical potential.

Table 8.—Recovery of Cr, Ni, and Mo from commercial pellet-plus-scrap heats 3 through 7, percent

Heat	Type of heat	Cr	Ni	Mo
3	Scrap plus 14 pct low-scale pellets	93.0	99.7	99.9
4	Scrap plus 19 pct low-scale pellets	93.7	89.7	95.0
5	Scrap plus 15 pct high-scale pellets	97.3	99.1	93.2
6	Scrap plus 14 pct high-scale pellets	90.8	91.9	82.8
7	Scrap plus 19 pct high-scale pellets	91.4	92.3	84.5

CONCLUSIONS

It has been shown that stainless steelmaking wastes such as flue dusts, mill scale, and grinding swarf can be pelletized and reduced in the arc furnace. This provides a means of recovering the contained scarce and valuable metals, while coincidentally solving problems of storage and waste disposal. The recovery procedure utilizes the reduction of metal oxides with carbon during the arc furnace melting, followed by a scavenging slag reduction of additional chromium oxide with ferrosilicon or Al.

One variation of the processing involves preparation of all-pellet smelting heats to produce master alloy ingot for recycle. This may be appropriate if furnace capacity is available in slack periods and large waste backlogs exist.

Alternatively, and recommended as being more economical, the waste-bearing pellets can be added directly to the arc furnace as some 10 to 20 pct of the total charge for production heats in lieu of part of the usual scrap or alloy charge required. The addition rate will depend on factors such as the rate of waste generation, waste backlog accumulation, and alloy product mix at a particular plant.

The dusts, scale, and swarf can be mixed and pelletized with little difficulty, providing both a means for adding carbon to the mix and a vehicle for charging to the furnace. Numerous varied combinations of pellet mix have been shown to be possible. Only conventional equipment is needed for agglomeration.

Usual recoveries of substantially greater than 90 pct of the Ni and Fe have been attained, and some 90 pct of the Cr and Mo appear consistently recoverable with proper control of variables. Other metals such as Mn are coincidentally recovered. Conventional arc furnaces were used throughout the testing.

The fact that this technology is readily transferable to an industrial scale was shown by the successful making of a number of demonstration heats ranging in size from 12.5 st for an all-pellet heat to about 19 st for a series of pellet-plus-scrap heats. The master alloy ingot from the all-pellet demonstration heat was used to make commercial stainless steel products without difficulty. No problems were encountered in these commercial stainless production heats to which up to 19 pct pellets were added in lieu of the normal scrap charge.

When the particular waste combination outlined in this paper is pelletized for recycle as a scrap substitute charge material, the pellets have a net value of more than $0.10/lb for oven drying or $0.14/lb for air drying, which implies an economically viable process.

Test results also indicate that a wide compositional variation of specialty steelmaking wastes can be incorporated into pellets for furnace charging.

REFERENCES

1. Federal Register. U.S. Environmental Protection Agency. Hazardous Waste Regulations. V. 45, No. 98, 1980, p. 33127.

2. Price, L. E. Tensions Mount in the EAF Dust Bowl. 33 Met. Producing, Feb. 1986, pp. 38–41.

3. Barnard, P. G., A. G. Starliper, W. M. Dressel, and M. M. Fine. Recycling of Steelmaking Dusts. BuMines TPR 52, 1972, 10 pp.

4. Dressel, W. M., P. G. Barnard, and M. M. Fine. Removal of Lead and Zinc and the Production of Prereduced Pellets From Iron and Steelmaking Wastes. BuMines RI 7927, 1974, 15 pp.

5. Higley, L. W., Jr., and M. M. Fine. Electric Furnace Steelmaking Dusts—A Zinc Raw Material. BuMines RI 8209, 1977, 15 pp.

6. Higley, L. W., Jr., and H. H. Fukubayashi. Method for Recovery of Zinc and Lead From Electric Furnace Steelmaking Dusts. Paper in Proceedings of the Fourth Mineral Waste Utilization Symposium. IIT Res. Inst., Chicago, IL, 1974, pp. 295–302.

7. Powell, H. E., W. M. Dressel, and R. L. Crosby. Converting Stainless Steel Furnace Flue Dusts and Wastes to a Recyclable Alloy. BuMines RI 8039, 1975, 24 pp.

8. Barnard, P. G., W. M. Dressel, and M. M. Fine. Arc Furnace Recycling of Chromium-Nickel From Stainless Steel Wastes. BuMines RI 8218, 1977, 10 pp.

9. Higley, L. W., Jr., L. A. Neumeier, M. M. Fine, and J. C. Hartman. Stainless Steel Waste Recovery System Perfected by Bureau of Mines Research. 33 Met. Producing, Nov. 1979, pp. 57–59.

10. Higley, L. W., Jr., R. L. Crosby, and L. A. Neumeier. In-Plant Recycling of Stainless and Other Specialty Steelmaking Wastes. BuMines RI 8724, 1982, 16 pp.

11. Neumeier, L. A., and M. J. Adam. In-Plant Recycling of Chromium-Bearing Specialty Steelmaking Wastes. Paper in Chromium-Chromite: Bureau of Mines Assessment and Research. Proceedings of Bureau of Mines Briefing Held at Oregon State University, Corvallis, OR, June 4–5, 1985, BuMines IC 9087, 1986, pp. 85–91.

12. Pargeter, J. K. Operating Experience With the Inmetco Process for the Recovery of Stainless Steelmaking Wastes. Paper in Proceedings of the Seventh Mineral Waste Utilization Symposium. IIT Res. Inst., Chicago, IL, 1980, pp. 118–126.

13. Fosnacht, D. R. Recycling of Ferrous Steel Plant Fines: State-of-the-Art. Iron and Steelmaker, v. 8, No. 4, Apr. 1981, pp. 22–26.

14. Peckner, D., and I. M. Bernstein. Handbook of Stainless Steels. McGraw-Hill, 1977, pp. 3–1—3–35.

15. Mueller, C. P. Recovery of Metallics From Specialty Steel Slags and Wastes. Pres. at AISI Symposium on Recovery of Alloys From Specialty Steel Wastes, Pittsburgh, PA, Oct. 21–22, 1981; information available from International Mill Service, Inc., Philadelphia, PA.

16. Lehigh University. Characterization, Recovery and Recycling of Electric Arc Furnace Dusts. Final rep. prepared for U.S. Dep. Commerce under project 99-26-09885-10, Feb. 1982, 313 pp.; NTIS PB 82-182585.

USING WASTES AS A SOURCE OF ZINC FOR ELECTROGALVANIZING

By V. R. Miller[1]

ABSTRACT

The Bureau of Mines investigated the use of Zn extracted from electric arc furnace (EAF) dust as a source of Zn for electrogalvanizing. The prepared sulfate electrolytes were used to coat steel sheet in flow cells at current densities up to 150 A/dm^2 to provide 90-g/m^2 Zn deposits. Electrochemical and physical properties of waste-derived coatings were compared with those of coatings produced from electrolytes prepared from pure ZnO and from an industrial process. These studies showed the properties to be similar in most cases.

INTRODUCTION

A dramatic increase in the demand for electrogalvanized steel has resulted from the construction, appliance, and especially the automotive industry needs *(1)*.[2] The amount of slab zinc used in 1986 for galvanized steel was estimated to be 47 pct of the total slab zinc consumption of 975,000 mt. An estimated 73 pct or 710,000 mt of this slab zinc was imported. Over 20 yr ago, it was estimated that 235,000 st of zinc could be recovered from domestic stack dusts *(2)*. In 1980, 75,000 st of Zn was contained in EAF dust alone *(3)*. This quantity of Zn was contained in about 400,000 st of EAF dust which has been declared a hazardous waste by the Environmental Protection Agency *(4)*.

Several studies and surveys have been carried out in recent years to examine the options for recovery of resources from EAF dust. Several processes, both pyrometallurgical and hydrometallurgical, have been proposed for treating EAF dust and these have been well documented in the literature. The bulk of these processes were aimed at recovering pure metals such as Zn. In the case of Zn, this requires stringent purification to produce electrolytes with impurities in the parts per billion range. However, for electrogalvanizing, some of the impurities have been shown to be beneficial *(5)*. Cobalt and chromium at low concentrations in electrogalvanizing baths have produced more corrosion-resistant coatings and Cd has enhanced wire drawability.

The Bureau of Mines demonstrated in previous research the feasibility of using Zn recovered from brass smelter flue dust to electrogalvanize steel wire in an industrial pilot plant *(6)*. This paper describes research on electrogalvanizing steel sheet with electrolytes produced from EAF dust and an EAF dust oxide fume produced from flash smelting the dust. The oxide fume differs from the EAF dust in that it contains the more volatile metals. Solutions from leaching the two products were purified as needed for electrogalvanizing and used in flow cells designed to simulate the hydrodynamics of an industrial line. Properties of deposits made with waste dust electrolytes were compared with the properties of deposits made using pure $ZnSO_4$ as well as industrial deposits.

EXPERIMENTAL

WASTE MATERIAL AND ELECTROLYTE

Table 1 contains a partial chemical analysis of the dusts used in the experimental work. The electrolyte from the EAF dust was prepared by mixing concentrated H_2SO_4 with the dust to sulfate it, then water leaching. The leach step involved mixing the sulfated dust with de-ionized water at 90° C for 1 h. The mixture was filtered; the liquor was reserved for electrolyte purification and the filter cake was combined with pure water for the wash step. The

Table 1.—Partial chemical analysis of dusts used, weight percent

Element	Oxide fume from flash smelter	Electric arc furnace (EAF) dust
Zn	35.4	31.3
Fe	7.5	19.6
Pb	6.5	5.2
Cd	.8	.1
Cu	.6	.2
Mn	.9	2.8
Mg	.4	1.3
Ca	.9	3.6
Cl	6.8	3.5
F	2.5	.1
Cr	.2	.3

[1] Supervisory research physicist, Rolla Research Center, Bureau of Mines, Rolla, MO.

[2] Italic numbers in parentheses refer to items in the list of references at the end of this paper.

wash step consisted of 30-min agitation at ambient temperature followed by filtration. The filter cake was then set aside for sampling and analysis. The wash water was returned to the leach reactors for starting the leach cycle on the next batch of sulfated dust. Typical combined extractions of Zn and Fe in the two steps were 92 and 11 pct, respectively.

The oxide fume electrolyte was prepared by direct H_2SO_4 leaching of the fume. The procedure was similar to that for the sulfated dust except that 450-g/L H_2SO_4 solution was used rather than deionized water. The wash step utilized pure water that was used, following filtration, for making the next acid leach solution. Typical leach liquor compositions are listed in table 2. The necessity of a degree of purification for the solutions is also evident when table 2 is examined in light of the need for low levels of Fe, Cu, Cd, Cl, and F.

Table 2.—Typical chemical analyses of leach solutions from oxide fume from flash smelter and electric arc furnace dust, grams per liter

Element	Oxide fume	EAF dust
Zn	158	155
Fe	35.3	10.1
Cu	3.0	<.01
Cd	.5	.4
Cl	11.7	18.6
F	5.2	.6
Pb	<.01	<.01

The Fe concentration was reduced to less than 0.1 g/L using a phosphate purification technique. The technique consisted of reducing the pH to 1.0, oxidizing the Fe with hydrogen peroxide, adding H_3PO_4 as a phosphate ion source, and raising the pH to 1.9 with lime. The Fe was subsequently precipitated as readily filterable $FePO_4$. The Cl levels were reduced using $CuSO_4$ and metallic Cu powder at 90° C, pH 2, for 2 h to form CuCl. Copper, cadmium, and lead were removed by cementation with Zn dust. Table 3 lists the chemical compositions of the electrolytes that were used to electrogalvanize the steel sheet. The Cl content of the oxide fume was high because of insufficient purification, which was not detected because of analytic error. It was detected when the electrolyte was rechecked after electrogalvanizing. Table 3 includes the pure zinc sulfate electrolyte that was prepared by dissolving French process ZnO in H_2SO_4 and H_2O. Zinc dust was added to the hot solution to insure the removal of Cd and Pb.

Table 3.—Electrolyte compositions used for electrogalvanizing steel sheet, grams per liter

Element	Pure $ZnSO_4$	EAF dust	Oxide fume
Zn	99	91	92
Fe	<.001	.025	.050
Cu	<.001	.004	.004
Cd	<.001	<.001	.002
Pb	<.002	.002	.002
Cl	<.001	.035	1.510
Co	<.001	<.001	.230
Ni	<.001	<.001	.140
Mn	<.001	2.94	1.41

STEEL PREPARATION

The steel sheet was supplied by Inland Steel and was 0.79-mm thick AKDQ alloy. As received, it had been sheared to size for the flow cells and oiled. The specimens were degreased with solvent, rinsed with ethanol, and dried in an airstream. The sheets were weighed to the nearest 0.0001 g. The sheets were then electrocleaned anodically in commercial alkaline cleaner for steel. Experimentation showed no significant change in weight, <0.001 g, before and after electrocleaning the sheets. The procedure following electrocleaning was to rinse the sheets in water, dip them in a 10-pct H_2SO_4 solution for 15 s to activate the surface, rinse in H_2O, place in the flow cell, and start the flow of electrolyte.

ELECTROGALVANIZING

Electrogalvanizing was done in two different size flow cells that used pumps to move the electrolyte past the stationary electrodes to simulate a moving line. The small cell used 4- by 5-cm sheet to yield a coated area of 20 cm^2. The anodes were Pb-1 pct Ag and were also 4 by 5 cm in size. The electrode spacing was 9 mm and with available flow rates, velocities at the cathode surface of up to 6 m/s were possible. Face velocities were used for flow rates to allow comparison with industrial electrogalvanizing line speeds. Five liters of electrolyte was required for operation of the pump to produce the desired flow rates.

The large cell coated 10- by 20-cm sheets and required 100 L of electrolyte. It also used Pb-1 pct Ag anodes with the electrode spacing being 9 mm. Time and current were adjusted for the current densities of 50 and 150 A/dm^2 to produce coatings of about 90 g/m^2. After the sheets were electrogalvanized, they were rinsed in H_2O, then ethanol, dried in air, and weighed to determine the amount of coating.

EXPERIMENTAL DESIGN

In conducting the research on the pure zinc sulfate electrolyte, the variables that were considered were current density, temperature, acid concentration (pH), Zn concentration, and face velocity of the electrolyte. Table 4 lists the variables and the upper and lower limits used in the experiments. A factorial design was used to gain the maximum information with a minimum of experimental work. The responses analyzed were current efficiency and preferred crystallographic orientation. Selected specimens were also subjected to electrochemical corrosion evaluation in addition to formability testing.

Table 4.—Experimental variables and test ranges

Variable	*Range*
Current density, A/dm^2	50–150
Temperature, °C	30–50
Acid concentration, pH	4.0–1.5
Zn concentration, g/L	90–150
Flow rate, m/s	2–5

The deposits prepared with electrolytes made from the waste dusts were evaluated in a similar manner using a factorial design. The two parameters, acid and Zn concentration, however, were held at 1.5 pH and 90 g/L, respectively.

ELECTROCHEMICAL CORROSION EVALUATION

Coupons were stamped from the electrogalvanized sheet to fit a flat specimen holder and yield a 1-cm^2 surface area. The coupons were degreased in boiling trichloroethylene, rinsed in ethanol, and dried in a filtered airstream.

The cell used was a commercially available 1-L glass vessel with various necks for electrodes, gas inlet and outlets, and thermometer *(7)*. The counterelectrode was Pt mesh, and the reference was a saturated calomel electrode. The medium was analytical reagent grade $(NH_4)_2SO_4$ of 1 mol/L concentration and pH of 6 ± 0.1. Prior to sample immersion, the medium was deaerated with oxygen-free N, and the gas purge continued throughout the experiments. All experiments were carried out at $25° \pm 1°$ C.

Impedance measurements were made at the open circuit potential (OCP) using a lock-in amplifier over a frequency range of 10 to 20,000 Hz having a peak amplitude of 5.15 mV (3.64 mV RMS). Measurements from 0.005 to 11 Hz were obtained in the time domain by an EG&G[3] fast fourier transform technique. The software performs the experiment and calculates the data points. The samples were immersed in the test medium for 1 h before measuring the electrochemical impedance.

FORMABILITY TESTS

Both compression and tension bend tests were used to evaluate the deposits. The compression samples were bent 180°, with the coating on the inside of the bend, and then straightened. Scotch brand tape was applied to the distorted area and removed. The relative amount of coating powdering was recorded. The tension samples were bent 180°, with the coating on the outside of the bend, and examined under low magnification to determine if peeling or flaking occurred in the deformed area. Then, the specimen was bent repeatedly back and forth over a mandrel until the steel fractured. The fracture area was examined under low magnification for separation or peeling of the coating. Prying with a sharp knife was used to indicate unsatisfactory adhesion by lift off of the coating *(8)*.

In addition to bend tests, drawing and ball punch deformation tests were conducted on coated sheet. Round 92-mm-diam blanks were punched from coated sheet and drawn into flanged cups approximately 43 mm in diameter and 42 mm deep. The ball punch deformation test was conducted in accordance with ASTM E643-78 *(9)* procedures. As an added indication of adhesion, a reverse ball punch test was also conducted on electrogalvanized sheet. In this test, the sheet was placed on the ram of the ductility tester, Zn side down, to form a 7.8-mm cone. The specimen was then removed and turned over with the top of the cone centered on the ram. The cone was then pushed back through the plate for a total of 14 mm. The condition of the Zn coating in the deformed area was then examined for flaking or peeling.

RESULTS AND DISCUSSION

CURRENT EFFICIENCY AND ORIENTATION

Current efficiency was calculated from the amount of electric charge used for a given sample and the weight of the deposit. Three specimens were coated for each set of conditions to obtain an average value. In the experimental work using the pure zinc sulfate electrolyte and small flow cell, the current efficiencies ranged from 95.2 to 99.0 pct. Thirteen out of the sixteen experimental combinations produced current efficiencies within 1 pct of each other in this range. This indicates little difference in the effects of the variables over the test ranges in table 4.

Similar results were obtained with the electrolytes prepared from the oxide fume and the EAF dust. The current efficiencies were in the same range of upper 90's values indicating no serious decrease due to the impurities present, especially the Cl. High levels of Cl did result in increased attack of the Pb-Ag anode producing nonconducting surface coatings, which resulted in higher voltages to hold the desired current settings.

The percentage of a particular crystallographic orientation that was used in the factorial analysis was arrived at by dividing the total count in the X-ray diffraction peak for that crystallographic plane by the total count for all planes and multiplying by 100. Table 5 lists some typical results obtained for selected conditions. For the pure Zn electrolyte, the predominant orientations were 002 and 103. It was noted that current density and Zn concentration played only a very minor role in either the orientation or current efficiency analysis.

Deposits produced from oxide fume electrolytes were different than those from the pure Zn electrolyte in that little (002) orientation was produced under any of the conditions. The majority of the deposits were 112 and 101. The same was true for the electrolyte from the EAF dust where there were higher percentages of all orientations other than 112 and 101. Examples of typical deposits are shown in the SEM photomicrographs in figure 1. The grain size of the deposits produced from waste electrolytes were also smaller than those from pure zinc oxide and from the industrial sample.

[3] Reference to specific products does not imply endorsement by the Bureau of Mines.

Preferred orientations of the industrial sample used for comparison were primarily 104, 103, 004, and 002, in order of descending percentage. Similar orientations were obtained for deposits prepared from pure electrolyte in the large cell.

ELECTROCHEMICAL CORROSION

Table 6 contains the ac data (electrochemical impedance spectroscopy) for selected samples from the tests on electrogalvanized samples. The values of polarization resistance (R_p) and double-layer capacitance (C_{dL}) have been shown in previous research *(10)* to be useful in monitoring the performance of electrogalvanized

Table 5.—Preferred crystallographic orientation of coated deposits prepared from different electrolytes at 500 A/dm², 90 g/L Zn, 1.5 pH, 60° C, 2 m/s, percent of total

Deposit source	002	004	101	102	103	104	110	112
Industrial	10	20	0	0	28	36	0	0
Pure ZnO	73	6	0	2	14	2	0	0
EAF dust	14	26	0	11	17	13	0	9
Oxide fume	0	0	39	4	1	0	5	45

Table 6.—Alternating current electrochemical impedance data for electrogalvanized steel in 1*M* $(NH_4)_2SO_4$ at 25° C after 1 h

Deposit source	Plating current density, A/dm²	Polarization resistance, (R_p), Ωcm²	Double-layer capacitance, (C_{dL}), μF/cm²
Industrial	60	1,600	15
Pure ZnO	50	1,625	17
	150	800	28
EAF dust	50	1,200	13
	150	600	20
Oxide fume	50	800	28
	150	500	42

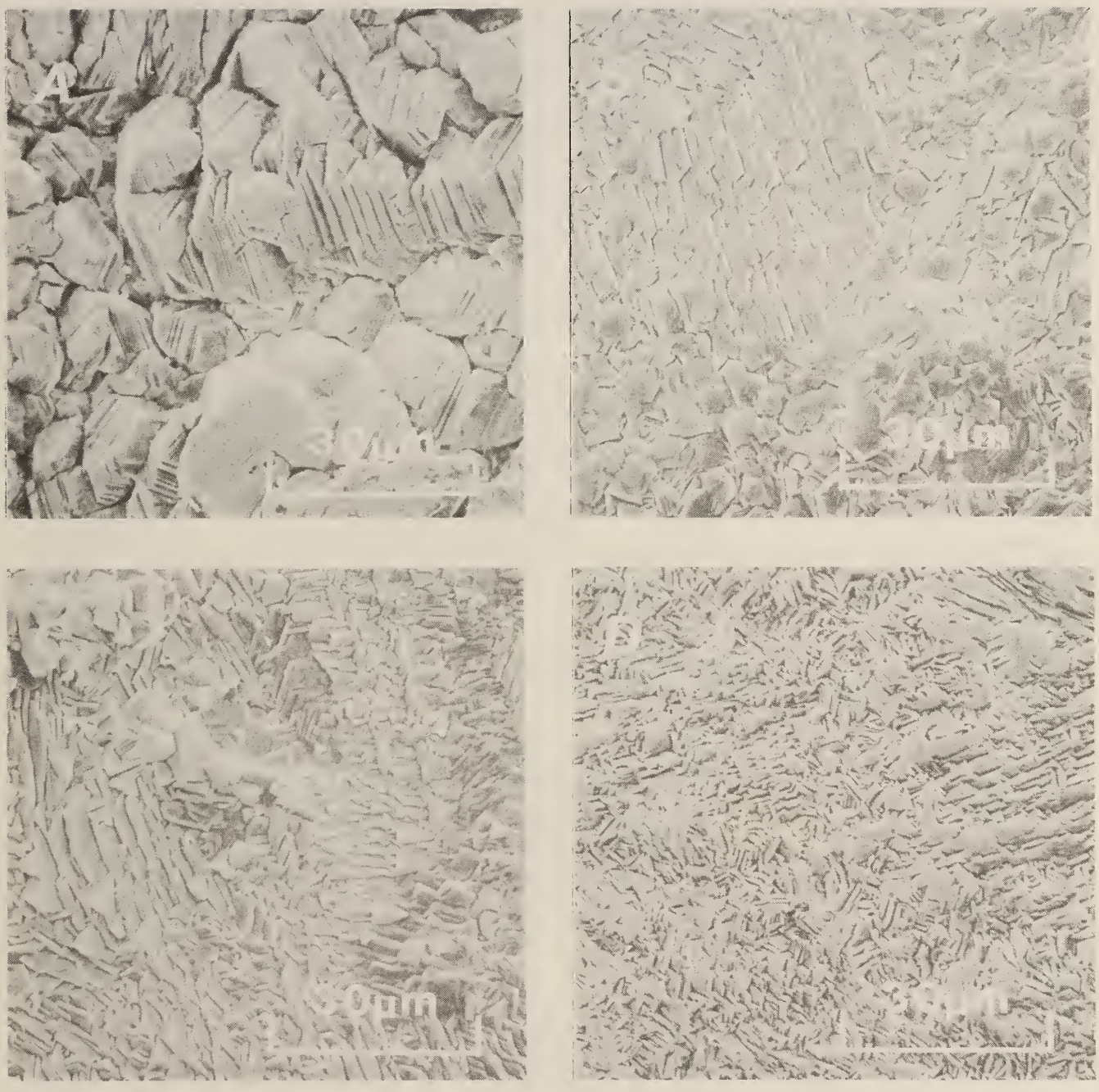

Figure 1.—SEM photomicrographs of electrogalvanized samples. *(A)* Industrial sample and samples electrogalvanized with *(B)* pure ZnO electrolyte, *(C)* EAF dust electrolyte, and *(D)* oxide fume electrolyte.

wire. It demonstrated that the corrosion rate of electrogalvanized steel was related to the ac impedance value of the polarization resistance in deaerated molar $(NH_4)_2SO_4$ under near-neutral conditions. The value of the double-layer capacitance was also reported to be related to the corrosion rate and to the surface condition of the metal coating. The corrosion rate ($i_{corr}R$) varies inversely as the polarization resistance. Thus, the larger the value of R_p the lower the corrosion rate. Low values of C_{dL} are usually obtained when there are surface films such as oxides or hydroxides of Zn and when the deposit is slowly corroding. Thus, low values indicate low corrosion rates when accompanied by large values of R_p.

It is seen in examining the electrochemical data in table 6, with the preceding in mind, that the corrosion rates are similar for the industrial, pure ZnO and EAF dust derived deposits that were plated at the lower current density. The deposit from the oxide fume exhibits a higher corrosion rate, which may be the result of the high Cl level in the electrolyte and the increased grain boundary area due to smaller grain size.

The data for the high-current-density deposits show what would amount to an increase in corrosion rate over the low-density plated samples. The EAF dust derived and the pure ZnO deposits are similar, with a possible advantage to the EAF dust deposit. Again, the

oxide fume exhibits values indicating higher corrosion rates over the pure ZnO and EAF dust deposits.

Results of salt spray corrosion tests by an independent laboratory on pure ZnO deposits indicated a similar trend. Only current density was significant in influencing salt spray results. Deposits plated at 50 A/dm^2 produced ASTM ratings of 8 to 9.5 *(11)*, while those at 150 A/dm^2 ranged from 4 to 6. The apparent reason is that current density influences nucleation and growth during electrodeposition and has a pronounced effect on grain size, with more active grain boundary material becoming predominant.

FORMABILITY TESTS

The results of selected bend tests are shown in table 7. All specimens bent in compression and straightened exhibited a few small cracks. However, only one specimen had some coating material removed with the tape. That sample was prepared with pure $ZnSO_4$ at a current density of 150 A/dm^2.

The tension bend tests resulted in small cracks on the industrial and oxide fume deposits. All others exhibited smooth bends. The examination of the coatings, after they were repeatedly bent through 180° until failure of the steel, indicated no separation or peeling of the coatings. Attempts to pry the coatings loose with a knife edge were unsuccessful, indicating good adhesion.

Microscopic examination of the drawn cup samples showed no cracking, flaking, or peeling of the Zn coatings, which indicates good ductility and adhesion. Examples of the drawn samples are shown in figure 2, which illustrates this.

The ball punch deformation test, used to evaluate the formability of sheet materials, was also used on the coated sheet. Samples plated from pure electrolyte at 60° C had cup heights and maximum loads similar to bare steel and commercial electrogalvanized sheet, while those plated at 35° C, with coarser-grained deposits, had lower cup heights and loads. Ball punch tests on samples prepared from EAF dust electrolyte indicated good formability as evidenced by cup heights and maximum loads similar to industrial samples. No peeling or flaking of the coating occurred in the area-of-rupture as shown in figure 3.

The reverse ball punch specimen shown in figure 4*A* is from a commercially coated sheet. The inner "ring," and just above it, is the area of severest deformation. There was no cracking, peeling, or flaking of the coating in this area. The specimens prepared with pure electrolyte were very similar to the commercial specimen. Figure 4*B* shows the EAF specimen, which exhibits some cracking at the ring. However, it was not possible to peel the coating at the cracks using a sharp knife point. This amount of cracking would not prevent the coating from being acceptable.

Table 7.—Bend test results on electrogalvanized steel sheet

Deposit source	Plating current density, A/dm^2	Compression		Tension	Bend rupture	
		Crack	Powdering	cracks	Bends	Peeling
Industrial	60	Yes	No	Small	12	No.
Pure ZnO	50	Yes	No	No	10	No.
	150	Yes	Moderate	No	9	No.
EAF dust	50	Yes	No	No	9	No.
	150	Yes	No	No	10	No.
Oxide fume	50	Yes	No	Small	10	No.
	150	Yes	No	No	11	No.

CONCLUSIONS

It has been shown that Zn from steel wastes such as EAF dusts can be used to successfully electrogalvanize steel sheet. Purification of the leach liquor is necessary, however, to reduce coextracted impurities Fe, Cu, Cd, and Cl. Electrogalvanizing tests in flow cells using pure and waste-derived electrolytes yielded good deposits at comparable current efficiencies which were in the 94- to 99-pct range. Deposits from waste electrolytes exhibited smaller grain size and less basal plane orientation than pure $ZnSO_4$ electrolyte.

Electrochemical corrosion evaluation of coated deposits showed that deposits from EAF dust, pure ZnO, and an industrial line have similar corrosion rates, while deposits from oxide fume with high Cl content have higher corrosion rates. Electrochemical data correlate with salt spray corrosion tests in showing that current density influences corrosion rate.

Bend, draw, and ball punch tests on coated steel sheet prepared from pure ZnO, EAF dust, and bend tests on oxide fume derived deposits indicated that the adhesion and ductility of the coatings were as good as those of an industrial sample.

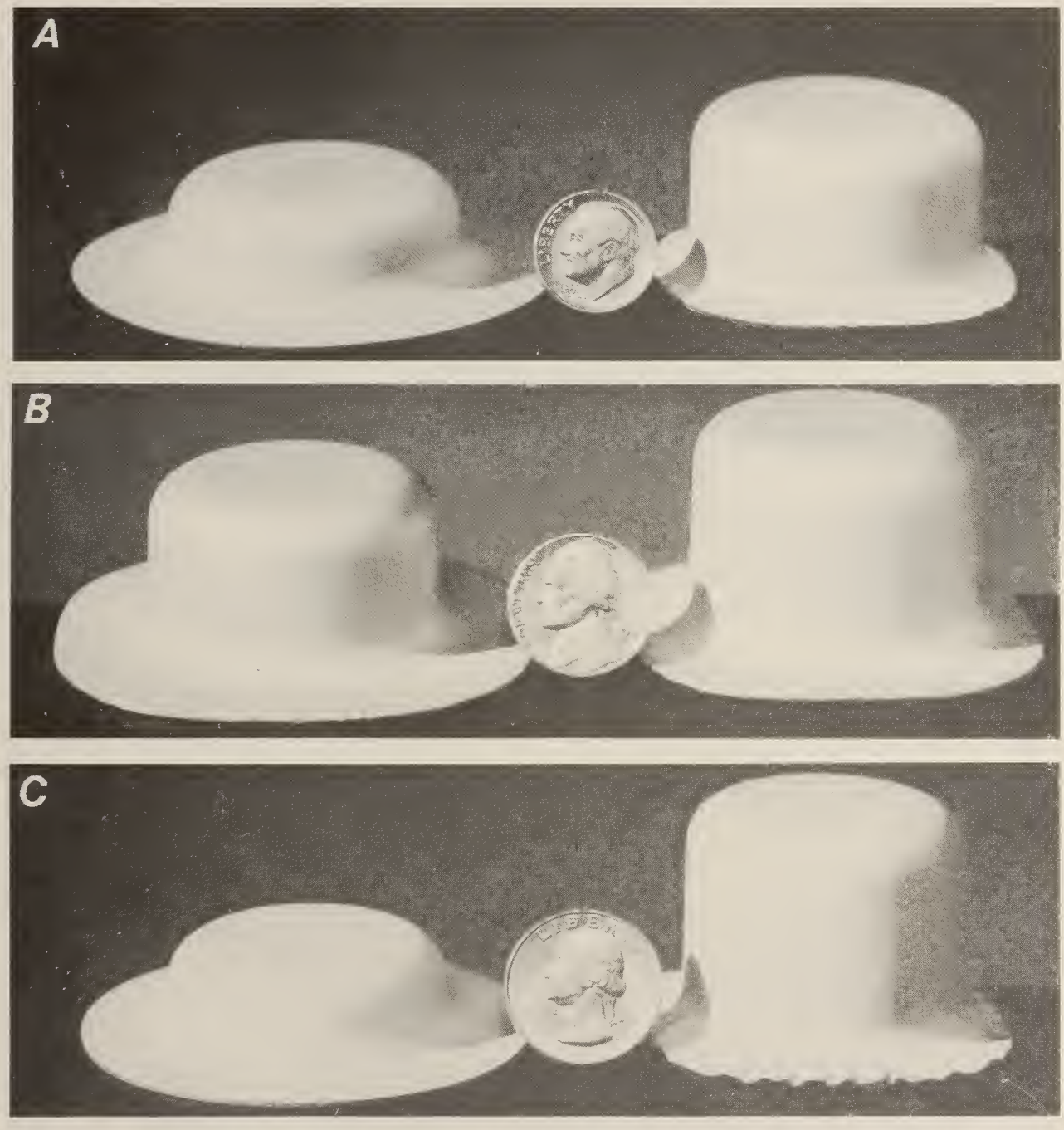

Figure 2.—Cups drawn from electrogalvanized samples. *(A)*, Industrial sample and cups drawn from samples electrogalvanized with *(B)* pure ZnO electrolyte and *(C)* EAF dust electrolyte.

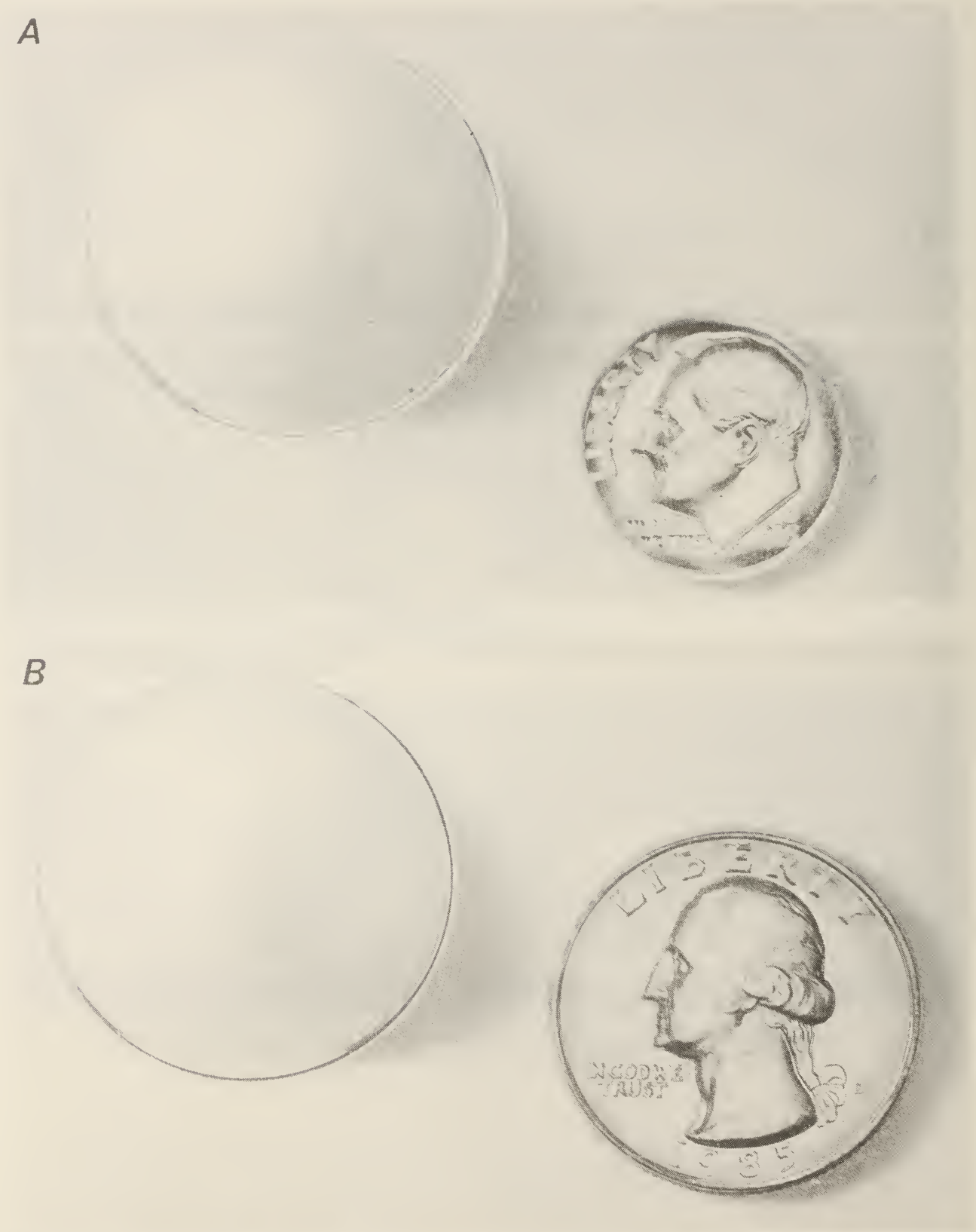

Figure 3.—Specimens from ball punch tests of electrogalvanized samples. *(A)* Industrial sample and *(B)* sample from EAF dust electrolyte.

Figure 4.—Specimens from reverse ball punch tests on electrogalvanized samples. *(A)* Industrial sample and *(B)* sample from EAF dust electrolyte.

REFERENCES

1. Jolly, J. H. Zinc. Sec. in BuMines Mineral Commodity Summaries 1987, pp. 180–181.

2. Carrillo, F. V., M. H. Hibpshman, and R. D. Rosenkranz. Recovery of Secondary Copper and Zinc in the United States. BuMines IC 8622, 1974, 58 pp.

3. Krishnan, E. R., and W. F. Kenner. Recovery of Metallic Values From Electric Arc Furnace Steelmaking Dusts. Paper in Proceedings of Symposium on Iron and Steel Pollution Abatement Technology for 1982. EPA Center for Environ. Res. Inf., Research Triangle Park, NC, 1983, 687 pp.

4. U.S. Code of Federal Regulations. Title 40—Protection of Environment; Chapter I—Environmental Protection Agency; Subchapter I—Solid Wastes. Part 261—Identification and Listing of Hazardous Waste; Subpart D—List of Hazardous Wastes, July 1, 1983.

5. Adaviya, T., M. Omura, K. Matsudo, and H. Naemura. Development of Corrosion-Resistant Electrogalvanized Steel. Plat. Surf. Finish., v. 68, No. 6, 1979, pp. 96–99.

6. Dattilo, M., E. R. Cole, Jr., and T. J. O'Keefe. Recycling of Zinc Waste for Electrogalvanizing. Conserv. & Recycling, v. 8, No. 3-4, 1985, pp. 399–409.

7. American Society for Testing and Materials. Standard Recommended Practice for Standard Reference Method for Making Potentiostatic and Potentiodynamic Anodic Polarization Measurements. G5–78 in 1982 Annual Book of ASTM Standards. Part 10—Metals—Mechanical, Fracture, and Corrosion Testing; Fatigue; Erosion and Wear; Effect of Temperature. Philadelphia, PA, 1982, pp. 906–916.

8. _____. Standard Test Methods for Adhesion of Metallic Coatings. B571–79 in 1982 Annual Book of ASTM Standards. Part 9, Metallic and Inorganic Coatings; Metal Powders, Sintered P/M Structural Parts. Philadelphia, PA, 1982, pp. 419–422.

9. _____.Standard Methods for Conducting a Ball Punch Deformation Test for Metallic Sheet Material. E643–78 in 1982 Annual Book of ASTM Standards. Part 10, Metals—Mechanical, Fracture, and Corrosion Testing; Fatigue, Erosion and Wear; Effect of Temperature. Philadelphia, PA, 1982, pp. 758–761.

10. Dattilo, M. The Use of AC Impedance to Determine the Corrosion Rate of Electrogalvanized Steel. Mater. Perf., v. 35, No. 11, Nov. 1986, pp. 18–22.

11. American Society for Testing and Materials. Standard Recommended Practice for Rating of Electroplated Panels Subjected to Atmospheric Exposure. B537–70 (Reapproved 1981) in 1982 Annual Book of ASTM Standards. Part 9, Metallic and Inorganic Coatings; Metal Powders, Sintered P/M Structural Parts. Philadelphia, PA, 1982, pp. 364–374.

ECONOMIC EVALUATION OF A TECHNIQUE TO PELLETIZE FLUE DUST AND OTHER WASTE FROM THE MANUFACTURE OF STAINLESS STEEL

By Joan H. Schwier[1]

ABSTRACT

Contained in this paper is an economic evaluation of a method to pelletize flue dust and other wastes from the manufacture of stainless steel. Bureau of Mines personnel have demonstrated that the alloying elements contained in this waste can be recovered if these pellets are used to replace a portion of the scrap fed to an electric arc furnace producing stainless steel. This evaluation considers two pellet drying options—heat dried and air dried.

The fixed capital cost for a plant addition required to produce 15 st of pellets per day is estimated to be about $974,000 for the heat-dried option and $560,000 for the air-dried option, based on second quarter 1987 equipment costs. The estimated annual operating cost per short ton of pellets to pelletize these wastes is approximately $117/st with the heat-dried option and $40/st with the air-dried option. The value of the pellets, based on the value of the contained alloying elements as ferroalloys, is estimated to be about $313/st. This indicates that the proposed pelletizing technique has economic potential.

INTRODUCTION

The manufacture of stainless steel results in the production of several wastes such as grinding swarf, mill scale, and flue dust from electric arc and argon-oxygen decarbonization furnaces. In an effort to recycle these wastes, the Bureau of Mines has investigated a technique to pelletize the wastes recovered from an electric-arc furnace. The original research[2] centered on smelting these pellets separately then recycling the recovered metal alloy as a replacement for the scrap portion of a stainless steel production heat.

Additional research has shown that it is also feasible to replace a portion of the scrap charge for stainless steel production heats with the pelletized waste. The pellets can compose from 10 to 20 pct of the total charge to the furnace. This enables recycling of the waste without the intermediate smelting stage. In this manner, it is expected that the alloying elements present in the waste can be recycled at minimum cost to the manufacturer.

This evaluation is the latest in a series of evaluations that has been used to help guide the research. The research work is described in another paper in this Information Circular, titled "Recycling of Stainless Steelmaking Dusts and Other Wastes," by L. A. Neumeier and M. J. Adam.

PROCESS DESCRIPTION

A plant addition has been designed to produce 15 st/d of pellets from stainless steel wastes, operating one shift per day, 5 days per week.

Wastes that are assumed to be available for the production of the pellets are grinding swarf, mill scale, and flue dusts from electric arc and argon-oxygen decarbonization furnaces. The flue dusts, mill scale, and grinding swarf are stored in open piles and moved daily to storage bins with a front-end loader. Mill scale is screened to separate it into three fractions—plus ¾ in, minus ¾ in plus 35 mesh, and minus 35 mesh. The plus ¾-in fraction is large enough to be recycled directly and is not included in the pellets. It is conveyed to a storage bin until needed in the furnace. Minus ¾-in plus 35-mesh mill scale is conveyed to a ball mill and crushed. The ball mill product is returned to the screen. Minus 35-mesh mill scale from the screen is conveyed to a storage bin.

In a zig-zag mixer, the mill scale is combined with grinding swarf and flue dusts from electric arc and argon-oxygen decarbonization furnaces. Coke breeze and portland cement are also added to the mixer. The coke breeze is required to reduce the oxidized

[1] Cost evaluation program assistant, Process Evaluation, Bureau of Mines, Washington, DC.

[2] Powell, H. E., W. M. Dressel, and R. L. Crosby. Converting Stainless Steel Furnace Flue Dust and Wastes to a Recyclable Alloy. BuMines RI 8039, 1975, 24 pp.

portion of the waste when the pellets are smelted. Portland cement is added as a binding agent.

The combined wastes are then conveyed to a balling drum for pelletization. The resulting green pellets, containing about 12 pct moisture, are dried by one of two methods, the heat-dried option using truck dryers or the air-dried option using the same type drying trucks, but without a dryer. In the heat-dried option, the pellets are air dried for 24 h before being completely dried in a heated dryer. Using the air-dried option, the pellets are dried in the open for several days. Either drying method produces pellets suitable for feeding to an electric arc furnace. The only difference in the plant designs for the two options is the addition of two truck dryers for the heat-dried option.

The evaluation is based on pellets produced from the materials presented in table 1. The composition of the dry pellets is shown in table 2. There is no reason to believe that the raw material ratios used in this study could not be changed to permit the use of varying quantities of each waste.

Table 1.—Materials used to make up the pellets, percent

Argon-oxygen decarbonization furnace flue dust	13.0
Electric arc furnace flue dust	17.4
Grinding swarf	39.1
Mill scale	17.4
Portland cement	4.4
Coke breeze	8.7
Total	100.0

Table 2.—Pellet composition (dry basis), percent

Chromium	9.5
Nickel	3.96
Molybdenum	.84
Manganese	2.0
Iron	41.8
Carbon	11.8
Silicon	3.5
Other	26.6
Total	100.00

ECONOMICS

The intent of an economic evaluation is to present capital and operating cost estimates of a commercial-size plant. In the preparation of any economic evaluation, it is necessary to make many assumptions. In general, the assumptions that are made are expected either to apply to the majority of the potential plants or to have only a small effect on the process capital and operating costs. An example of such an assumption is that the plant operates one shift per day, 5 days per week.

If an assumption would be necessary that may not apply to a majority of plants or may have a major effect on capital or operating costs, then it is generally not included in the evaluation. An example of such an exclusion is that land cost and pond construction costs have not been included in the capital or operating cost estimates. When an assumption has been made or deliberately excluded, this fact is documented.

A detailed description of the estimating techniques used in this evaluation has been published.[3]

CAPITAL COSTS

The capital cost estimate is of the general type called a study estimate by Weaver and Bauman.[4] This type of estimate, prepared from a flowsheet and a minimum of equipment data, can be expected to be within 30 pct of the actual cost. Equipment costs are from informal cost quotations from equipment manufacturers and from capacity-cost data. The costs of the major items of equipment and their accessories are tabulated in the appendix to this paper.

The estimated fixed capital costs for plant additions capable of producing 15 st/d of pellets, on a second quarter 1987 basis (Marshall and Swift (M and S) index of 808.0), are approximately $974,000 for the heat-dried option and $560,000 for the air-dried option, as shown in table 3. Because this is a plant addition, the cost to hook up to existing plant facilities and utilities is estimated as 2 pct of the total section costs.

Factors for piping, etc., except for the electrical factor, are assigned to each section, using as a basis the effect fluids, solids, or a combination of fluids and solids may have on the process equipment. The electrical factor is based on the motor horsepower requirements for each section. A factor of 10 pct, referred to as miscellaneous, is added to each section to cover minor equipment and construction costs that are not shown with the equipment listed.

For each section, the field indirect cost, which covers field supervision, inspection, temporary construction, equipment rental, and payroll overhead, is estimated at 10 pct of the direct cost. Engineering cost is estimated at 10 pct, and administration and overhead cost is estimated at 5 pct of the construction cost. A contingency allowance of 10 pct and a contractor's fee of 5 pct are included in the section costs.

The costs of plant facilities and plant utilities are estimated as 2 pct each of the total process section costs and include the same field indirect costs, engineering, administration and overhead, contingency allowance, and contractor's fee as are included in the section costs. Included under plant facilities are the cost of material and labor for auxiliary buildings such as offices, shops, laboratories, and cafeterias, and the cost of nonprocess equipment such as office furniture, and safety, shop, and laboratory equipment. Also

Table 3.—Estimated capital cost,[1] heat-dried and air-dried options

	Heat dried	Air dried
Fixed capital:		
Mill-scale preparation section	$142,000	$142,000
Mixing and pelletization section	726,900	357,600
Subtotal	868,900	499,600
Plant facilities, 2 pct of above subtotal	17,400	10,000
Plant utilities, 2 pct of above subtotal	17,400	10,000
Total plant cost	903,700	519.600
Land cost	0	0
Subtotal	903,700	519,600
Interest during construction period	70,700	40,400
Fixed capital cost	974,400	560,000
Working capital:		
Raw material and supplies inventory	2,400	2,200
Product and in-process inventory	39,600	14,800
Accounts receivable	39,600	14,800
Available cash	30,600	9,500
Working capital cost	112,200	41,300
Capitalized startup cost	9,700	5,600
Subtotal	121,900	46,900
Total capital cost	1,096,300	606,900

[1] Basis: M and S equipment cost index of 808.0.

[3] Peters, F. A. Economic Evaluation Methodology. BuMines IC 9147, 1987, 21 pp.

[4] Weaver, J. B., and H. C. Bauman. Cost and Profitability Estimation. Sec. 25 in Perry's Chemical Engineers's Handbook, ed. by R. H. Perry and C. H. Chilton. McGraw-Hill, 5th ed., 1973, p. 47.

included are labor and material costs for site preparation such as clearing, grading, drainage, roads, and fences. The costs of water, power, and steam distribution systems are included under plant utilities.

Working capital is defined as the funds in addition to fixed capital, land investment, and startup costs that must be provided to operate the plant. Working capital, also shown in table 3, is estimated from the following items: (1) Raw material and supplies inventory (cost of raw material and operating supplies for 30 days), (2) product and in-process inventory (total operating cost for 30 days), (3) accounts receivable (total operating cost for 30 days), and (4) available cash (direct expenses for 30 days).

Capitalized startup costs are estimated as 1 pct of the fixed capital costs, and are shown in table 3. The cost of land is not included in this estimate.

OPERATING COSTS

The estimated annual operating cost is based on the average of 260 days of operation per year, one shift per day, over the life of the plant. The operating costs are divided into direct, indirect, and fixed costs.

Direct costs include raw materials, utilities, direct labor, plant maintenance, payroll overhead, and operating supplies. Raw materials and utility requirements per short ton of pellets are shown in the appendix. The shipping charge must be added to the cost of the raw material because the plant location has not been selected. Payroll overhead, estimated as 35 pct of direct labor and maintenance labor, includes vacation, sick leave, social security, and fringe benefits.

Plant maintenance is separately estimated for each piece of equipment and for the buildings, electrical system, piping, plant utility distribution systems, and plant facilities.

The indirect costs include the expenses of control laboratories, accounting, plant protection and safety, plant administration, marketing, and company overhead. These costs are estimated as 40 pct of the direct labor and maintenance costs. Research and overall company administrative costs outside the plant are not included.

Fixed costs include the cost of taxes (excluding income taxes), insurance, and depreciation. Depreciation is based on a straight-line, 20-yr period.

The net operating cost per short ton of pellets is $117 for the heat-dried option; and $40 for the air-dried option. These costs are presented in table 4. Included in this cost is a credit of 1 cent per pound ($20/st) for the reduced landfill requirements. If the dusts

Table 4.—Estimated annual operating cost, heat-dried and air-dried options

	Heat-dried costs		Air-dried costs	
	Annual	Per st pellets	Annual	Per st pellets
Direct cost:				
Raw materials:				
Portland cement at $60/st	$10,300	$2.64	$10,300	$2.64
Coke breeze at $32/st	13,400	3.44	13,400	3.44
Argon-oxygen decarbonization dust at $0.00/st	0	.00	0	.00
Electric arc furnace flue dust at $0.00/st	0	.00	0	.00
Grinding swarf at $0.00/st	0	.00	0	.00
Mill scale at $0.00/st	0	.00	0	.00
Replacement balls for grinding at $0.27/lb	100	.03	100	.03
Total	23,800	6.11	23,800	6.11
Utilities:				
Electric power at $0.05/kW·h	2,600	.67	900	.23
Process water at $0.25/Mgal	100	.03	100	.03
Natural gas at $5.25/MMBtu	202,000	51.79	NAP	NAP
Total	204,700	52.49	1,000	.26
Direct labor:				
Labor at $10.50/h	65,500	16.79	43,700	11.21
Supervision, 20 pct of labor	13,100	3.36	8,700	2.23
Total	78,600	20.15	52,400	13.44
Plant maintenance:				
Labor	12,400	3.18	6,400	1.64
Supervision, 20 pct of maintenance labor	2,500	.64	1,300	.33
Materials	12,400	3.18	6,400	1.64
Total	27,300	7.00	14,100	3.61
Payroll overhead, 35 pct of above payroll	32,700	8.38	21,000	5.38
Operating supplies, 20 pct of plant maintenace	5,500	1.41	2,800	.72
Total direct cost	372,600	95.54	115,100	29.52
Indirect cost, 40 pct of direct labor and maintenace	42,400	10.87	26,600	6.82
Fixed cost:				
Taxes, 1 pct of total plant cost	9,000	2.31	5,200	1.33
Insurance, 1 pct of total plant cost	9,000	2.31	5,200	1.33
Depreciation, 20-yr life	48,700	12.49	28,000	7.18
Total operating cost	481,700	123.52	180,100	46.18
Credit:				
Reduced landfill requirements at $0.01/lb	23,700	6.08	23,700	6.08
Net operating cost	458,000	117.44	156,400	40.10

NAP Not applicable.

are declared as hazardous waste, the disposal cost would be at least $200/st. The grinding swarf and mill scale may have a market value; but a cost for them is not included in the operating cost.

PRODUCT VALUE

To estimate the value of the pellets, it is assumed that the contained alloying elements will have a value equal to their price as a ferroalloy or metal. These values, per pound are, nickel, $2.10; chromium as ferrochrome, $0.42; molybdenum, $3.20; and manganese as ferromanganese, $0.33. Based on the composition listed in table 2, the value of the pellets is about $313/st. Based on the chromium and nickel values alone, the pellet value is about $246/st. In either case the value of the metal contained in the pelletized waste is much higher than the cost to pelletize it.

It should be noted that the pellet value listed in the preceding paragraph is only an estimate and at best will only be representative of pellets with the same composition. For a particular location, with its own unique wastes, the value of pellets will vary significantly from the value presented. It is expected, however, that the values given are sufficiently representative to allow anyone interested in the Bureau's recycling technique to make a decision as to whether additional consideration is warranted.

TECHNICAL EVALUATION

The technique to pelletize the stainless steel waste, as presented in this paper, utilizes standard agglomeration techniques and should present no problems in scale-up to a commercial size. Pellets produced at the Bureau's Rolla (MO) Research Center were used to replace part of the scrap charge to an electric arc furnace at a commercial stainless steel manufacturer and were successfully smelted. The results of this testing can be obtained from the research personnel at the Rolla Research Center. It appears, therefore, that the proposed recycling technique has been sufficiently developed to allow serious consideration of it for adaptation on a commercial scale.

The use of the proposed process has two potential advantages. First, the alloying elements previously lost in the wastes will be recycled, which will lower the overall operating cost for the stainless steel manufacturer. Also, because chromium and nickel are almost totally imported, their recycle will reduce the U.S. dependence on these imports. The second advantage will be a reduction in the landfill requirements of the stainless steel manufacturer. Processing the wastes can only increase the environmental acceptability of a plant.

Wastes produced by a stainless steel plant will vary from plant to plant as well as from day to day. This is due to the variety of alloys produced and to variations in equipment and procedures. The Bureau's recycling technique, however, should be applicable to any fine stainless steel manufacturing waste.

APPENDIX.—HEAT-DRIED AND AIR-DRIED OPTIONS

Table A-1.—Raw material and utility requirements per short ton of pellets

		Heat dried	Air dried
Raw materials:			
Portland cement	st	0.044	0.044
Coke breeze	st	.107	.107
Argon-oxygen decarbonization dust	st	.130	.130
Electric arc furnace flue dust	st	.174	.174
Grinding swarf	st	.391	.391
Mill scale	st	.174	.174
Replacement balls for grinding	lb	.067	.067
Utilities:			
Electric power	kW·h	13.467	4.533
Process water	Mgal	.133	.133
Natural gas	MMBtu	9.867	Nap

Nap Not applicable.

Table A-2.—Equipment cost summary, mill scale preparation section, heat-dried and air-dried options

Item	*Equipment*[1]	*Labor*	*Total*
Mill-scale hopper	$800	$300	$1,100
Belt conveyor	7,700	1,300	9,000
Vibrating screen	10,700	1,400	12,100
Bucket conveyor	1,400	400	1,800
Storage bin	1,800	700	2,500
Bucket elevator	3,000	900	3,900
Belt conveyor	7,000	1,200	8,200
Ball mill	3,500	200	3,700
Mill-scale storage bin	300	100	400
Total	36,200	6,500	42,700
Total equipment cost × factor indicated:			
Foundations, × 0.695			25,200
Structures, × 0.080			2,900
Instrumentation, × 0.050			1,800
Electrical, × 0.362			13,100
Piping, × 0.200			7,200
Painting, × 0.020			700
Miscellaneous, × 0.100			3,600
Total			54,500
Total direct cost			97,200
Field indirect, 10 pct of total direct cost			9,700
Total construction cost			106,900
Engineering, 10 pct of total construction cost			10,700
Administration and overhead, 5 pct of total construction cost			5,300
Subtotal			122,900
Contingency, 10 pct of above subtotal			12,300
Subtotal			135,200
Contractor's fee, 5 pct of above subtotal			6,800
Section cost			142,000

[1] Basis: M and S equipment cost index of 808.0.

Table A-3.—Equipment cost summary, mixing and pelletization section, heat-dried option

Item	*Equipment*[1]	*Labor*	*Total*
Argon-oxygen decarbonization dust storage bin	$2,000	$700	$2,700
Argon-oxygen decarbonization dust feeder	1,000	100	1,100
Electric arc furnace flue dust storage bin	2,000	700	2,700
Electric arc furnace flue dust feeder	1,000	100	1,100
Grinding swarf storage bin	2,000	700	2,700
Grinding swarf feeder	1,000	100	1,100
Portland cement storage bin	4,200	1,200	5,400
Portland cement feeder	1,000	200	1,200
Coke breeze storage bin	3,000	1,200	4,200
Coke breeze feeder	1,000	100	1,100
Belt conveyor from storage	10,000	2,100	12,100
Mixer (zig-zag)	1,300	100	1,400
Belt conveyor	7,700	1,400	9,100
Pelletizer	48,000	600	48,600
Belt conveyor	5,800	900	6,700
6-truck dryer[2]	68,500	2,400	70,900
9-truck dryer[2]	97,000	2,600	99,600
Pellet storage bin	2,600	1,000	3,600
Bucket conveyor	6,200	1,900	8,100
Total	265,300	18,100	283,400
Total equipment cost × factor indicated:			
Foundations, × 0.228			60,400
Structures, × 0.080			21,200
Insulation, × 0.020			5,300
Instrumentation, × 0.050			13,300
Electrical, × 0.109			29,000
Piping, × 0.200			53,100
Painting, × 0.020			5,300
Miscellaneous, × 0.100			26,500
Total			214,100
Total direct cost			497,500
Field indirect, 10 pct of total direct cost			49,800
Total construction cost			547,300
Engineering, 10 pct of total construction cost			54,700
Administration and overhead, 5 pct of total construction cost			27,400
Subtotal			629,400
Contingency, 10 pct of above subtotal			62,900
Subtotal			692,300
Contractor's fee, 5 pct of above subtotal			34,600
Section cost			726,900

[1] Basis: M and S equipment cost index of 808.0.
[2] Includes cost of truck.

Table A-4.—Equipment cost summary, mixing and pelletization section, air-dried option

Item	Equipment[1]	Labor	Total
Argon-oxygen decarbonization dust storage bin	$2,000	$700	$2,700
Argon-oxygen decarbonization dust feeder	1,000	100	1,100
Electric arc furnace flue dust storage bin	2,000	700	2,700
Electric arc furnace flue dust feeder	1,000	100	1,100
Grinding swarf storage bin	2,000	700	2,700
Grinding swarf feeder	1,000	100	1,100
Portland cement storage bin	4,200	1,200	5,400
Portland cement feeder	1,000	200	1,200
Coke breeze storage bin	3,000	1,200	4,200
Coke breeze feeder	1,000	100	1,100
Belt conveyor from storage	10,000	2,100	12,100
Mixer (zig-zag)	1,300	100	1,400
Belt conveyor	7,700	1,400	9,100
Pelletizer	48,000	600	48,600
Belt conveyor	5,800	900	6,700
Pellet storage bin	2,600	1,000	3,600
Bucket conveyor	6,200	1,900	8,100
Total	99,800	13,100	112,000
Drying trucks			16,500
Total equipment cost × factor indicated:			
Foundations, × 0.463			46,200
Structures, × 0.080			8,000
Instrumentation, × 0.050			5,000
Electrical, × 0.241			24,100
Piping, × 0.200			20,000
Painting, × 0.020			2,000
Miscellaneous, × 0.100			10,000
Total			115,300
Total direct cost			244,700
Field indirect, 10 pct of total direct cost			24,500
Total construction cost			269,200
Engineering, 10 pct of total construction cost			26,900
Administration and overhead, 5 pct of total construction cost			13,500
Subtotal			309,600
Contingency, 10 pct of above subtotal			31,000
Subtotal			340,600
Contractor's fee, 5 pct of above subtotal			17,000
Section cost			357,600

[1] Basis: M and S equipment cost index of 808.0.

U.S. GOVERNMENT PRINTING OFFICE: 1988 — 547-000/80,059

U.S. Department of the Interior
Bureau of Mines—Prod. and Distr.
Cochrans Mill Road
P.O. Box 18070
Pittsburgh, Pa. 15236

☐ Do not wish to receive this material, please remove from your mailing list.

☐ Address change. Please correct as indicated.